

Abdominal fat-related biomarkers and metabolic health

Dissertation
zur Erlangung des Doktorgrades (PhD)
der Medizinischen Fakultät
der Rheinischen Friedrich-Wilhelms-Universität
Bonn

Lidia Ximena Orozco Ruiz

aus Michoacán, Mexico

2022

Angefertigt mit der Genehmigung
der Medizinischen Fakultät der Universität Bonn

1. Gutachterin: Prof. Dr. Dr. Monique M.B. Breteler
2. Gutachterin: Prof. Dr. Ute Nöthlings

Tag der Mündlichen Prüfung: 08.06.2022

Aus dem Deutschen Zentrum für Neurodegenerative Erkrankungen (DZNE e.V.), Populationsbezogene Gesundheitsforschung

Direktorin: Prof. Dr. Dr. Monique M.B. Breteler

Table of Contents

List of abbreviations	5
1. Abstract	6
2. Introduction & Aims with references	7
2.1 Obesity prevalence	7
2.2 Obesity Paradox	8
2.3 Abdominal fat	8
2.4 Abdominal adipose tissue expansion and metabolic complications.....	9
2.4.1 Hypoxia, macrophages infiltration and inflammatory cytokines	10
2.4.2 Glucose and lipid metabolism	10
2.4.3 Metabolic differences between VAT and SAT	11
2.5 Methods to assess abdominal obesity.....	12
2.5.1 Anthropometric measurements.....	12
2.5.2 Imaging methods	12
2.6 Metabolomic biomarkers of abdominal fat and metabolic health.	13
2.6.1 Metabolomics.....	15
2.7 Aim.....	16
2.8 References	16
3. Publications	23
3.1 FatSegNet: A fully automated deep learning pipeline for adipose tissue segmentation on abdominal dixon MRI.	23
3.2 Metabolic Profiling of Human Plasma and Urine, Targeting Tryptophan, Tyrosine and Branched Chain Amino Acid Pathways.....	36
3.3 Association of abdominal MRI visceral and subcutaneous adipose tissue with cardiometabolic risk markers and their comparison with anthropometric measurements (Submitted).....	60

3.4 Branched-chain and aromatic amino acids related to visceral adipose tissue impact metabolic health risk markers.....	83
4. <i>General discussion</i>.....	93
5. <i>Acknowledgement</i>.....	99
6. <i>Statement</i>	100

List of abbreviations

VAT	Visceral adipose tissue
SAT	Subcutaneous adipose tissue
BMI	Body mass index
WC	Waist circumference
WHR	Waist-to-hip ratio
WHtR	Waist-to-height ratio
MRI	Magnetic resonance imaging
FAs	Fatty acids
FFA	Free-fatty acids
MU	Metabolically unhealthy
MH	Metabolically healthy
CVD	Cardiovascular diseases
T2D	Type 2 diabetes
TNFα	Tumor necrosis factor alpha
IL-6	Interleukin 6
GLUT4	glucose transporter type 4
BCAA	Branched-chain amino acids
AAA	Aromatic amino acids
Trp	Tryptophan
Val	Valine
Ile	Isoleucine
Leu	Leucine
Tyr	Tyrosine
KP	Kynurenine pathway
IDO1	Indoleamine 2,3-dioxygenase-1 enzyme
WHO	World Health Organization
UHPLC-ESI-MS/MS	Ultrahigh performance liquid chromatography–electrospray ionization tandem mass spectrometry.

1. Abstract

Obesity is considered one of the major risk factors for chronic diseases and mortality. Although body mass index (BMI) is generally used to classify obesity, BMI can lead to the misclassification of individuals at cardiometabolic risk. Some individuals with a high BMI actually have a low cardiovascular disease (CVD) risk. The limited suitability of BMI for risk classification is due to the lack of information regarding body fat distribution, particularly abdominal fat. Beyond BMI, other anthropometric measurements such as waist circumference (WC), waist to hip ratio (WHR), and waist to height ratio (WHtR) are commonly used as proxies for abdominal fat. However, also their associations with cardiometabolic risk and thus validity as risk markers remain questionable. Abdominal fat consists of visceral and subcutaneous adipose tissue (VAT and SAT), two metabolically different fat compartments. However, the relationships of VAT and SAT with cardiometabolic risks are rather complex and not yet completely understood. In this thesis, I aimed to investigate the association of abdominal fat, as assessed through anthropometric and abdominal MRI measurements, with cardiometabolic risk markers of metabolic health. To enable this, I first collaborated with experts of artificial intelligence in medical imaging, and targeted metabolomics analysis, to develop the measures to be used (fat segmentation; metabolic profiling). Next, I investigated the interplay of abdominal fat-related biomarkers and metabolic health. The analyses were based on the first 5000 participants from the baseline examination of the Rhineland Study. My main findings are 4-fold. First, I confirmed that larger VAT volumes are more metabolically detrimental than SAT in women, whereas VAT and SAT are associated with cardiometabolic risk markers to a similar extent in men. Second, I observed that among anthropometric measurements, WC is the best surrogate marker for VAT. However, none of the anthropometric measurements added further information on cardiometabolic risk markers above that offered by VAT alone, suggesting that abdominal MRI measurements cannot be replaced if we want to understand underlying mechanisms linking adiposity and metabolic diseases. Third, I found that larger VAT volume in metabolically unhealthy persons might alter the metabolism of branched-chain (BCAA) and aromatic amino acids (AAA). And lastly, my research suggests that BCAA and AAA downstream metabolites might be involved in the mechanisms that underlie the relationship of abdominal VAT with metabolic health.

2. Introduction & Aims with references

2.1 Obesity prevalence

Obesity is considered one of the major health problems around the world and is one of the main causes of non-communicable diseases such as CVD, type 2 diabetes (T2D), musculoskeletal disorders, and some types of cancer (Heymsfield and Wadden, 2017) (GBD 2015 Obesity Collaborators, 2017) (World Health Organization, 2021). Historically, obesity has been assessed by the Quetelet index. This index was first reported in 1835 by Alphonse Quetelet, who attempted to define the average man using data from the heights and weights of the French and Scottish armies. His results showed that body weight increases as the square of the body height (Eknoyan, 2006) (Rössner, 2007). The Quetelet index, later called BMI, is calculated by dividing weight in kilograms by the square of body height measured in meters (kg/m^2). The World Health Organization (WHO) established several cut-off values of BMI to classify the population as underweight ($\text{BMI} < 18.5$), normal weight ($18.5 \leq \text{BMI} < 24.9$), overweight ($25 \leq \text{BMI} < 29.9$), and obese ($\text{BMI} \geq 30$) (WHO Consultation, 2000). Epidemiological studies have reported that worldwide the prevalence of overweight and obesity has risen significantly over the past three decades. Overall, about 13% of the adult population worldwide (11% of men and 15% of women) were obese in 2016 (World Health Organization, 2021).

The prevalence of overweight and obesity has increased in both developed and developing countries, but patterns differ between men and women. In developed countries, men have higher rates of overweight and obesity, while in developing countries, women exhibit higher rates, and this relationship persists over time (Jaacks et al., 2019). In Germany, the obesity prevalence is also increasing despite strategies implemented by the Federal Government. The German Health Interview and Examination Survey for Adults (DEGS1) reported in 2013 that 24% of women and 23% of men were obese (Mensink et al., 2013). More recently, the German Health Update (GEDA) study series, using self-reported data on height and weight, reported that 46.7% of women and 61.6% of men in Germany were overweight, and the overall prevalence of obesity was 18.1% for both sexes (Schienkiewitz et al., 2017).

2.2 Obesity Paradox

Increases in BMI contribute to a high proportion of deaths due to CVD and T2D (GBD 2015 Obesity Collaborators, 2017). However, a considerable proportion of BMI-related deaths occurred in people without obesity (Afshin et al., 2017). Several studies found a non-linear (U-shaped curve) association of BMI with CVD and mortality, in which individuals with a BMI threshold of 25 to 30 kg/m² (overweight) have a lower mortality risk compared with individuals at a low (normal weight) and high spectrum (obesity) of BMI (Berrington de Gonzalez et al., 2010; Di Angelantonio et al., 2016; Flegal et al., 2007; Song et al., 2015). This so-called “obesity paradox” has raised the importance of a further subclassification of obesity groups according to their metabolic profile. For instance, studies have reported that there is a subset of individuals with a high BMI that can be considered metabolically healthy (MH) as they present a healthy metabolic profile, characterized by high insulin sensitivity, a favourable lipid profile, and low pro-inflammatory cytokine levels, and normal blood pressure. Conversely, another subset of individuals with normal or low BMI are metabolically unhealthy (MU) (Wildman et al., 2008)(Stefan et al., 2013). Body fat distribution, and specifically abdominal fat, is a cornerstone in understanding the complex relationships between obesity and metabolic diseases and is considered an essential factor in the mechanisms involved in converting MH phenotype to MU (Hwang et al., 2015). A challenge for population research into obesity is that the easily obtainable measure of BMI does not directly depict body fat, and even less, abdominal fat distribution (Sommer et al., 2020).

2.3 Abdominal fat

Abdominal fat is an important risk factor for chronic diseases (Després, 2012). One of the first pieces of research studying the effects of abdominal fat distribution on cardiometabolic risk was done by Jean Vague more than 50 years ago. His work drew attention to sex differences in abdominal fat accumulation, with men tending to accumulate fat around the trunk and upper body (android obesity) while women store more fat around the thighs and hips (gynoid obesity) (Vague, 1956). Abdominal adipose tissue is distributed principally in two main compartments: subcutaneous adipose tissue (SAT) and visceral adipose tissue (VAT).

Anatomically, SAT is defined as the adipose tissue layer found between the dermis and the aponeuroses and fasciae of the muscles. The main areas for subcutaneous fat deposition are the femoral-gluteal regions, back, and anterior abdominal wall. SAT represents about 80% of all body fat of a healthy individual (Ibrahim, 2010).

Abdominal VAT, a term originating from the Latin “viscera” word, stands for “organs in the cavities of the body” and can be distributed in three main body cavities: intrathoracic (ITAT), intraabdominal (IAAT), and intrapelvic (IPAT). Although the anatomical definition for VAT varies across studies, the majority define VAT as the abdominal fat accumulated in the IAAT cavity. This region is usually localized 5 cm below the lumbar 4th or from the lumbar 5th to the slice corresponding to the superior border of the liver (Shen et al., 2003). Usually, VAT quantification also includes the fat surrounding the retroperitoneal organs, such as the pancreas, kidneys, duodenum, ascending colon, and descending colon (Nauli and Matin, 2019), and represents approximately 10 to 20% of the total body fat in men and 5 to 8% of total body fat in women. Because of its anatomical position, venous blood from visceral fat is drained directly to the liver through the portal vein (Ibrahim, 2010).

2.4 Abdominal adipose tissue expansion and metabolic complications

Adipose tissue is an endocrine organ, and one of its main functions is to store fat and release it in response to energy needs (Rosen and Spiegelman, 2014). Adipocytes are the representative cells of the adipose tissue, storing fat as triglycerides and free fatty acids (FFAs). In a response to an excess of energy intake, there is an increased demand for fat storage in the adipocytes by absorbing FFAs and triglycerides in the postprandial period. As a result, adipocytes expand increasing the cell numbers via preadipocyte differentiation (hyperplasia) and increasing the cell size by lipid droplet expansion (hypertrophy) (Ghaben and Scherer, 2019)(Arner et al., 2010). Hyperplasia is known as a healthier mechanism of expansion because adipocytes keep a normal physiological process storing excess of FFAs and triglycerides. It is suggested that SAT is the initial site for fat storage, however, once the storage capacity of SAT adipocytes is exceeded, they reach a limit of expansion and become hypertrophic. Those hypertrophic adipocytes start to accumulate in the VAT or in organs that are not adapted to store fat (ectopic fat) (Ibrahim, 2010). Ectopic fat is mainly accumulated in the major glucose reg-

ulatory or peripheral organs such as the liver, skeletal muscle, pancreas, and heart. This type of fat accumulation is considered “lipotoxic” because interferes with normal insulin signaling, promotes insulin resistance, and increases the risk of T2D (Chait and den Hartigh, 2020).

Although the expansion of SAT adipocytes, in response to an excess of energy intake, occurs principally through hypertrophy rather than hyperplasia (Rosen and Spiegelman, 2014), the size and number of adipocytes within VAT and SAT can highly vary at a population level (Suárez-Cuenca et al., 2021). Several cellular pathways and genetic factors have been proposed to be involved in the regulation of adipocyte size and morphology (Tandon et al., 2018) (Ye et al., 2022) (Macotella et al., 2012). The way adipocytes expand determines the metabolic complications of abdominal fat (Suárez-Cuenca et al., 2021) by activating selective mechanisms that lead to inter-individual differences in cardiometabolic risk (Suárez-Cuenca et al., 2021) (Tandon et al., 2018) such as promoting inflammation, disrupting insulin sensitivity, and impairing lipid metabolism.

2.4.1 Hypoxia, macrophages infiltration and inflammatory cytokines

Hypertrophic adipocytes expand by increasing their size and can rapidly reach the local limit of tissue oxygen diffusion, becoming hypoxic. Acute hypoxia leads to cell death and triggers physiologic stimuli for collagen breakdown and infiltration of macrophages. Macrophages are the main inflammatory cell type that infiltrates the adipose tissue and contribute considerably to the local levels of pro-inflammatory molecules. An increased rate of collagen synthesis and rates of adipocyte necrosis is associated with high levels of pro-inflammatory cytokines such as tumor necrosis factor-alpha (TNF- α), interleukin 6 (IL-6), and a decrease of anti-inflammatory cytokines such as leptin and adiponectin (Ghaben and Scherer, 2019). Pro-inflammatory cytokines secreted in the adipose tissue antagonize insulin action and promote systemic inflammation (Smith and Kahn, 2016).

2.4.2 Glucose and lipid metabolism

Adipocytes play an important role in the regulation of glucose and insulin homeostasis. The relationship between adipocytes and glucose homeostasis is mainly regulated by glucose transporter type 4 (GLUT4), the major insulin-regulated glucose transporter (Abel et al., 2001) Hypertrophic adipocytes show a reduced expression of glucose

transporter type 4 (GLUT4), which leads to a decrease of *de novo* lipid synthesis and impair glucose uptake in the adipocytes, affecting the capability of adipocytes to store and (re-) esterify fatty acids (FAs), and causing high circulating levels of FAs (Smith and Kahn, 2016). An excess of FFA can cause metabolic disturbance in several ways. FFA may interact with insulin receptors and cause decreased insulin sensitivity, inhibit glucose uptake, and stimulate glyconeogenesis. Additionally, FFAs are substrates for hepatic triglyceride production and influence the assembly and secretion of very-low-density lipoproteins (VLDL) (Arner, 1995). Thus, elevated FFAs levels promote hepatic lipid accumulation, contributing to glucose intolerance, hypertriglyceridemia, insulin resistance, and hyperinsulinemia (Smith and Kahn, 2016) (Ebbert and Jensen, 2013). Metabolic dysfunction of hypertrophic adipocytes can also lead to increase production of lipid species that can accumulate in non-adipose organs, causing organ failure (Chaurasia and Summers, 2015).

2.4.3 Metabolic differences between VAT and SAT

Adipocytes from VAT and SAT show heterogeneous functionality and mechanisms that may underlie their differential contributions to cardiometabolic risk.

It has been shown that hypertrophic adipocytes from VAT are more insulin-resistant, have a higher rate of insulin-stimulated glucose uptake (Ibrahim, 2010) (Ye et al., 2022), and secrete higher concentrations of pro-inflammatory cytokines compared with SAT adipocytes (Kranendonk et al., 2015). VAT has a higher rate of lipolysis than SAT and direct access to the liver through the portal system. Thus, VAT provides direct FFAs and cytokines to the liver and other non-fat tissues, increasing the risk of developing hepatic insulin resistance and T2D (Arner, 1995) (Rytka et al., 2011)

In addition, based on the “gut-to-adipose tissue axis” theory, higher inflammation in VAT might be highly influenced by lipopolysaccharide from the gut microbiome because of the VAT’s proximity to the intestine (Hersoug et al., 2018) (Hersoug et al., 2016).

Previous work has also shown that SAT adipocytes have a higher rate of differentiation in response to different stimuli than VAT adipocytes, indicating that SAT fat expands mainly by hyperplasia, whereas VAT expands by hypertrophy (Macotela et al., 2012). Moreover, adipocyte precursor cells (APCs) of VAT and SAT showed different gene ex-

pression signatures. These differences in the genetic background might also explain the differences concerning cardiometabolic risk (Macotela et al., 2012).

Still, the association of VAT and SAT with cardiometabolic risk at the population level is complex, and accurately measuring abdominal fat is essential to getting a more comprehensive understanding of the underlying mechanisms of metabolic health.

2.5 Methods to assess abdominal obesity

2.5.1 Anthropometric measurements

Anthropometric measurements are indirect and non-invasive methods to assess body composition. They are widely used in epidemiological studies because of their feasibility in clinical practice. Beyond the already mentioned BMI, other measures such as WC, WHR, and WHtR are used in clinical practice to estimate abdominal obesity (Cornier et al., 2011; Neeland et al., 2019). Some epidemiological studies have shown the superiority of these surrogates over BMI when evaluating risk for CVD (Bodenant et al., 2011)(Kidy et al., 2017) or risk of mortality (Pischon et al., 2008). For instance, the European Prospective Investigation into Cancer and Nutrition (EPIC) reported that the associations of BMI with the risk of death followed a J-shaped curve, with higher risks of death observed in both the lower and upper BMI categories. Interestingly, they found a stronger association between high WC with mortality risk in individuals with low BMI (Pischon et al., 2008). Worldwide, the estimation of obesity prevalence comes from extensive national data that rely on BMI (World Health Organization, 2021). However, anthropometric measurements are an indirect measurement of adiposity and are sensitive to different types of measurement errors because of a lack of standardized techniques (Ulijaszek and Kerr, 1999). Measures of circumferences can be influenced by muscles and bones and do not accurately discriminate between VAT and SAT (Bosy-Westphal et al., 2010).

2.5.2 Imaging methods

An accurate assessment of VAT and SAT is essential for identifying individuals at higher risk of CVD and investigating the underlying mechanisms involved in the relationship of abdominal obesity with cardiometabolic risk.

The development of body fat measurement techniques started many years ago, from dissection and chemical analysis of cadavers (Martin et al., 2003) (Janssens et al., 1994) to less invasive techniques. Nowadays, there is a wide range of invasive and non-invasive methods for body composition analysis, of which imaging techniques such as computed tomography (CT) and MRI are considered the gold standard for abdominal fat assessment. Nonetheless, due to the high radiation exposure with CT scans, MRI measurements are preferred (Borga et al., 2018) (Cornier et al., 2011).

MRI uses quantitative fat water imaging, which is a precise measurement of regional adipose tissue and lean tissue. The basis for quantitative fat water imaging is fat water separated, or Dixon imaging, where the different magnetic resonance frequencies of protons in fat and water are used for separating the two signals into a fat image and a water image (Dixon, Thomas, 1984). Abdominal MRI scans can be done by single-slice or multiple-slice acquisition. However, multiple-slices are preferred for a more accurate abdominal fat volume quantification (Shuster et al., 2012). Since MRI does not induce radiation, there is no limited time for scanning which reduces the uncertainty of their locations (Borga et al., 2018). The localization and quantification of VAT and SAT volumes are done with manual and/or semi-automated segmentation methods. However, manual segmentation methods are time-consuming, expensive, and introduce significant intra- and inter-operator variability (West et al., 2016). With the increasing demand for accurate quantification of abdominal adipose tissue in large cohort studies, automated quantification methods are needed (West et al., 2016). Nonetheless, the performance of automated segmentation is challenging because of the complex structures and shapes of the adipose across individuals and the inherent properties of Dixon images such as low-intensity contrast between adipose tissue classes, inhomogeneous signals, and potential organ motion. Thus, the development and validation of robust automated pipelines for large population-based studies are essential (Estrada et al., 2020).

2.6 Metabolomic biomarkers of abdominal fat and metabolic health.

The link between abdominal adipose tissue and metabolic health can be mediated by biomarkers such as metabolites. These molecules are signatures of environmental exposures and they can also be used as biomarkers to classify individuals at risk for certain diseases (Wild, 2005).

Studies have shown that obesity is associated with disorders in protein metabolism (Guillet et al., 2011), especially the metabolism of branched-chain (BCAA) and aromatic amino acids (AAA). BCAA and AAA are considered essential amino acids because they must be obtained from the diet. The main metabolites from BCAA are Isoleucine (Ile), leucine (Leu), and Valine (Val). They are involved in protein synthesis and insulin secretion. Phenylalanine (Phe), tryptophan (Trp), and tyrosine (Tyr) belong to the AAA amino acids. They serve as precursors for the synthesis of many biologically/neurologically active compounds that are essential for maintaining normal biological functions (Han et al., 2019). However, an imbalance between protein intake and protein catabolism can cause physiological problems (Neinast et al., 2019). Alteration in protein breakdown is the primary source of elevated concentrations of BCAA and AAA in circulation. High circulating BCAA and AAA have been associated with obesity (Cusotto et al., 2020), insulin resistance (Wiklund et al., 2016), and cardiometabolic risk factors (Cheng et al., 2012). They have also been established as biomarkers to predict the future development of T2D (Wang et al., 2011), metabolic syndrome, dyslipidemia, and hypertension (Yamakado et al., 2015).

Interestingly, studies have shown that adipocytes play an important role in the obesity-related alteration of amino acid metabolism. Trp can be further metabolized in downstream metabolites by three main pathways: the kynurenine pathway (KP), the serotonin pathway, and indole derivatives under the direct or indirect control of the microbiota (Agus et al., 2018). The highest proportion of Trp metabolism is through KP (Badawy and Guillemin, 2019). This pathway is mainly regulated by the indoleamine 2,3-dioxygenase-1 (IDO1) enzyme, activated by proinflammatory cytokines in the adipose tissue (Wolowczuk et al., 2012). Certain downstream metabolites of the KP are neurotoxic and have been associated with chronic diseases (Chen and Guillemin, 2009).

Likewise, BCAA metabolism can be regulated in adipocytes. Animal (Herman et al., 2010) and human (Lackey et al., 2013) studies have shown that in adipocytes, the expression of BCAA catabolic enzyme is decreased, particularly in the VAT of MU obese individuals (Lackey et al., 2013). This suppression of BCAA catabolism in adipose tissue can cause systemic elevations of BCAAs in the circulation. Thus, the measurement of BCAA and AAA-derived circulating metabolites is becoming increasingly important.

2.6.1 Metabolomics

Metabolomic analysis can profile metabolites in biofluids, cells, and tissues to identify metabolites and metabolic pathways that are associated with particular phenotypes or diseases. There are mainly two approaches to metabolite identification, untargeted and targeted metabolomics.

Untargeted metabolomics aims to measure the broadest range of metabolites present in an extracted sample without a priori knowledge of the metabolome, with the advantage of possibly identifying novel metabolites. Targeted metabolomic analyses, on the other hand, measure the concentrations of a predefined set of metabolites. A standard curve for a concentration range of the metabolite of interest is prepared, so that accurate quantification can be gained. This type of analysis can be used to obtain exact concentrations of metabolites identified by untargeted metabolomics, providing analytical validation. Through the use of internal standards, analysis can be undertaken in a quantitative or semi-quantitative manner (Johnson et al., 2016) (Roberts et al., 2012). The validation of targeted and robust methods that cover a large number of putative metabolites such as BCAA, AAA, and AAA-breakdown metabolites is needed.

2.7 Aim

The overarching goal of this thesis was to identify abdominal fat-related biomarkers associated with cardiometabolic risk markers. For this, I first contributed to developing and validating an automated deep learning pipeline for localizing, segmenting, and quantifying VAT and SAT from MRI Dixon fat images (Chapter 3.1). Moreover, I also contributed to validating a UHPLC-ESI-MS/MS method for targeted quantification of putative metabolites from BCAA and AAA metabolism (Chapter 3.2). I next used the data on abdominal adipose tissue distribution to investigate the relation of VAT and SAT with anthropometric measurements and cardiometabolic risk factors (Chapter 3.3). Furthermore, I investigated the relationship of VAT and SAT with circulating BCAA, AAA, and AAA-breakdown metabolites across metabolic health status and evaluated the association of those metabolites with cardiometabolic risk markers, and whether they mediate the link between abdominal adipose tissue and metabolic health (Chapter 3.4).

Towards the end of this thesis (Chapter 4), I will discuss my main results in the context of what is already known, how my findings contribute to a better understanding of the complex associations between VAT and SAT with cardiometabolic risk, and give directions for further research on this important topic.

2.8 References

- Abel ED, Peroni O, Kim JK, Boss O, Hadro E, Minnemann T, et al. 2001. Adipose-selective targeting of the GLUT4 gene impairs insulin action in muscle and liver. *Nature* 409: 729–733
- Afshin A, Forouzanfar MH, Reitsma MB, Sur P, Estep K, Lee A, et al. 2017. Health effects of overweight and obesity in 195 countries over 25 years. *N Engl J Med* 377: 13–27
- Agus A, Planchais J, Sokol H. Gut Microbiota Regulation of Tryptophan Metabolism in Health and Disease. *Cell Host Microbe*. 2018; 23:716–724;
- Arner E, Westermark PO, Spalding KL, Britton T, Rydén M, Frisén J, et al. 2010. Adipocyte turnover: Relevance to human adipose tissue morphology. *Diabetes* 59:105–109

- Arner P. 1995. Differences in lipolysis between human subcutaneous and omental adipose tissues. *Ann Med* 27:435–438
- Badawy AAB, Guillemin G. 2019. The Plasma [Kynurenine]/[Tryptophan] Ratio and Indoleamine 2,3-Dioxygenase: Time for Appraisal. *Int J Tryptophan Res* 12
- Berrington de Gonzalez A, Hartge P, Cerhan JR, Flint AJ, Hannan L, MacInnis RJ, et al. 2010. Body-Mass Index and Mortality among 1.46 Million White Adults. *N Engl J Med* 363:2211–2219
- Bodenant M, Kuulasmaa K, Wagner A, Kee F, Palmieri L, Ferrario MM, et al. 2011. Measures of abdominal adiposity and the risk of stroke: The monica risk, genetics, archiving and monograph (MORGAM) study. *Stroke* 42:2872–2877
- Borga M, West J, Bell JD, Harvey NC, Romu T, Heymsfield SB, et al. 2018. Advanced body composition assessment: From body mass index to body composition profiling. *J Investig Med* 66:887–895
- Bosy-Westphal A, Booke C-A, Blöcker T, Kossel E, Goele K, Later W, et al. 2010. Measurement Site for Waist Circumference Affects Its Accuracy As an Index of Visceral and Abdominal Subcutaneous Fat in a Caucasian Population. *J Nutr* 140:954–961
- Chait A, den Hartigh LJ. 2020. Adipose Tissue Distribution, Inflammation and Its Metabolic Consequences, Including Diabetes and Cardiovascular Disease. *Front Cardiovasc Med* 7:1–41
- Chaurasia B, Summers SA. 2015. Ceramides - Lipotoxic Inducers of Metabolic Disorders. *Trends Endocrinol Metab* 26:538–550
- Chen Y, Guillemin GJ. 2009. Kynurenine pathway metabolites in humans: Disease and healthy states. *Int J Tryptophan Res* 2:1–19
- Cheng S, Rhee EP, Larson MG, Lewis GD, McCabe EL, Shen D, et al. 2012. Metabolite profiling identifies pathways associated with metabolic risk in humans. *Circulation* 125:2222–2231
- Cornier MA, Després JP, Davis N, Grossniklaus DA, Klein S, Lamarche B, et al. 2011. Assessing adiposity: A scientific statement from the american heart association. *Circulation* 124:1996–2019
- Cussotto S, Delgado I, Anesi A, Dexpert S, Aubert A, Beau C, et al. 2020. Tryptophan Metabolic Pathways Are Altered in Obesity and Are Associated With Systemic

Inflammation. *Front Immunol* 11:557

Després JP. 2012. Body fat distribution and risk of cardiovascular disease: An update. *Circulation* 126: 1301–1313.

Di Angelantonio E, Bhupathiraju SN, Wormser D, Gao P, Kaptoge S, de Gonzalez AB, et al. 2016. Body-mass index and all-cause mortality: individual-participant-data meta-analysis of 239 prospective studies in four continents. *Lancet* 388:776–786

Dixon, Thomas W. 1984. Simple Proton Spectroscopic Imaging. *Radiology* 153: 189–194

Ebbert JO, Jensen MD. 2013. Fat depots, free fatty acids, and dyslipidemia. *Nutrients* 5:495–508

Eknoyan G. 2006. A History of Obesity, or How What Was Good Became Ugly and Then Bad. *Adv Chronic Kidney Dis* 13:421–427

Estrada S, Lu R, Conjeti S, Orozco-Ruiz X, Panos-Willuhn J, Breteler MMB, et al. 2020. FatSegNet: A fully automated deep learning pipeline for adipose tissue segmentation on abdominal dixon MRI. *Magn Reson Med* 83:1471–1483

Flegal KM, Graubard BI, Williamson DF, Gail MH. 2007. Cause-specific excess deaths associated with underweight, overweight, and obesity. *J Am Med Assoc* 298:2028–2037

GBD 2015 Obesity Collaborators. 2017. Health effects of overweight and obesity in 195 countries over 25 years. *N Engl J Med* 377:13–27

Ghaben AL, Scherer PE. 2019. Adipogenesis and metabolic health. *Nat Rev Mol Cell Biol* 20:242–258

Guillet C, Masgrau A, Boirie Y. 2011. Is protein metabolism changed with obesity? *Curr Opin Clin Nutr Metab Care* 14:89–92

Han Q, Phillips RS, Li J. 2019. Editorial: Aromatic amino acid metabolism. *Front Mol Biosci* 6:1–3

Herman MA, She P, Peroni OD, Lynch CJ, Kahn BB. 2010. Adipose tissue Branched Chain Amino Acid (BCAA) metabolism modulates circulating BCAA levels. *J Biol Chem* 285:11348–11356

Hersoug LG, Møller P, Loft S. 2016. Gut microbiota-derived lipopolysaccharide uptake and trafficking to adipose tissue: Implications for inflammation and obesity. *Obes Rev* 17:297–312

- Hersoug LG, Møller P, Loft S. 2018. Role of microbiota-derived lipopolysaccharide in adipose tissue inflammation, adipocyte size and pyroptosis during obesity. *Nutr Res Rev* 31:153–163
- Heymsfield SB, Wadden TA. 2017. Mechanisms, Pathophysiology, and Management of Obesity. *N Engl J Med* 376:254–266
- Hwang YC, Hayashi T, Fujimoto WY, Kahn SE, Leonetti DL, McNeely MJ, et al. 2015. Visceral abdominal fat accumulation predicts the conversion of metabolically healthy obese subjects to an unhealthy phenotype. *Int J Obes* 39:1365–1370
- Ibrahim MM. 2010. Subcutaneous and visceral adipose tissue: Structural and functional differences. *Obes Rev* 11:11–18
- Jaacks LM, Vandevijvere S, Pan A, McGowan CJ, Wallace C, Imamura F, et al. 2019. The obesity transition: stages of the global epidemic. *Lancet Diabetes Endocrinol* 7:231–240
- Janssens V, Thys P, Clarys JP, Kvis H, Chowdhury B, Zinzin E, et al. 1994. Post-mortem limitations of body composition analysis by computed tomography. *Ergonomics* 37:207–216
- Johnson CH, Ivanisevic J, Siuzdak G. 2016. Metabolomics: Beyond biomarkers and towards mechanisms. *Nat Rev Mol Cell Biol* 17:451–459
- Kidy FF, Dhalwani N, Harrington DM, Gray LJ, Bodicoat DH, Webb D, et al. 2017. Associations Between Anthropometric Measurements and Cardiometabolic Risk Factors in White European and South Asian Adults in the United Kingdom. *Mayo Clin Proc* 92:925–933
- Kranendonk MEG, van Herwaarden JA, Stupkova T, Jager W de, Vink A, Moll FL, et al. 2015. Inflammatory characteristics of distinct abdominal adipose tissue depots relate differently to metabolic risk factors for cardiovascular disease: Distinct fat depots and vascular risk factors. *Atherosclerosis* 239:419–427.
- Lackey DE, Lynch CJ, Olson KC, Mostaedi R, Ali M, Smith WH, et al. 2013. Regulation of adipose branched-chain amino acid catabolism enzyme expression and cross-adipose amino acid flux in human obesity. *Am J Physiol - Endocrinol Metab* 304:1175–1187
- Macotella Y, Emanuelli B, Mori MA, Gesta S, Schulz TJ, Tseng YH, et al. 2012. Intrinsic differences in adipocyte precursor cells from different white fat depots. *Diabetes*

61:1691–1699

- Martin AD, Janssens V, Caboor D, Clarys JP, Marfell-Jones MJ. 2003. Relationships between visceral, trunk and whole-body adipose tissue weights by cadaver dissection. *Ann Hum Biol* 30:668–677
- Mensink GBM, Schienkiewitz A, Haftenberger M, Lampert T, Ziese T, Scheidt-Nave C. 2013. Overweight and obesity in Germany Results of the German Health Interview and Examination Survey for Adults (DEGS1). *Bundesgesundheitsblatt - Gesundheitsforsch - Gesundheitsschutz* 56:786–794
- Nauli AM, Matin S. 2019. Why Do Men Accumulate Abdominal Visceral Fat? *Front Physiol* 10:1–10
- Neeland IJ, Ross R, Després JP, Matsuzawa Y, Yamashita S, Shai I, et al. 2019. Visceral and ectopic fat, atherosclerosis, and cardiometabolic disease: a position statement. *Lancet Diabetes Endocrinol* 7: 715–725
- Neinast M, Murashige D, Arany Z. 2019. Branched Chain Amino Acids. *Annu Rev Physiol* 81:139–164
- Pischon T, Boeing H, Hoffmann K, Bergmann M, Schulze MB, Overvad K, et al. 2008. General and Abdominal Adiposity and Risk of Death in Europe. *N Engl J Med* 359:2105–2120
- Roberts LD, Souza AL, Gerszten RE, Clish CB. 2012. Targeted metabolomics. *Curr Protoc Mol Biol* 1
- Rosen ED, Spiegelman BM. 2014. What we talk about when we talk about fat. *Cell* 156:20–44
- Rössner S. 2007. Adolphe Quetelet (1796 – 1874). *Obes Rev* 7881
- Rytka JM, Wueest S, Schoenle EJ, Konrad D. 2011. The portal theory supported by venous drainage-selective fat transplantation. *Diabetes* 60:56–63
- Schienkiewitz A, Mensink GBM, Kuhnert R, Journal CL. 2017. Overweight and obesity among adults in Germany. *J Heal Monit* 2:20–27
- Shen W, Wang ZM, Punyanita M, Lei J, Sinav A, Kral JG, et al. 2003. Adipose tissue quantification by imaging methods: A proposed classification. *Obes Res* 11: 5–16
- Shuster A, Patlas M, Pinthus JH, Mourtzakis M. 2012. The clinical importance of visceral adiposity: A critical review of methods for visceral adipose tissue analysis. *Br J Radiol* 85:1–10

- Smith U, Kahn BB. 2016. Adipose tissue regulates insulin sensitivity: role of adipogenesis, de novo lipogenesis and novel lipids. *J Intern Med* 280:465–475
- Sommer I, Teufer B, Szelag M, Nussbaumer-Streit B, Titscher V, Klerings I, et al. 2020. The performance of anthropometric tools to determine obesity: a systematic review and meta-analysis. *Sci Rep* 10: 1–12
- Song X, Jousilahti P, Stehouwer CDA, Söderberg S, Onat A, Laatikainen T, et al. 2015. Cardiovascular and all-cause mortality in relation to various anthropometric measures of obesity in Europeans. *Nutr Metab Cardiovasc Dis* 25: 295–304
- Stefan N, Häring HU, Hu FB, Schulze MB. 2013. Metabolically healthy obesity: Epidemiology, mechanisms, and clinical implications. *Lancet Diabetes Endocrinol* 1:152–162
- Suárez-Cuenca JA, De La Peña-Sosa G, De La Vega-Moreno K, Banderas-Lares DZ, Salamanca-García M, Martínez-Hernández JE, et al. 2021. Enlarged adipocytes from subcutaneous vs. visceral adipose tissue differentially contribute to metabolic dysfunction and atherogenic risk of patients with obesity. *Sci Rep* 11:1–11
- Tandon P, Wafer R, Minchin JEN. 2018. Adipose morphology and metabolic disease. *J Exp Biol* 121
- Ulijaszek SJ, Kerr DA. 1999. Anthropometric measurement error and the assessment of nutritional status. *Br J Nutr* 82:165–177
- Vague J. 1956. The degree of masculine differentiation of obesities: a factor determining predisposition to diabetes, atherosclerosis, gout, and uric calculous disease. *Am J Clin Nutr* 4: 20–34.
- Wang TJ, Larson MG, Vasan RS, Cheng S, Rhee EP, McCabe E, et al. 2011. Metabolite profiles and the risk of developing diabetes. *Nat Med* 17:448–453
- West J, Leinhard OD, Romu T, Collins R, Garratt S, Bell JD, et al. 2016. Feasibility of MR-based body composition analysis In large scale population studies. *PLoS One* 11:1–14
- WHO Consultation. 2000. Obesity: preventing and managing the global epidemic. Report of a World Health Organization Consultation. *World Health Organ Tech Rep Ser* 894: 1–253
- Wiklund P, Zhang X, Pekkala S, Autio R, Kong L, Yang Y, et al. 2016. Insulin resistance is associated with altered amino acid metabolism and adipose tissue dysfunction in

normoglycemic women. *Sci Rep* 6:1–11

- Wild CP. 2005. Complementing the genome with an “exposome”: The outstanding challenge of environmental exposure measurement in molecular epidemiology. *Cancer Epidemiol Biomarkers Prev* 14:1847–1850
- Wildman RP, Muntner P, Reynolds K, McGinn AP, Rajpathak S, Wylie-Rosett J, et al. 2008. The obese without cardiometabolic risk factor clustering and the normal weight with cardiometabolic risk factor clustering prevalence and correlates of 2 phenotypes among the US population (NHANES 1999-2004). *Arch Intern Med* 168:1617–1624
- Wolowczuk I, Hennart B, Leloire A, Bessede A, Soichot M, Taront S, et al. 2012. Tryptophan metabolism activation by indoleamine 2,3-dioxygenase in adipose tissue of obese women: An attempt to maintain immune homeostasis and vascular tone. *Am J Physiol Regul Integr Comp Physiol* 303:135–143
- World Health Organization. 2021. Obesity and Overweight.; doi:<https://www.who.int/news-room/fact-sheets/detail/obesity-and-overweight>. Available: <https://www.who.int/news-room/fact-sheets/detail/obesity-and-overweight>
- Yamakado M, Nagao K, Imaizumi A, Tani M, Toda A, Tanaka T, et al. 2015. Plasma Free Amino Acid Profiles Predict Four-Year Risk of Developing Diabetes, Metabolic Syndrome, Dyslipidemia, and Hypertension in Japanese Population. *Sci Rep* 5:1–12
- Ye RZ, Richard G, Gévry N, Tchernof A, Carpentier AC. 2022. Fat Cell Size: Measurement Methods, Pathophysiological Origins, and Relationships With Metabolic Dysregulations. *Endocr Rev* 43:35–60

3. Publications

3.1 FatSegNet: A fully automated deep learning pipeline for adipose tissue segmentation on abdominal dixon MRI.

Received: 27 March 2019 | Revised: 17 August 2019 | Accepted: 6 September 2019
DOI: 10.1002/mrm.28022

FULL PAPER

Magnetic Resonance in Medicine

FatSegNet: A fully automated deep learning pipeline for adipose tissue segmentation on abdominal dixon MRI

Santiago Estrada^{1,2}  | Ran Lu² | Sailesh Conjeti¹ | Ximena Orozco-Ruiz² |
Joana Panos-Willuhn² | Monique M. B. Breteler^{2,3}  | Martin Reuter^{1,4,5} 

¹Image Analysis, German Center for Neurodegenerative Diseases (DZNE), Bonn, Germany

²Population Health Sciences, German Center for Neurodegenerative Diseases (DZNE), Bonn, Germany

³Faculty of Medicine, Institute for Medical Biometry, Informatics and Epidemiology (IMBIE), University of Bonn, Bonn, Germany

⁴A.A. Martinos Center for Biomedical Imaging, Massachusetts General Hospital, Boston, Massachusetts

⁵Department of Radiology, Harvard Medical School, Boston, Massachusetts, USA

Correspondence

Santiago Estrada, DZNE, Venusberg-Campus 1 BLDG 99, 53127 Bonn, Germany.
Email: santiago.estrada@dzne.de

Funding information

Diet-BB Competence Cluster in Nutrition Research, Federal Ministry of Education and Research (BMBF), Grant/Award Number: 01EA1410C and FKZ: 01EA1809C; JPI HDHL on Biomarkers for Nutrition and Health, BMBF, Grant/Award Number: 01EA1705B; National Institutes of Health (NIH), Grant/Award Number: R01NS083534 and R01LM012719

Purpose: Introduce and validate a novel, fast, and fully automated deep learning pipeline (FatSegNet) to accurately identify, segment, and quantify visceral and subcutaneous adipose tissue (VAT and SAT) within a consistent, anatomically defined abdominal region on Dixon MRI scans.

Methods: FatSegNet is composed of three stages: (a) Consistent localization of the abdominal region using two 2D-Competitive Dense Fully Convolutional Networks (CDFNet), (b) Segmentation of adipose tissue on three views by independent CDFNets, and (c) View aggregation. FatSegNet is validated by: (1) comparison of segmentation accuracy (sixfold cross-validation), (2) test–retest reliability, (3) generalizability to randomly selected manually re-edited cases, and (4) replication of age and sex effects in the Rhineland Study—a large prospective population cohort.

Results: The CDFNet demonstrates increased accuracy and robustness compared to traditional deep learning networks. FatSegNet Dice score outperforms manual raters on VAT (0.850 vs. 0.788) and produces comparable results on SAT (0.975 vs. 0.982). The pipeline has excellent agreement for both test–retest (ICC VAT 0.998 and SAT 0.996) and manual re-editing (ICC VAT 0.999 and SAT 0.999).

Conclusions: FatSegNet generalizes well to different body shapes, sensitively replicates known VAT and SAT volume effects in a large cohort study and permits localized analysis of fat compartments. Furthermore, it can reliably analyze a 3D Dixon MRI in ~1 minute, providing an efficient and validated pipeline for abdominal adipose tissue analysis in the Rhineland Study.

KEYWORDS

deep learning, dixon MRI, neural networks, semantic segmentation, subcutaneous adipose tissue, visceral adipose tissue

This is an open access article under the terms of the Creative Commons Attribution License, which permits use, distribution and reproduction in any medium, provided the original work is properly cited.

© 2019 The Authors *Magnetic Resonance in Medicine* published by Wiley Periodicals, Inc. on behalf of International Society for Magnetic Resonance in Medicine

1 | INTRODUCTION

The excess of body fat depots is an increasing major public health issue worldwide and an important risk factor for the development of metabolic disorders and reduced quality of life.^{1,2} While the body mass index (BMI) is a widely used indicator of adipose tissue accumulation in the body, it does not provide information on fat distribution³ neither with respect to different fat tissue types nor with respect to deposit location. Different compartments of adipose tissue are associated with different physiopathological effects.^{4,5} Abdominal adipose tissue (AAT), composed of subcutaneous and visceral adipose tissue (SAT and VAT), has long been associated with an increased risk of chronic cardiovascular diseases, glucose impairment, and dyslipidemia.^{6,7} Recently, several studies have indicated a stronger relation between the accumulation of VAT with an adverse metabolic and inflammatory profile compared to SAT.^{8,9} Therefore, an accurate and independent measurement of VAT and SAT volumes (VAT-V and SAT-V) is of significant clinical and research interest.

Currently, the gold standard for measuring VAT-V and SAT-V is the manual segmentation of abdominal fat images from Dixon magnetic resonance (MR) scans—a very expensive and time-consuming process. Thus, especially for large studies, automatic segmentation methods are required. However, achieving good accuracy is challenging due to complex AAT structures, a wide variety of VAT shapes, large anatomical differences across subjects, and the inherent properties of the Dixon images: low intensity contrast between adipose tissue classes, inhomogeneous signals, and potential organ motion. So far, those limitations impeded the widespread implementation of automatic and semi-automatic techniques based on intensity and shape features, such as fuzzy-clustering,¹⁰ k -means clustering,¹¹ graph cut^{12,13} active contour methods,¹⁴ and statistical shape models.¹⁵

Recently, fully convolutional neural networks (F-CNNs)^{16,17} have been widely adopted in the computer vision community for pixel/voxel-wise image segmentation in an end-to-end fashion to overcome above-mentioned challenges. With these methods there is no need to extract manual features, divide images into patches, or implement sliding window techniques. F-CNNs can automatically extract intrinsic features and integrate global context to resolve local ambiguities thereby improving the results of the predicted models.¹⁷ Langer et al¹⁸ proposed a three-channel UNet for AAT segmentation, which is a conventional architecture for 2D medical image segmentation.¹⁹ While this method showed promising results, we demonstrate that our network architecture outperforms the traditional UNet for segmenting AAT on our images with a wide range of anatomical variation. More recent architectures such as the SD-Net²⁰ and Dense-UNet, a densely connected network,²¹ have the potential to improve generalizability and robustness by encouraging feature

re-usability and strengthening information propagation across the network.²¹ In prior work, we introduced a competitive dense fully convolutional network (CDFNet)²² as a new 2D F-CNN architecture that promotes feature selectivity within a network by introducing maximum attention through a maxout activation unit.²³ The maxout boosts performance by allowing the creation of specialized sub-networks that target a specific structure during training.²⁴ Therefore, this approach facilitates the learning of more complex structures^{22,24} with the added benefit of reducing the number of training parameters relative to the aforementioned networks.

In this paper, we propose FatSegNet, a novel fully automated deep learning pipeline based on our CDFNet architecture to localize and segment VAT and SAT on abdominal Dixon MR images from the Rhineland Study, an ongoing large population-based cohort study.^{25,26} To constrain AAT segmentations to a consistent anatomically defined region, the proposed pipeline consists of three stages:

1. **Localization** of the abdominal region using a semantic segmentation approach by implementing CDFNet models on sagittal and coronal planes; we use the lumbar vertebrae positions as reference points for selecting the region of interest.
2. **Segmentation** of VAT and SAT within the abdominal region through 2D CDFNet models on three different planes (axial, sagittal, and coronal).
3. **A view aggregation** stage where the previous generated label maps are combined to generate a final 3D segmentation.

We initially evaluate and compare the individual stages of the pipeline with other deep learning approaches in a sixfold cross-validation. We show that the proposed network architecture (CDFNet) improves segmentation performance and simultaneously reduces the number of required training parameters in step 1 and 2. After asserting segmentation accuracy, we evaluate the whole pipeline (FatSegNet) with respect to robustness and reliability against two independent test sets: a manually edited and a test–retest set. Finally, we present a case study on unseen data comparing the VAT-V and SAT-V calculated from the FatSegNet segmentations against BMI to replicate age and sex effects on these volumes in a large cohort.

2 | METHODS

2.1 | Data

2.1.1 | MR imaging acquisition

MR image acquisition was performed at two different sites both with identical 3T Siemens MAGNETOM Prisma MR scanners (Siemens Healthcare, Erlangen, Germany).

The body coil was used for signal reception of a three-dimensional two-point Dixon sequence (acquisition time = 12 s, echo time TE1 = 1.23 ms, TE2 = 2.46 ms, repetition time TR = 4.12 ms, axial field of view = 500 mm × 437 mm, flip angle = 6°, left-right readout bandwidth = 750 Hz/pixel, partial Fourier factor 6/8 × 5/8). Based on a preceding moving-table abdominal localizer, the field-of-view was centered on the middle of the third lumbar vertebra (L, L3). Data were acquired during a single breath-hold in supine position with arms placed at the sides. The image resolution was finally interpolated from 2.0 mm × 2.7 mm × 10.0 mm to 2.0 mm × 2.0 mm × 5.0 mm (matrix size = 256 × 224 × 72).

2.1.2 | Datasets

The Rhineland Study is an ongoing population-based prospective cohort (<https://www.rheinland-studie.de/>) which enrolls participants aged 30 years and above at baseline from Bonn, Germany. The study is carried out in accordance with the recommendations of the International Council for Harmonisation (ICH) Good Clinical Practice (GCP) standards (ICH-GCP). Written informed consent was obtained from all participants in accordance with the Declaration of Helsinki.

The first 641 subjects from the Rhineland Study with BMI and abdominal MR Dixon scans are included. The sample presents a mean age of 54.2 years (range 30 to 95) and 55.2% of the subjects are women. The BMI of the participants ranges from 17.2 to 47.7 kg/m² with a mean of 25.2 kg/m². Subjects were stratified into two subsets: 38 scans were manually annotated for training and testing; the remaining 603 subjects were segmented using the proposed pipeline. After visual inspection, 16 subjects were excluded due to poor image quality or extreme motion artifacts (e.g. potentially caused by breathing). Thus, 587 participants were used for the case study analysis and a subset of 50 subjects were randomly

selected for manual corrections of the predicted label maps. This manually edited set and an independent test–retest set of 17 healthy young volunteers were used to assess reliability of the automated segmentation and volume estimates.

Ground truth data

38 subjects were randomly selected from sex and BMI strata to ensure a balanced population distribution. These scans were manually annotated by two trained raters without any semi-automated support such as thresholding, which can reduce accuracy in the ground truth and lead to overestimation of the performance of the proposed automated method.

Specific label schemes were created for each individual task of the pipeline. For localizing the abdominal region, raters divided the scans into three different blocks defined by the location of the vertebrae as follows: the abdominal region (from lower bound of twelfth thoracic vertebra (Th12) to the lower bound of L5), the thoracic region (all above the lower bound of Th12), and the pelvic region (everything below the lower bound of L5), as illustrated in Figure 1E). For AAT segmentation, 60 slices per subject were manually labeled into three classes: SAT, VAT, and bone with neighbouring tissues. The bone was labeled to prevent bone marrow from being misclassified as adipose tissue. In order to improve spatial context and prevent misclassification of the arms, the dataset was complemented by a synthetic class defined as “other tissue” that was composed of any soft tissue inside the abdomen cavity that is not VAT or SAT. The manual annotations are illustrated in Figure 1B,C. Furthermore, four subjects were labeled by both raters to evaluate the inter-rater variability.

Test–retest data

17 additional subjects were recruited with the exclusive purpose of measuring the acquisition protocol reliability.

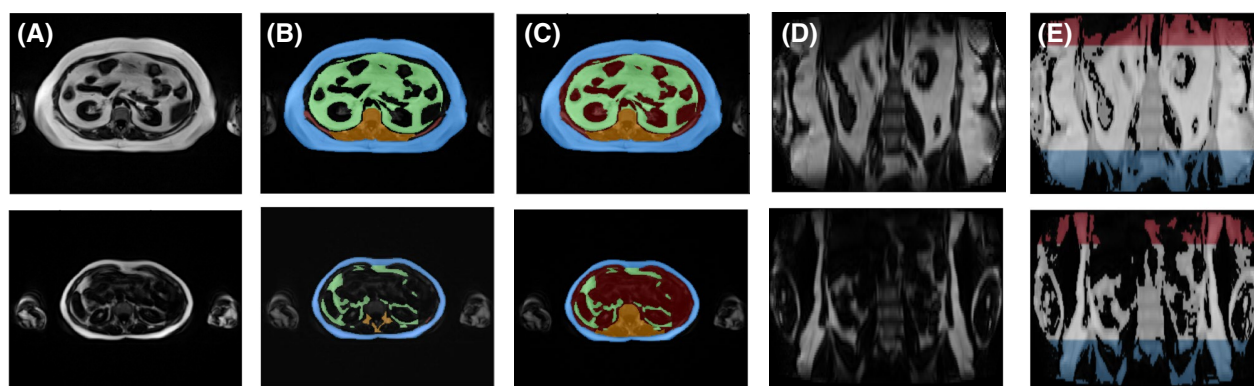


FIGURE 1 MR Dixon images and ground truth from two subjects with different BMI (obese (upper), normal (lower)). A, Fat images: axial plane. B, Initial manual segmentation (blue: SAT, green: VAT, orange: bone and surrounding structures). C, Ground truth with additional synthetic class (red: other-tissue) and filled-in bone structures (orange). D, Fat images: coronal plane. E, Ground truth for localization of region of interest (red: thoracic region, white: abdominal region (region of interest), blue: pelvic region)

The group presents a mean age of 25.5 years (range: 20 to 31) and 65.0% of the participants are women; all of them have a normal BMI (BMI <25 kg/m²). Subjects were scanned in two consecutive sessions. Before starting the second session, subjects were removed from the scanner and re-positioned.

2.2 | FatSegNet pipeline

The FatSegNet is to be deployed as a post-processing adipose analysis pipeline for the abdominal Dixon MR images acquired in the Rhineland Study. Therefore, it should meet the following requirements: (1) be fully automated, (2) segment the different adipose tissue types within the anatomically defined abdominal region, and (3) be robust to body type variations and generalizable in presence of high population heterogeneity. Following the prior conditions, we designed FatSegNet as a fully automated deep learning pipeline for adipose segmentation (Figure 2).

The proposed pipeline consists of three stages: (1) the abdominal region is localized by averaging bounding boxes from two abdominal segmentation maps generated by CDFNets on the sagittal and coronal view. For each view a bounding box is set to the full image width. The height is extracted by localizing the highest and lowest slice with at least 85% of none background voxels classified as abdominal region. Highest and lowest slice position are averaged across the views. (2) Afterward, adipose tissue is segmented within the abdominal region by three CDFNets on different views (axial, coronal, and sagittal) with standardized input sizes (zero padding). (3) Finally, a view aggregation network merges the predicted label maps from the previous stage into a final segmentation; the implemented multi-view scheme is designed to improve segmentation of structures that are not clearly visible due to

poor lateral resolution. This 2.5D strategy produces a fully automated pipeline to accurately segment adipose tissue inside a consistent anatomically defined abdominal region.

2.2.1 | Pipeline components

Competitive dense fully convolutional network (CDFNet)

For the segmentation task, we introduce the CDFNet architecture due to its robustness and generalizability properties. The proposed network improves feature selectivity and, thus, boosts the learning of fine-grained anatomies without increasing the number of learned parameters.²² We implemented the CDFNet by suitably adopting the Dense-UNet architecture proposed by Roy et al²⁷ and extending it toward competitive learning via maxout activations.²⁴

The Dense-UNet proposed in²⁷ follows the usual dumbbell like architecture with four dense-block encoders, four dense-block decoders and one bottleneck layer. Each dense-block is based on short-range skip connections between convolutional layers as introduced for densely connected neural networks²⁸; the dense connection approach stacks multiple convolutional layers in sequence and the input of a layer is iteratively concatenated with the outputs of the previous layers. This type of connectivity improves feature reusability, increases information propagation, and alleviates vanishing gradients.²⁸ The architecture additionally incorporates the traditional long-range skip connections between all encoder and decoder blocks of the same spatial resolution as introduced by Ronnenberger et al¹⁹ which improves gradient flow and spatial information recovery.

Within the Dense-UNet, the information aggregation through these connections is performed by concatenation layers. Such a design increases the size of the output feature map along the feature channels, which in turn results in the need to

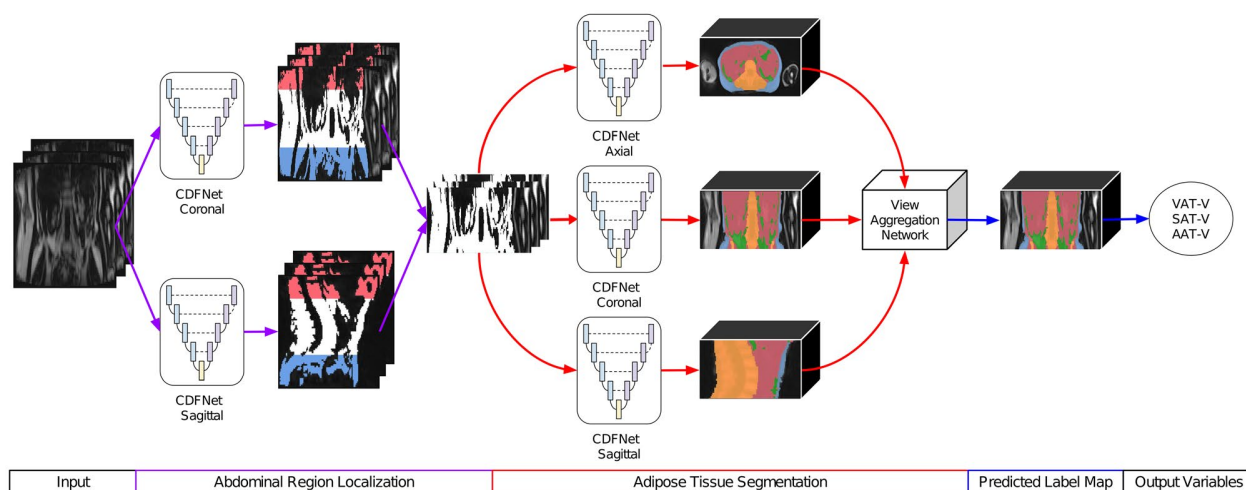


FIGURE 2 Proposed FatSegNet Pipeline for segmenting AAT. The pipeline is divided into three stages: First, localization of abdominal region. Then, tissue segmentation on the abdominal region and finally, view aggregation. Both local and global volume estimates of individual structures are calculated on the final prediction

learn filters with a higher number of parameters. Goodfellow et al introduced the idea of competitive learning through max-out activations,²³ which was adapted by Liao and Carneiro²⁴ for competitive pooling of multi-scale filter outputs. Both²³ and²⁴ proved that the use of maxout competitive units boosts performance by creating a large number of dedicated sub-networks within a network that learns to target specific sub-tasks and reduces the number of required parameters significantly, which in turn can prevent over-fitting.

The maxout is a simple feed-forward activation function that chooses the maximum value from its inputs.²³ Within a CNN, a maxout feature map is constructed by taking the maximum across multiple input feature maps for a particular spatial location. The proposed CDFNet uses competitive layers (maxout activation) instead of concatenation layers. Our preliminary results²² demonstrate that these competitive units promote the formation of dedicated local sub-networks in each of the densely connected blocks within the encoder and the decoder paths. This encourages sub-modularity through a network-in-network design that can learn more efficiently. Toward this, we propose two novel architectural elements targeted at introducing competition within the short- and long-range connections, as follows:

1. Local Competition—Competitive Dense Block (CDB):

By introducing maxout activations within the short-range skip connections of each of the densely connected convolutional layers (at the same resolution), we encourage local competition during learning of filters. The multiple convolution layers in each block prevent filter co-adaptation.

2. Global Competition—Competitive Un-pooling Block (CUB):

We introduce a maxout activation between a long-range skip connection from the encoder and the features up-sampled from the prior lower resolution decoder block. This promotes competition between finer feature maps with smaller receptive fields (skip connections) and coarser feature maps from the decoder path that spans much wider receptive fields encompassing higher contextual information.

In brief, the proposed CDFNet comprises a sequence of four CDBs, constituting the encoder path (down-sampling block), and four CDBs constituting the decoder path (up-sampling block), which is joined via a bottleneck layer. The bottleneck consists of a 2D convolutional layer followed by a Batch Normalization. The skip-connections from each of the encoder blocks feed into the CUB that subsequently forward features into the corresponding decoder block of the same resolution as illustrated in Figure 3.

View aggregation network

The proposed view aggregation network is designed to regularize the prediction for a given voxel by considering spatial information from the coronal, axial, and sagittal view. The network, therefore, merges the probability maps of the three different CDFNets from the previous stage by applying a $(3 \times 3 \times 3)$ 3D-convolution (30 filters) followed by a Batch Normalization. Then a $(1 \times 1 \times 1)$ 3D-convolution is employed to reduce the feature maps to the desired number of classes ($n = 5$). The final prediction probabilities are obtained via a concluding softmax layer (as illustrated in Supporting Information Figure S1). Our approach learns to weigh each view differently on a voxel

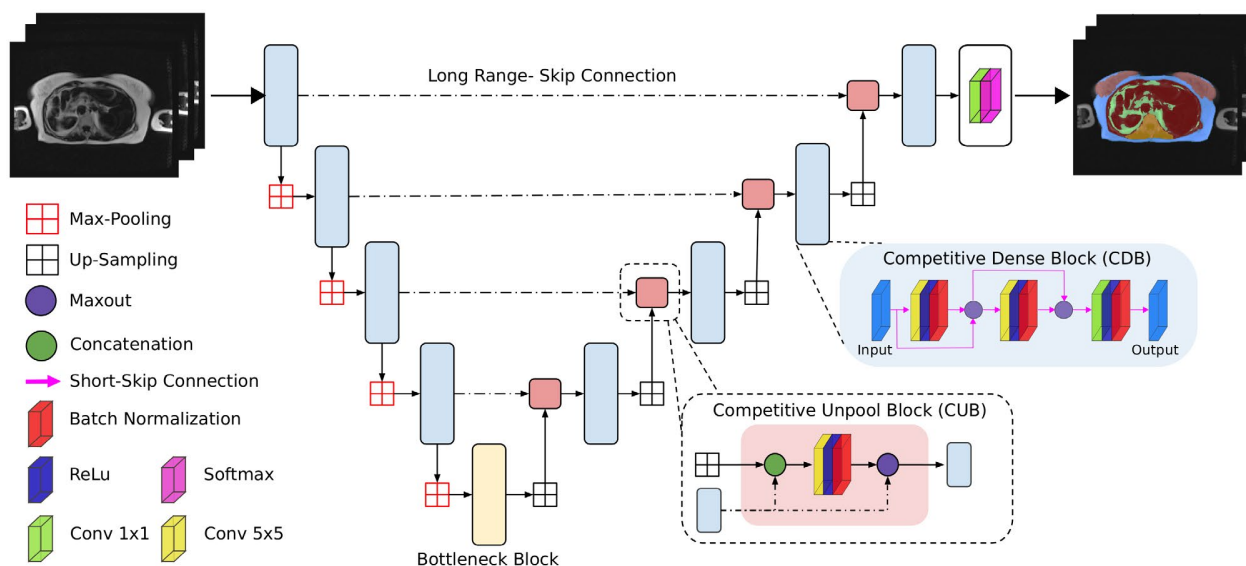


FIGURE 3 Proposed network architecture: Competitive Dense Fully Convolutional Network (CDFNet), with 4 competitive dense blocks (CDB) on each encoder and decoder path and 4 competitive unpool blocks (CUB) between them. CDB and CUB induce local and global competition within the network. Note—the output filters for all convolutional layers in CUB, CDB, and Bottleneck were standardized to 64 channels

level, compared to standard hard-coded global view aggregation schemes. Such hard-coded weighting schemes can be suboptimal when working with anisotropic voxels sizes (e.g., here $2\text{ mm} \times 2\text{ mm} \times 5\text{ mm}$) as resolution differences impose a challenge when combining the spatial information from the finer (within-plane) and coarser (across slice) resolutions. Additionally, in the presence of high variance, abdominal body shapes across subjects segmentation benefit from data-driven approaches that can flexibly adopt weights to individual situations and even spatial locations, which are not possible if hard-coded global weights are being used.

2.3 | Experimental setup

For training and testing the pipeline, we perform a sixfold cross-validation subject-space split on the ground truth dataset. For each fold, 32 subjects are used for training and 6 held out for testing; the test sets splits are approximately balanced based on their BMI classification (underweight [BMI $< 18.5\text{ kg/m}^2$], normal [$18.5 \leq \text{BMI} < 25\text{ kg/m}^2$], overweight [$25 \leq \text{BMI} < 30\text{ kg/m}^2$], and obese [BMI $\geq 30\text{ kg/m}^2$]). This selection process ensures that all BMI categories are used for bench-marking the cross-validation models. Additionally, a final model is implemented using 33 subjects for training holding out 5 subjects spanning different BMI levels for a final performance sanity check (visual quality check and stability of Dice score). Given the limited ground truth data, for all models a validation set to assess convergence during training was created by randomly separating 15% of the slices from the corresponding training set. This allows evaluating performance and generalizability on a completely separate test set.

2.3.1 | Baselines and comparative methods

We validate the FatSegNet by comparing the performance of each stage of the pipeline against the cross-validation test sets using Dice score index (DSC) to measure similarity between the prediction and the ground truth. Let M (ground truth) and P (prediction) denote the labels binary segmentation, the Dice score index is defined as

$$DSC = \frac{2 \cdot |M \cap P|}{|M| + |P|} \quad (1)$$

where $|M|$ and $|P|$ represents the number of elements in each segmentation and $|M \cap P|$ the number of common elements. Therefore, the DSC ranges from 0 to 1 and a higher DSC represents a better agreement between segmentations.

Additionally, we benchmark the proposed CDFNet models for abdominal region localization and AAT delineation with state-of-the-art segmentation F-CNNs such as UNet,¹⁹ SD-Net,²⁰ and Dense-UNet.²⁷ We use the probability maps generated from the aforementioned networks to train the view aggregation model and measure performance with and without

view aggregation. The proposed view aggregation performance for each FCNNs is compared against two non-data-driven (hard-coded) methods: equally balanced weights for all views and axial focus weights (accounting for higher in-plane resolution, axial = 0.5, coronal = 0.25, sagittal = 0.25). Finally, to permit a fair comparison, all benchmark networks follow the same architecture of four encoder blocks, four decoders blocks, and one bottleneck layer as illustrated in Figure 3 with an input image size of 224×256 . Note, significant differences between our proposed methods and comparative baselines are evaluated by a Wilcoxon signed-rank test²⁹ after multiple comparisons correction using a one-sided adaptive FDR.³⁰

The aforementioned models are implemented in Keras³¹ with a TensorFlow back-end using an NVIDIA Titan Xp GPU with 12 GB RAM and the following parameters: batch size of 8, momentum set to 0.9, constant weight decay of 10^{-06} , and an initial learning rate of 0.01 decreased by a order of 10 every 20 epochs. The models are trained for 60 epochs with an early-stopping criterion (no relevant changes on the validation loss after the last 8 epochs—convergence was observed around 50 epochs). A composite loss function of median frequency balanced logistic loss and Dice loss²⁰ is used. This loss function emphasizes the boundaries between classes and supports learning of unbalanced classes such as VAT. Finally, online data augmentation (translation, rotation and global scaling) is performed to increase training set size and improve the networks generalizability. Note, the FatSegNet implementation is available at <https://github.com/reuter-lab/FatSegNet>.

2.3.2 | Pipeline reliability

We assess the FatSegNet reliability by comparing the difference of VAT-V and SAT-V across sessions for each subject of the test–retest and manually edited set. Given a predicted label map and $N_i(l)$ the number of voxels classified as l (VAT or SAT) in session i (test–retest, or manual–automated), the absolute percent difference (APD(l)) of a label volume measures variability across sessions. It is defined as

$$APD(l) = \frac{2 \cdot |N_1(l) - N_2(l)|}{N_1(l) + N_2(l)} \cdot 100 \quad (2)$$

Additionally, we calculate the agreement of total VAT-V and SAT-V between sessions by an intra-class correlation (ICC) using a two-way fixed, absolute agreement and single measures ICC(A,1).³²

2.3.3 | Case study analysis on the Rhineland study

We compare the volumes of abdominal adipose tissue (AAT-V, SAT-V, and VAT-V) generated from FatSegNet with BMI on the unseen dataset. A fast quality control is

TABLE 1 Mean (and standard deviation) Dice scores (cross-validation) of the FCNN models for abdominal adipose tissue segmentation

Models (PRM) ^a	Subcutaneous (SAT)				Visceral (VAT)			
	Axial	Coronal	Sagittal	V. Aggregation	Axial	Coronal	Sagittal	V. Aggregation
UNet (~20 M)	0.965 (0.029) ^b	0.960 (0.034) ^b	0.960 (0.035) ^b	0.972 (0.019) ^b	0.810 (0.111) ^b	0.804 (0.113) ^b	0.820 (0.101)	0.837 (0.095) ^b
SD-Net (~1.5M)	0.969 (0.027) ^b	0.954 (0.040) ^b	0.956 (0.034) ^b	0.972 (0.020) ^b	0.820 (0.097) ^b	0.812 (0.099) ^b	0.822 (0.091) ^b	0.843 (0.081) ^b
Dense-UNet (~3.3M)	0.972 (0.025) ^b	0.959 (0.037) ^b	0.963 (0.029) ^b	0.975 (0.019) ^b	0.824 (0.091) ^b	0.814 (0.097) ^b	0.827 (0.090) ^b	0.847 (0.080) ^b
Proposed (~2.5M)	0.970 (0.025)	0.966 (0.029)	0.966 (0.027)	0.975 (0.018)	0.826 (0.095)	0.826 (0.085)	0.824 (0.092)	0.850 (0.076)
Inter-rater variability	0.982 (0.018)				0.788 (0.060)			

Note: We show FDR corrected significance indicators of Wilcoxon signed-rank test²⁹ comparing the proposed CDFNet vs. benchmark FCNNs.

^aThe approximately number of learn parameters reported is for the models without the View Aggregation Network.

^bStatistical difference using a one-sided adaptive FDR multiple comparison correction³⁰ at a level of 0.05.

performed to identify drastic failure cases. The differences among BMI groups are evaluated with a one-way analysis of variance (ANOVA) with subsequent Tukey’s honest significant difference (HSD) post hoc comparisons. The associations of volumes of abdominal adipose tissue and BMI are assessed using partial correlation and linear regression after accounting for age, sex, and height of the abdominal region. Separate linear regression analyses are performed to explore the effect of age on SAT-V and VAT-V in men and women. All the statistical analyses are performed in R.³³

3 | RESULTS

3.1 | Method validation

3.1.1 | Localization of abdominal region

For assessing the performance of abdominal region detection after creation of an average bounding box from the coronal and sagittal views the average Dice overlap (sixfold cross-validation) was calculated, as illustrated on the Supporting Information Figure S2. We observe that all models perform extremely well on the relatively easy task of localizing the desired abdominal region (DSC >0.96). There is no significant difference between the models; however, we use our CDFNet because it requires substantially less parameters (see Table 1) compared to the UNet and Dense-UNet.

3.1.2 | Segmentation of AAT

In Table 1, we present the average Dice score (sixfold cross-validation) for VAT and SAT for each individual view as well as for the view aggregation model. Here, we observe that all methods work extremely well for SAT segmentation. Nevertheless, our proposed CDFNet outperforms the UNet and SD-Net on all single-view models and, when compared with the Dense-UNet, there is significant improvement in the sagittal and coronal views. For the more challenging task of VAT recognition, which is a more fine-grained compartment with large shape variation, the proposed CDFNet outperforms the SD-Net on all single planes; when compared with Dense-UNet and U-Net, there is only significant improvement in the axial and coronal plane. Nonetheless, CDFNet achieves this performance with ~30% (Dense-UNet) and ~80% (UNet) less parameters, demonstrating that the proposed architecture improves feature selectivity and simplifies network learning. Furthermore, fewer parameters can help decrease overfitting error, especially when training with limited annotated data, and thus improve generalizability.

Note, that Dice scores increase and difference of pairwise comparisons is slightly reduced after the view aggregation (Table 1), showing that this steps helps all individual networks to reach a better performance by introducing spatial

TABLE 2 Mean (and standard deviation) Dice scores (cross-validation) of hard-coded balanced weights, hard-coded axial focus weights, and the proposed view aggregation for abdominal adipose tissue segmentation

Single-view model	Subcutaneous (SAT)			Visceral (VAT)		
	Balanced	Axial focus	Proposed	Balanced	Axial focus	Proposed
UNet	0.970 (0.026)	0.970 (0.026)	0.972 (0.019)	0.830 (0.098) ^a	0.829 (0.099) ^a	0.837 (0.095)
SD-Net	0.970 (0.026) ^a	0.972 (0.025) ^a	0.972 (0.020)	0.839 (0.084) ^a	0.838 (0.085) ^a	0.843 (0.082)
Dense-UNet	0.973 (0.025)	0.974 (0.024) ^a	0.975 (0.019)	0.841 (0.081) ^a	0.840 (0.082) ^a	0.847 (0.080)
CDFNet	0.972 (0.025) ^a	0.973 (0.024)	0.975 (0.018)	0.844 (0.077) ^a	0.841 (0.080) ^a	0.850 (0.076)

Note: We show FDR corrected significance indicators of Wilcoxon signed-rank test²⁹ comparing the proposed data-driven aggregation scheme vs. each hard-coded method.

^aStatistical difference using a one-sided adaptive FDR multiple comparison correction³⁰ at a level of 0.05.

TABLE 3 Mean absolute percent difference (APD) and interclass correlation agreement (ICC(A,1)) for the volumes estimates of VAT and SAT across sessions of the manually edited and test–retest set

Metric	Manually edited set		Test–retest set	
	SAT-V	VAT-V	SAT-V	VAT-V
ICC [95% CI]	0.999 [0.999-1.000]	0.999 [0.994-0.999]	0.996 [0.986-0.999]	0.998 [0.995-0.999]
APD (SD)	0.149% (0.424)	1.398% (0.963)	3.254% (2.524)	2.957% (2.600)

information from multiple views and regularizing the prediction maps. The proposed data-driven aggregation scheme outperforms (DSC) the hard-coded models for SAT and with statistically significance for VAT as shown in Table 2. Furthermore, learned weights are spatially varying and can adjust to subject-specific anatomy, which in turn can improve generalizability. We empirically observe that the aggregation model smoothes the label maps slightly, resulting in visually more appealing boundaries. It also significantly reduces the arms from being misclassified as adipose tissue which can otherwise be observed in different views, especially on overweight and obese subjects, where arms are located closer to the abdominal cavity, as seen Supporting Information Figure S3.

Finally it should be highlighted, that all single-view and the view aggregation models achieve similarly excellent results on the SAT segmentation compared to inter-rater variability and outperform the manual raters for the more challenging VAT segmentation by a margin.

3.1.3 | FatSegNet reliability

Table 3 presents the reliability metrics evaluated on the test–retest and the manually edited test set. The proposed pipeline presents only a small absolute percent volume difference (APD) for VAT and SAT, and excellent agreement between the predicted and corrected segmentation maps. It must be noted, that APD is larger for both tissue types in the test–retest setting as it also includes variance from acquisition noise (e.g. motion artefacts, non-linearities based on different positioning) in addition to potential variances of the processing pipelines. Nevertheless, we observe excellent agreement

(ICC) between sessions for the test–retest dataset for both adipose tissue types.

3.2 | Case study: Analysis of Rhineland study data

3.2.1 | The characteristics of the study population

After visual quality inspection, 16 scans were flagged due to image artefacts, such as motion or low contrast (see Figure 4C,D for two examples). The characteristics of the remaining 587 participants with valid data on BMI and volumes of abdominal adipose tissue are presented in Supporting Information Table S1. The mean (SD) age of the subjects is 54.2 (13.3) years, and 54.7% are women. 311 (53.0%) subjects are normal weight, 209 (35.6%) overweight, and 67 (11.4%) obese. We observed a BMI increase with age ($\beta = 0.03$, $P = .007$) and a borderline significance of age difference among BMI groups ($P = .052$, ANOVA). Obvious differences are observed in AAT-V, VAT-V, and SAT-V across BMI groups ($P < .001$, ANOVA). VAT-V to SAT-V ratio is higher in overweight and obese participants compared to those with normal weight ($P < .001$), but there is no difference between overweight and obese ($P = .505$).

3.2.2 | The association between abdominal adipose tissue volumes and BMI

BMI shows a strong positive correlation with AAT-V and SAT-V (AAT-V: $r = .88$, $P < .001$; SAT-V: $r = .85$, $P < .001$),

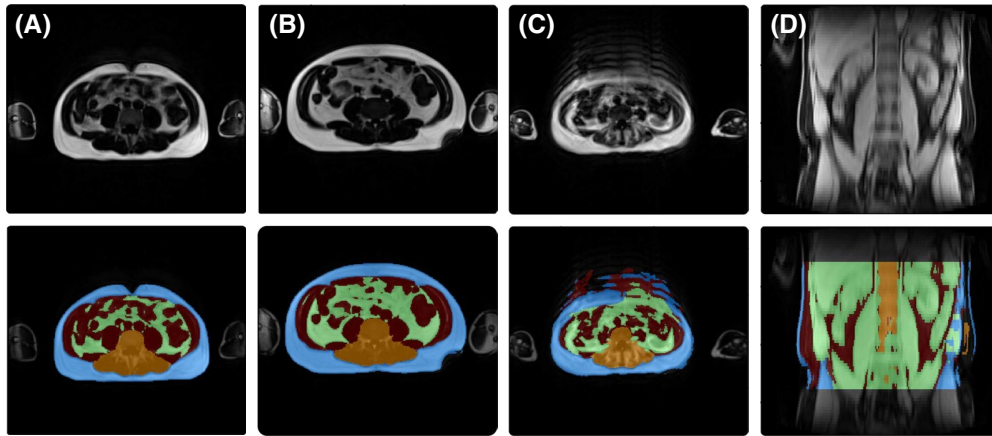


FIGURE 4 Examples of FatSegNet predictions and excluded cases on the Rhineland Study. (A, B) Subjects with different body shapes and accurate segmentations. (C, D) Excluded subjects from the case study due to extreme motion noise (C), or low image contrast quality (D).

but only a moderate correlation with VAT-V ($r = 0.65$, $P < .001$) after adjusting for age, sex, and abdominal region height. As illustrated in Figure 5, both SAT-V and VAT-V are positively associated with BMI after accounting for age, sex, and abdominal region height ($P < .001$). The accumulation of SAT-V is higher than VAT-V as BMI increases.

3.2.3 | Influence of age and sex on VAT-V and SAT-V

The influence of age and sex on VAT-V and SAT-V follows different patterns (as illustrated in Figure 6). Men tend to have lower SAT and higher VAT compared to women ($P < .001$). VAT-V significantly increase with age in both men and women. Conversely, SAT-V is weakly associated with age in women ($\beta = 0.02$, $P = .012$), but not in men ($\beta = -0.01$, $P = .337$).

4 | DISCUSSION

In our study, we established, validated, and implemented a novel deep learning pipeline to segment and quantify the components of abdominal adipose tissue, namely, VAT-V, SAT-V, and AAT-V on a fast acquisition abdominal Dixon MR protocol for subjects from the Rhineland Study, a large population-based cohort. The proposed pipeline is fully automated and requires approximately 1 minute for analyzing a subject's whole volume. Moreover, since the pipeline is based on deep learning models, it can be easily updated and retrained as the study progresses and new manual data are generated—which can further improve overall pipeline robustness and generalizability, providing a pragmatic solution for a population-based study.

The proposed pipeline, termed FatSegNet implements a three-stage design with the CDFNet architecture at the core for localizing the abdominal region and segmenting

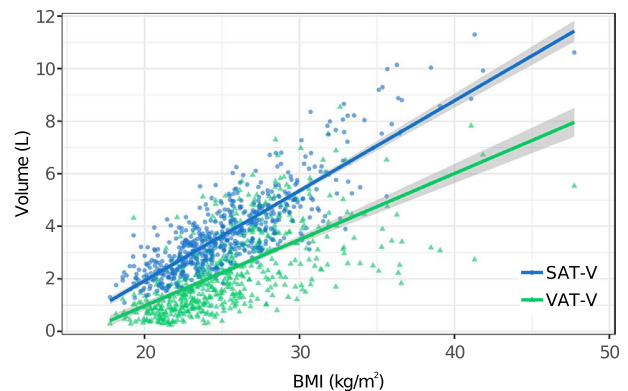


FIGURE 5 Association of BMI with SAT-Volume and VAT-Volume

the AAT. The introduction of our CDFNet inside the pipeline boosts the competition among filters to improve feature selectivity within the networks. CDFNet introduces competition at a local scale by substituting concatenation layers with maxout activations that prevent filter co-adaptation and reduce the overall network complexity. It also induces competition at a global scale through competitive unpooling. This network design, in turn, can learn more efficiently.

For the first stage of the pipeline, i.e. localization of the abdominal region, all FCNNs can successfully determine the upper and lower limit of the abdominal region from a segmentation prediction map. However, our CDFNet requires significantly fewer parameters compared to the traditional UNet and Dense-UNet. Furthermore, the localization block is able to identify the abdominal region correctly even in cases with scoliosis (curved spine) as illustrated in Figure 7F. For the more challenging task of segmenting AAT, we demonstrate that CDFNet recovers VAT significantly better than traditional deep learning variants that rely on

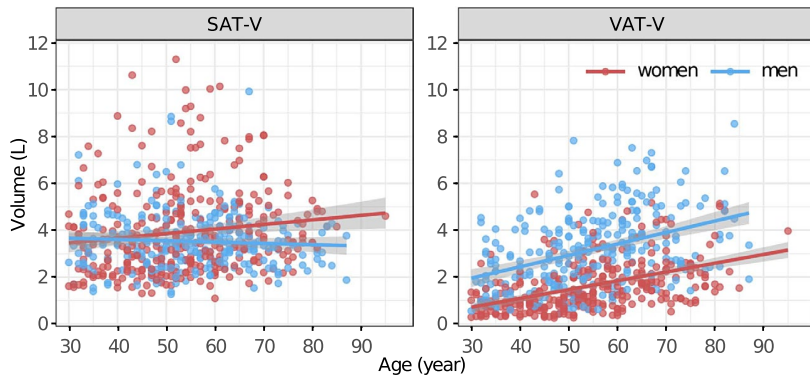


FIGURE 6 The association between age and SAT-Volume and VAT-Volume in men and women

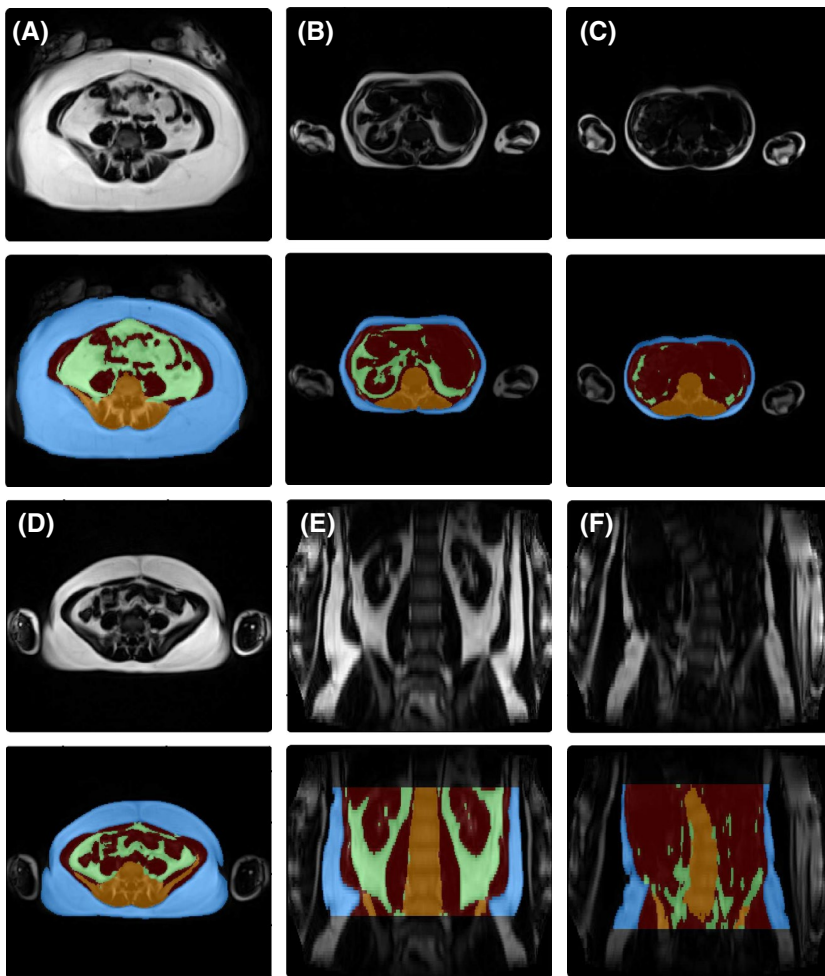


FIGURE 7 Examples of FatSegNet predictions on the Rhineland Study. (A-F) Accurate automatic segmentation of different body shapes. Extreme cases: A, arms are in front of the abdominal cavity, and F, deviated spine

concatenation layers. Additionally, each individual CDFNet view model outperforms manual raters for segmenting the complex VAT and accomplishes equivalent results on SAT. The selection of an inhomogeneous BMI testing set ensures that our method is evaluated for different body types and avoids biases, as better segmentation performance can be achieved on subjects with high content of AAT compared to lean subjects.^{34,35} Moreover, images from individuals with high AAT could be accompanied by other types of issues,

such as fat shadowing (Figure 7D), or arms located in close proximity to the abdominal cavity (Figure 7A,D,E). These issues are mitigated by our view aggregation model that regularizes the predicted segmentation by combining the spatial context from different views ultimately improving segmentation of tissue boundaries. Moreover, this approach automatically prevents misclassification of arms whereas previous deep learning AAT segmentation methods required manual removal of the upper extremities in a pre-processing step.¹⁸

Note, that we prefer the 2D over a full 3D approach in this work. A full 3D network architecture has more parameters, requiring significantly more expert annotated training data (full 3D cases) and/or artificial data augmentation, which could increase the chance of overfitting—in addition to increased GPU memory requirements.

As demonstrated on the Rhineland Study data, the proposed pipeline exhibits high robustness and generalizability across a wide range of age, BMI, and a variety of body shapes as seen in Figures 7 and 4A,B. FatSegNet successfully identifies the AAT in different abdomen morphologies, spine curvatures, adipose shadowing, arms positioning, or intensity inhomogeneities. Furthermore, the pipeline has a high test–retest reliability between the calculated volumes of VAT and SAT without the need of any image pre-processing (bias-correction, image registration, etc.) or manual selection of a slice or region. Furthermore, the manually edited test set demonstrates a high similarity of automated and manual labels and excellent agreement of volume estimates. However, as is usual with any automated method, segmentation reliability decreases when input images have low quality as illustrated in Figure 4C,D where the scans present severe motion/breathing artifacts or very low-image contrast. In order to detect these problematic images in large studies, an automated or manual quality control protocol should be implemented before passing images to automated pipelines.

In accordance with previous studies on smaller data sets,^{13,36} our data showed a lower correlation of BMI with VAT-V than with AAT-V and SAT-V. We also observed a sex difference of the SAT-V and VAT-V accumulation as previously reported^{37,38}: men were more likely to have higher VAT-V and lower SAT-V compared to women. Moreover, we further explored the association between age with SAT-V and VAT-V and found an obvious age effect on the accumulation of VAT-V in both men and women, and a weak age effect on SAT-V in women but not in men. This discrepancy was previously observed by Machann et al,³⁷ who assessed the body composition using MRI in 150 healthy volunteers aged 19 to 69 years. They reported a strong correlation between VAT-V and age both in men and women, whereas SAT-V only slightly increased with age in women. The fact that our results replicate these previous findings on a large unseen dataset corroborates stability and sensitivity of our pipeline.

In conclusion, we have developed a fully automated post-processing pipeline for adipose tissue segmentation on abdominal Dixon MRI based on deep learning methods. While reducing the number of required parameters, the pipeline outperforms other deep learning architectures and demonstrates high reliability. Furthermore, the proposed method was successfully deployed in a large population-based cohort, where it replicated well known SAT-V and VAT-V age and sex associations and demonstrated generalizability across a large

range of anatomical differences, both with respect to body shape and fat distribution.

ACKNOWLEDGEMENTS

We would like to thank the Rhineland Study group for supporting the data acquisition and management, as well as Mohammad Shahid for his support on the deployment of the FatSegNet method into the Rhineland Study processing pipeline. Furthermore we acknowledge Tony Stöcker and his team for developing and implementing the Dixon MRI sequence used in this work. This work was supported by the Diet-Body-Brain Competence Cluster in Nutrition Research funded by the Federal Ministry of Education and Research (BMBF), Germany (grant numbers 01EA1410C and FKZ: 01EA1809C), by the JPI HDHL on Biomarkers for Nutrition and Health (HEALTHMARK), BMBF (grant number 01EA1705B), the NIH R01NS083534, R01LM012719, and an NVIDIA Hardware Award.

ORCID

Santiago Estrada  <http://orcid.org/0000-0003-0339-8870>

Monique M. B. Breteler  <https://orcid.org/0000-0002-0626-9305>

Martin Reuter  <https://orcid.org/0000-0002-2665-9693>

REFERENCES

1. Padwal R, Leslie WD, Lix LM, Majumdar SR. Relationship among body fat percentage, body mass index, and all-cause mortality: a cohort study. *Ann Int Med.* 2016;164:532–541.
2. Ng M, Fleming T, Robinson M, et al. Global, regional, and national prevalence of overweight and obesity in children and adults during 1980–2013: a systematic analysis for the Global Burden of Disease Study 2013. *The Lancet.* 2014;384:766–781.
3. Tomiyama AJ, Hunger JM, Nguyen-Cuu J, Wells C. Misclassification of cardiometabolic health when using body mass index categories in NHANES 2005–2012. *Int J Obesity.* 2016;40:883–886.
4. Linge J, Borga M, West J, et al. Body composition profiling in the UK biobank imaging study. *Obesity.* 2018;26:1785–1795.
5. Després JP. Body fat distribution and risk of cardiovascular disease: an update. *Circulation.* 2012;126:1301–1313.
6. Kissebah AH, Vydellingum N, Murray R, Evans DJ, Kalkhoff RK, Adams PW. Relation of body fat distribution to metabolic complications of obesity. *J Clinical Endocrinol Metabolism.* 1982;54:254–260.
7. Despres JP, Moorjani S, Lupien PJ, Tremblay A, Nadeau A, Bouchard C. Regional distribution of body fat, plasma lipoproteins, and cardiovascular disease. *Arteriosclerosis Thrombosis Vascular Biol.* 1990;10:497–511.
8. Després JP, Lemieux I. Abdominal obesity and metabolic syndrome. *Nature.* 2006;444:881–887.
9. De Laroche E, Côté J, Gilbert G, et al. Visceral/epicardial adiposity in nonobese and apparently healthy young adults:

- association with the cardiometabolic profile. *Atherosclerosis*. 2014;234:23–29.
10. Zhou A, Murillo H, Peng Q. Novel segmentation method for abdominal fat quantification by MRI. *J Magn Reson Imaging*. 2011;34:852–860.
 11. Thörmer G, Bertram HH, Garnov N, et al. Software for automated MRI-based quantification of abdominal fat and preliminary evaluation in morbidly obese patients. *J Magn Reson Imaging*. 2013;37:1144–1150.
 12. Christensen AN, Larsen CT, Mandrup CM, et al. Automatic segmentation of abdominal fat in MRI-Scans, using graph-cuts and image derived energies. In: *Scandinavian Conference on Image Analysis*. Tromsø, Norway: Springer; 2017:109–120.
 13. Sadananthan SA, Prakash B, Leow MKS, et al. Automated segmentation of visceral and subcutaneous (deep and superficial) adipose tissues in normal and overweight men. *J Magn Reson Imaging*. 2015;41:924–934.
 14. Mosbech TH, Pilgaard K, Vaag A, Larsen R. Automatic segmentation of abdominal adipose tissue in MRI. In: *Scandinavian Conference on Image Analysis*. Ystad, Sweden: Springer; 2011: 501–511.
 15. Wald D, Teucher B, Dinkel J, et al. Automatic quantification of subcutaneous and visceral adipose tissue from whole-body magnetic resonance images suitable for large cohort studies. *J Magn Reson Imaging*. 2012;36:1421–1434.
 16. Badrinarayanan V, Kendall A, Cipolla R. Segnet: a deep convolutional encoder-decoder architecture for image segmentation. *IEEE Trans Pattern Anal Mach Intelligence*. 2017;39: 2481–2495.
 17. Long J, Shelhamer E, Darrell T. Fully convolutional networks for semantic segmentation. In Proceedings of the IEEE conference on computer vision and pattern recognition, Boston, MA, 2015. pp. 3431–3440.
 18. Langner T, Hedström A, Mörwald K, et al. Fully convolutional networks for automated segmentation of abdominal adipose tissue depots in multicenter water–fat MRI. *Magn Reson Med*. 2019;81:2736–2745.
 19. Ronneberger O, Fischer P, Brox T. U-net: convolutional networks for biomedical image segmentation. In *International Conference on Medical image computing and computer-assisted intervention*. Munich, Germany: Springer; 2015:234–241.
 20. Roy AG, Conjeti S, Sheet D, Katouzian A, Navab N, Wachinger C. Error corrective boosting for learning fully convolutional networks with limited data. In: *International Conference on Medical Image Computing and Computer-Assisted Intervention*. Quebec City, Canada: Springer; 2017:231–239.
 21. Jégou S, Drozdal M, Vazquez D, Romero A, Bengio Y. The one hundred layers tiramisù: fully convolutional densenets for semantic segmentation. In: *2017 IEEE Conference on IEEE Computer Vision and Pattern Recognition Workshops (CVPRW)*. Honolulu, HI: 2017:1175–1183.
 22. Estrada S, Conjeti S, Ahmad M, Navab N, Reuter M. Competition vs. concatenation in skip connections of fully convolutional networks. In: *International Workshop on Machine Learning in Medical Imaging*. Granada, Spain: Springer; 2018: 214–222.
 23. Goodfellow IJ, Warde-Farley D, Mirza M, Courville A, Bengio Y. Maxout networks. In Proceedings of the 30th International Conference on International Conference on Machine Learning–Volume 28 JMLR. org, Atlanta, GA, 2013. pp. III–1319.
 24. Liao Z, Carneiro G. A deep convolutional neural network module that promotes competition of multiple-size filters. *Pattern Recognition*. 2017;71:94–105.
 25. Breteler MM, Stöcker T, Pracht E, Brenner D, Stirnberg R. MRI in the Rhineland study: a novel protocol for population neuroimaging. *Alzheimer's Dementia*. 2014;10:P92.
 26. Stöcker T. Big data: the Rhineland study. In Proceedings of the 24th Scientific Meeting of the International Society for Magnetic Resonance in Medicine (Singapore); 2016. <https://index.miramart.com/ISMIRM2016/PDFfiles/6865.html>.
 27. Roy AG, Conjeti S, Navab N, et al. QuickNAT: a fully convolutional network for quick and accurate segmentation of neuroanatomy. *NeuroImage*. 2019;186:713–727.
 28. Huang G, Liu Z, Van Der Maaten L, Weinberger KQ. Densely connected convolutional networks. In: *2017 IEEE Conference on Computer Vision and Pattern Recognition (CVPR)*. Honolulu, HI: IEEE; 2017:2261–2269.
 29. Wilcoxon F. Individual comparisons by ranking methods. *Biometrics Bull*. 1945;1:80–83.
 30. Benjamini Y, Krieger AM, Yekutieli D. Adaptive linear step-up procedures that control the false discovery rate. *Biometrika*. 2006;93:491–507.
 31. Chollet F, et al. Keras; 2015. <https://keras.io/getting-started/faq/#how-should-i-cite-keras>.
 32. McGraw KO, Wong SP. Forming inferences about some intraclass correlation coefficients. *Psychol Methods*. 1996;1:30–46.
 33. R Core Team. *R: a language and environment for statistical computing*. R Foundation for Statistical Computing, Vienna, Austria; 2013. <http://www.R-project.org/>
 34. Kullberg J, Ahlström H, Johansson L, Frimmel H. Automated and reproducible segmentation of visceral and subcutaneous adipose tissue from abdominal MRI. *Int J Obesity*. 2007;31:1806–1817.
 35. Addeman BT, Kutty S, Perkins TG, et al. Validation of volumetric and single-slice MRI adipose analysis using a novel fully automated segmentation method. *J Magn Reson Imaging*. 2015;41:233–241.
 36. Sun J, Xu B, Freeland-Graves J. Automated quantification of abdominal adiposity by magnetic resonance imaging. *Am J Human Biol*. 2016;28:757–766.
 37. Machann J, Thamer C, Schnoedt B, et al. Age and gender related effects on adipose tissue compartments of subjects with increased risk for type 2 diabetes: a whole body MRI/MRS study. *Magn Reson Mater Phys Biol Med*. 2005;18:128–137.
 38. Kuk JL, Lee S, Heymsfield SB, Ross R. Waist circumference and abdominal adipose tissue distribution: influence of age and sex. *Am J Clinical Nutrition*. 2005;81:1330–1334.

SUPPORTING INFORMATION

Additional supporting information may be found online in the Supporting Information section at the end of the article.

FIGURE S1 View aggregation Network. The proposed network is composed of a initial 3D convolution layer with 30 channels, followed by a batch normalization and a 3D convolutional layer for reducing the feature map dimensionality into the number of classes($n = 5$)

FIGURE S2 Step 1: Abdominal region localization. Dice scores box-plot: Average Dice score (cross-validation) of the abdominal

region detection comparing the Proposed CDFNet vs. other FCNN architectures. The Dice scores are calculated on the average abdominal region generated from the average bounding boxes of the sagittal and coronal model. There is no significant difference between models, nonetheless, the proposed method achieves the same performance with $\sim 30\%$ and $\sim 80\%$ less parameters compared to Dense-UNet and UNet, respectively

FIGURE S3 Comparison of single view model (left) vs. view aggregation (right): AAT predictions of two unseen subjects: A, normal subject, B, obese subject. View aggregation avoids arm-misclassification (red boxes) and improves SAT (purple box)

TABLE S1 Case study analysis on the Rhineland Study data. Characteristics of the participants ($n = 587$) showing mean (SD) for continuous and counts (PCT) for categorical variables

How to cite this article: Estrada S, Lu R, Conjeti S, et al. FatSegNet: A fully automated deep learning pipeline for adipose tissue segmentation on abdominal dixon MRI. *Magn Reson Med.* 2020;83:1471–1483. <https://doi.org/10.1002/mrm.28022>

3.2 Metabolic Profiling of Human Plasma and Urine, Targeting Tryptophan, Tyrosine and Branched Chain Amino Acid Pathways



metabolites



Article

Metabolic Profiling of Human Plasma and Urine, Targeting Tryptophan, Tyrosine and Branched Chain Amino Acid Pathways

Andrea Anesi ^{1,†} , Josep Rubert ^{2,†} , Kolade Oluwagbemigun ³ , Ximena Orozco-Ruiz ⁴,
Ute Nöthlings ³ , Monique M.B. Breteler ^{4,5} and Fulvio Mattivi ^{2,6,*}

- ¹ Department of Food Quality and Nutrition, Research and Innovation Centre, Fondazione Edmund Mach (FEM), Via E. Mach 1, 38010 San Michele all' Adige, Italy; andrea.anesi@fmach.it
- ² CIBIO, Department of Cellular, Computational and Integrative Biology, Via Sommarive 9, 38123 Povo, Italy; josep.rubert@unitn.it
- ³ Nutritional Epidemiology, Institute of Nutrition and Food Sciences, University of Bonn, Endenicher Allee 19b, 53115 Bonn, Germany; koluwagb@uni-bonn.de (K.O.); noethlings@uni-bonn.de (U.N.)
- ⁴ Population Health Sciences, German Center for Neurodegenerative diseases (DZNE), Venusberg-Campus 1-Building 99, 53127 Bonn, Germany; Ximena.Orozco-Ruiz@dzne.de (X.O.-R.); monique.breteler@dzne.de (M.M.B.B.)
- ⁵ Institute for Medical Biometry, Informatics and Epidemiology (IMBIE), Faculty of Medicine, University of Bonn, Venusberg-Campus 1-Building 11, 53127 Bonn, Germany
- ⁶ University of Trento, Department of Physics, Bioorganic Chemistry Laboratory, Via Sommarive 14, 38123 Povo, Italy
- * Correspondence: fulvio.mattivi@unitn.it; Tel.: +39-0461-615-259
- † These authors contributed equally to this work.

Received: 2 October 2019; Accepted: 28 October 2019; Published: 1 November 2019



Abstract: Tryptophan and tyrosine metabolism has a major effect on human health, and disorders have been associated with the development of several pathologies. Recently, gut microbial metabolism was found to be important for maintaining correct physiology. Here, we describe the development and validation of a UHPLC-ESI-MS/MS method for targeted quantification of 39 metabolites related to tryptophan and tyrosine metabolism, branched chain amino acids and gut-derived metabolites in human plasma and urine. Extraction from plasma was optimised using 96-well plates, shown to be effective in removing phospholipids. Urine was filtered and diluted ten-fold. Metabolites were separated with reverse phase chromatography and detected using triple quadrupole MS. Linear ranges (from ppb to ppm) and correlation coefficients ($r^2 > 0.990$) were established for both matrices independently and the method was shown to be linear for all tested metabolites. At medium spiked concentration, recovery was over 80% in both matrices, while analytical precision was excellent (CV < 15%). Matrix effects were minimal and retention time stability was excellent. The applicability of the methods was tested on biological samples, and metabolite concentrations were found to be in agreement with available data. The method allows the analysis of up to 96 samples per day and was demonstrated to be stable for up to three weeks from acquisition.

Keywords: tryptophan metabolism; tyrosine metabolism; branched chain amino acids; gut microbiota metabolites; targeted metabolomics; LC-MS/MS; human plasma; urine; clinical studies

1. Introduction

The emerging field of “nutrition-microbiome-human health” has raised many unanswered questions regarding the complex relationship and interplay of gut microbiota, their metabolites in

homeostasis and human physiology. Results from epidemiological studies, clinical trials and recent meta-analyses have supported the link between mood disorders, obesity and gut microbiota [1–3], and recent data have strikingly indicated that emotional stress, anxiety and depression may influence the development of gastrointestinal disorders and cancer [4–8]; however, the relationship between them is still unclear. It has been suggested that gut microbial metabolites act on the gut epithelium, modulating downstream signalling pathways involved in the control of digestion, metabolism, immunity, the brain and pain [9–13].

Indeed, during the last few years, the link between gut microbiota and the brain has been investigated in depth [3,14–16], demonstrating that depression is associated with decreased gut microbiota richness and diversity [17]. The concept of the “brain-gut-microbiome axis” has recently been introduced to describe the complex interactions between gut microbiota and human physiology [18].

Tryptophan (TRP) metabolism has claimed to be a key player in neurophysiology and depression [14,17–20], regulation of immune response and inflammation, inflammatory bowel diseases [21], metabolic syndrome and obesity [18]. TRP is an essential amino acid bearing an indole group critical for protein synthesis, but it also serves as a substrate for the generation of several bioactive compounds. In mammals, about 95% of ingested TRP is catabolised through the kynurenine pathway (KP) [20,22,23] into a range of metabolites known to be involved in inflammation, immune response and excitatory neurotransmissions [22,24] (Figure 1). Kynurenine (KYN) and its metabolites are known for their beneficial effects on the central nervous system [20].

Minor pathways of TRP degradation lead to synthesis of the neurotransmitter serotonin (5-HT) via the hydroxylation pathway, tryptamine (TRY) via decarboxylation and indole-3-pyruvic acid via transamination pathways [11,23]. Several bacteria have the ability to synthesize 5-HT from dietary TRP, and are therefore able to modulate the brain-gut axis [25]. Gut microbiota can also produce indole and its derivatives, such as indole-3-propionic acid (IPA), indole-3-lactic acid (ILA) and indole-3-aldehyde (IALD) [26]. Indole is synthesized from TRP via the tryptophanase enzyme and this metabolite is able to maintain host-microbe homeostasis on the mucosal surface [26–28]. Hepatic sulfonation of indole leads to the production of indoxyl sulfate (IS), a cytotoxic metabolite that induces renal and vascular dysfunction [29,30]. IPA is a potent antioxidant able to reduce DNA damage and lipid peroxidation, and to maintain mucosal homeostasis and intestinal barrier functions [31,32]. *Clostridium sporogenes* is the predominant IPA producer, but a recent work demonstrated that four other gut bacteria can synthesize it: *Peptostreptococcus anaerobius* CC14N and three strains of *Clostridium cadaveris* [33]. ILA is an intermediate of IPA production from TRP operated by *C. sporogenes*, but it is also produced by *Bifidobacterium* spp [34]. ILA was also identified as a potential biomarker for alcohol-induced liver disease in Ppara mouse model [35]. IALD is produced from bacteria belonging to the *Lactobacillus* genera and helps to maintain host-microbial homeostasis [36].

The importance of qualitatively and quantitatively understanding gut microbiota regulation of TRP metabolism in healthy and diseased conditions thus appears to be clear. On the other hand, emerging evidence has also shown that different concentrations in human biofluids (blood and urine) and tissues of branched chain amino acids (BCAAs), such as L-methionine (MET), L-valine (VAL), L-isoleucine (ILE) and L-leucine (LEU) among others, might play an unrecognised and crucial role in the development of intestinal health [37,38], depression [39] and cancer [40]. In the light of these facts, it is clear that there is a complex inter-kingdom regulatory network and interactions occurring between the host, microbiome, and diet.

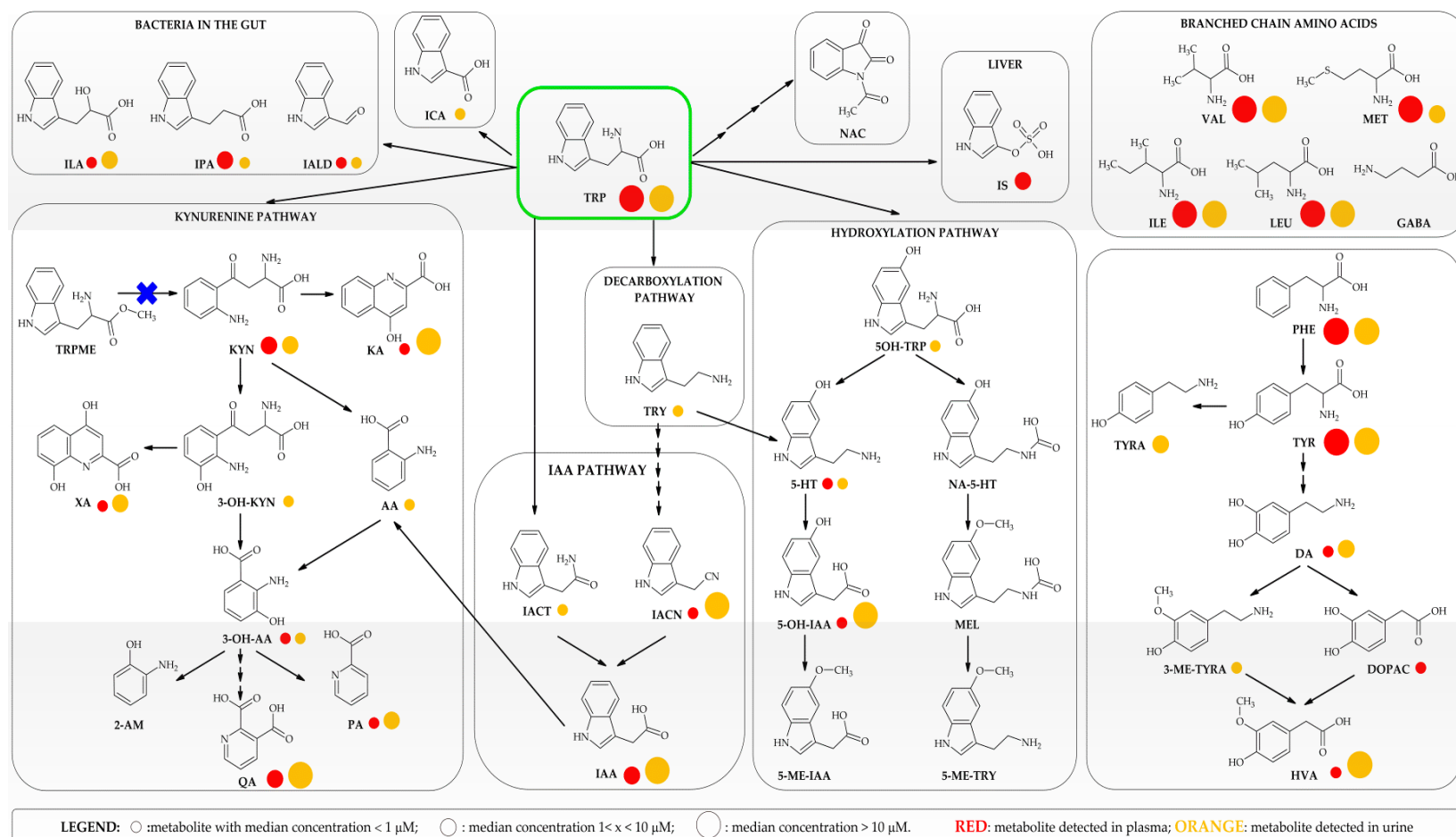


Figure 1. Principal branches of the TRP and TYR metabolic pathways covered in this analytical method and structures of the main BCAAs. Red circles represent the metabolites detected in plasma, orange circles those detected in urine. The size of the circle is proportional to the median concentration in each biofluid. ○: metabolite with median concentration of < 1 μM; ○: metabolite with median concentration of 1 < x < 10 μM; ○: metabolite with median concentration of > 10 μM.

Accurate quantitation of TRP derived metabolites and BCAAs in plasma, serum and urine is becoming increasingly important, since subtle changes may be responsible for mechanistic responses. However, to date the development and validation of a single robust targeted method providing broad coverage and suitable for the main biofluids is still lacking. More frequently, only a few metabolites related to KP have been monitored [41–48]. Zhu and colleagues reported on the quantitation of 19 metabolites in urine and human serum, including microbial derived metabolites [49]. One main drawback of this method, which could limit applicability in clinical studies requiring the inclusion of a large number of samples, is the number of laborious steps proposed for metabolite extraction, which requires the use of single tubes, 1 h incubation at $-20\text{ }^{\circ}\text{C}$ to ensure protein precipitation and three centrifugation steps.

In 2016, Marcos and co-workers proposed a method for quantitation of 17 TRP metabolites and BCAAs in urine and plasma [50]. Again, the procedure for extraction of metabolites from plasma limited the processing of a large sample set. More recently, Whiley and colleagues (2019) published a thoroughly validated method for the quantitation of 18 TRP metabolites in serum and plasma based on Phenomenex PHREE SPE 96-well plate extraction that allows high-throughput sample preparation [51]. The study, which to our knowledge represents the state-of-the-art in the field, covers the quantitative analysis of 18 metabolites associated with KP and 5-HT degradation pathways, but did not cover BCAAs or gut-derived metabolites.

Here, we present a validated analytical method for the simultaneous separation and detection of 39 metabolites in both plasma and urine using Ultra High Performance Liquid Chromatography-Electrospray-Ionization-Tandem Mass Spectrometry (UHPLC-ESI-MS/MS). Preliminary application of this method in two independent epidemiological studies across the lifespan of the Dortmund Nutritional and Anthropometric Longitudinally Designed (DONALD) Study and the Rhineland Study allowed us to establish the typical ranges for these 39 metabolites present in the human biofluids of two German populations.

Legend: TRP: L-tryptophan; KYN: kynurenine; KA: kynurenic acid; 3-OH-KYN: 3-hydroxy kynurenine; 3-OH-AA: 3-hydroxy-anthranilic acid; AA: anthranilic acid; XA: xanthurenic acid; QA: quinolinic acid; PA: picolinic acid; 2-AM: 2-aminophenol; 5-OH-TRP: 5-hydroxy-L-tryptophan; 5-HT: serotonin; 5-OH-IAA: 5-hydroxyindole-3-acetic acid; 5-ME-IAA: 5-methoxyindole-3-acetic acid; NA-5-HT: *N*-acetyl-5-hydroxytryptamine; MEL: melatonin; 5-ME-TRY: 5-methoxytryptamine; TRY: tryptamine; IACN: indole-3-acetonitrile; IAA: indole-3-acetic acid; IACT: indole-3-acetamide; ILA: indole-3-lactic acid; IPA: indole-3-propionic acid; IALD: indole-3-carboxaldehyde; IS: indoxyl sulfate; NAC: 1-acetylisatin; ICA: indole-3-carboxylic acid; TRPME: tryptophan methyl ester; PHE: phenylalanine; TYR: tyrosine; TYRA: tyramine; DA: dopamine; 3-ME-TYRA: 3-methoxy-*p*-tyramine; DOPAC: 3,4-dihydroxyphenyl acetic acid; HVA: homovanillic acid; GABA: gamma-aminobutyric acid; ILE: L-isoleucine; LEU: L-leucine; VAL: L-valine; MET: L-methionine.

2. Results

2.1. Liquid Chromatography and Mass Spectrometry

Two Multiple Reaction Monitoring (MRM) transitions were optimised for each target compound by changing Collision Energy (CE) and Cone Voltage (CV). The one displaying the highest intensity was selected as the quantifier ion (Q), while the less intense one was selected as the qualifier ion (q). MS parameters and retention times (RT) are reported in Table 1.

Table 1. Internal standard used for quantification, RT (min) and MS parameters (parent *m/z*, polarity, quantifier and qualifier ions *m/z*, CV and CE) for the selected analytes. A Waters ACQUITY HSST3 (1.8 μm , 2.1 \times 150 mm) column was used for metabolite separation.

Metabolite	Internal Standard	RT (min)	Parent <i>m/z</i>	ESI	Q <i>m/z</i>	q <i>m/z</i>	CV (V)	CE (eV)
γ -aminobutyric acid	MET-d ₄	1.16	104.03	+	68.95	86.14	12	14
l-valine	MET-d ₄	1.47	118.03	+	55.01	72.02	12	18
picolinic acid	MET-d ₄	1.53	124.00	+	77.96	105.87	26	10
dopamine-d ₄		1.66	158.16	+	94.85	122.4	12	22
dopamine	DA-d ₄	1.67	154.22	+	91.02	119.01	12	20
methionine-d ₄		1.68	154.09	+	59.17	62.95	12	16
methionine	MET-d ₄	1.68	150.22	+	104.02	56.04	12	10
2-aminophenol	TRP-d ₅	1.70	110.16	+	92.00	65.01	20	14
quinolinic acid	MET-d ₄	1.80	168.22	+	77.98	106.03	14	16
3-hydroxykynurenine	TRP-d ₅	2.01	225.176	+	110.02	162.01	14	18
tyrosine-d ₄		2.04	186.16	+	140.11	93.95	12	14
tyrosine	TYR-d ₄	2.07	182.17	+	136.07	90.96	18	16
l-isoleucine	MET-d ₄	2.25	132.09	+	86.00	69.00	10	12
tyramine	TYR-d ₄	2.25	138.12	+	76.68	103.97	10	24
l-leucine	MET-d ₄	2.38	132.09	+	86.00	43.00	10	12
serotonin-d ₄		2.93	181.16	+	118.14	146.05	12	26
serotonin	5-HT-d ₄	3.02	177.22	+	115.09	132.18	10	26
5-hydroxy-tryptophan	TRP-d ₅	3.00	221.29	+	162.01	134.02	12	18
3-methoxy- <i>p</i> -tyramine	TYR-d ₄	3.02	168.22	+	91.00	119.05	8	20
kynurenine	TRP-d ₅	3.53	209.12	+	94.01	146.08	14	16
dl-phenylalanine	TYR-d ₄	3.61	166.22	+	120.10	103.01	14	20
3-hydroxyanthranilic acid	TRP-d ₅	4.75	154.22	+	80.01	108.01	10	22
tryptophan-d ₅		4.90	210.16	+	150.09	122.11	12	18
tryptophan	TRP-d ₅	4.94	205.29	+	146.06	118.01	12	16
1-acetylisatin	TRP-d ₅	4.94	190.01	+	148.01	162.01	18	10
DOPAC-d ₅		4.99	172.11	-	128.04	99.99	14	8
3,4-dihydroxyphenyl acetic acid	DOPAC-d ₅	5.04	167.07	-	123.05	94.99	14	8
xanthurenic acid	TRP-d ₅	5.03	206.09	+	160.00	132.02	20	18
kynurenic acid-d ₅		5.41	195.09	+	149.06	121.08	24	18
kynurenic acid	KA-d ₅	5.44	190.09	+	143.99	116.00	20	20
tryptamine	TRP-d ₅	5.45	161.13	+	127.20	117.40	12	24
5-methoxytryptamine	TRP-d ₅	5.60	191.20	+	159.09	143.08	12	22
5-hydroxyindole acetic acid-d ₅		5.71	197.16	+	150.16	122.17	16	14
5-hydroxyindole acetic acid	5-OH-IAA-d ₅	5.74	192.23	+	146.27	91.00	18	14
<i>N</i> -acetyl-5-hydroxytryptamine	TRP-d ₅	5.86	219.20	+	160.07	115.09	16	16
tryptophan methyl ester	TRP-d ₅	6.07	219.14	+	160.00	132.02	12	18

Table 1. Cont.

Metabolite	Internal Standard	RT (min)	Parent m/z	ESI	Q m/z	q m/z	CV (V)	CE (eV)
homovanillic acid	DOPAC-d ₅	6.20	181.09	-	137.08	121.99	8	10
indoxyl sulfate	TRP-d ₅	6.24	212.04	-	80.08	132.02	24	20
indole-3-acetamide	TRP-d ₅	6.53	175.05	+	102.99	76.95	14	30
anthranilic acid	TRP-d ₅	6.78	138.22	+	91.99	65.04	10	22
indole-3-lactic acid	TRP-d ₅	6.96	206.11	+	160.09	130.02	18	10
indole-3-carboxylic acid	TRP-d ₅	7.15	162.08	+	116.03	88.95	16	20
melatonin	TRP-d ₅	7.31	233.22	+	174.08	159.05	16	14
5-methoxyindole acetic acid	TRP-d ₅	7.35	206.17	+	160.17	145.05	16	16
indole-3-carboxaldehyde	TRP-d ₅	7.36	146.09	+	118.05	90.97	22	24
indole-3-acetonitrile	TRP-d ₅	7.52	130.22	+	76.95	102.99	30	22
indole-3-acetic acid	TRP-d ₅	7.53	176.09	+	130.00	102.99	18	12
indole-3-propionic acid	TRP-d ₅	8.06	190.11	+	130.02	54.96	12	16

With our chromatographic setup, GABA was practically non-retained and eluted with the chromatographic front. The 150 mm column enabled separation of ILE from LEU, as highlighted in Figure 2 for the BEH (panel A) and HSST3 (B) columns. The HSST3 column provided baseline separation of ILE (RT: 2.25 min) from LEU (RT: 2.38 min).

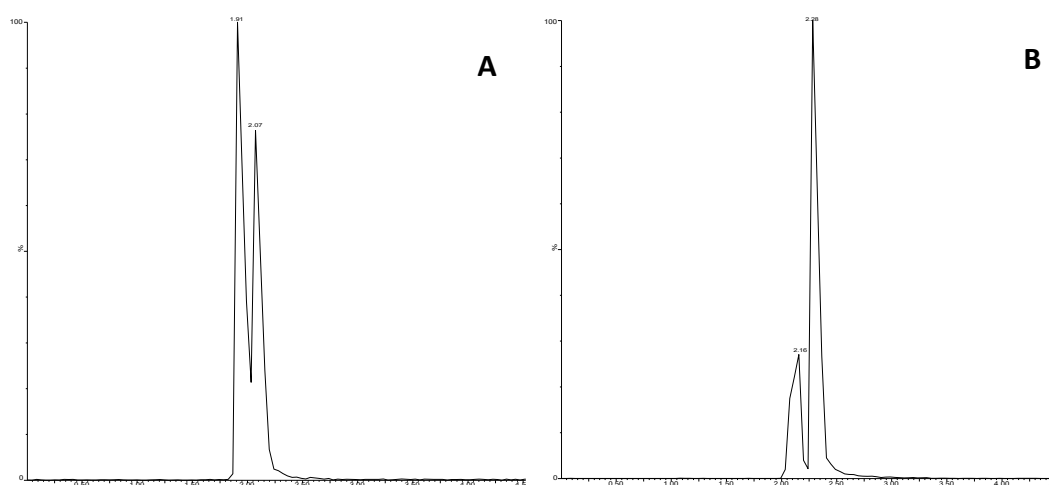


Figure 2. MRM ($132.096 > 86.0$) for ILE (left peak) and LEU (right peak) in plasma samples. (A): Waters ACQUITY BEH C₁₈ 1.7 μm , 2.1×150 mm; (B): Waters ACQUITY HSST3 1.8 μm , 2.1×150 mm.

The presence of different substituents on the indole moiety enabled separation of all indole derivatives within 8.5 min. The total run time, including column re-equilibration, was 14 min. This made it possible to acquire up to 96 samples (one 96-well plate) in 24 h. Directing flow waste during non-acquisition time enabled us to acquire up to 300 samples per batch without significant signal losses for both matrices.

2.2. Linearity and Limit of Quantification (LOQ)

The linearity range for each metabolite was established by using calibration curves in water with 0.1% formic acid (FA), since it was impossible to obtain analyte-free matrices (blanks). Linearity ranges covered 4+ orders of magnitude, from a few ppb to ppm. The availability of a large number of samples obtained from two independent German observational and epidemiological studies across the lifespan

allowed us to finely tune calibration. Working calibration ranges were specifically designed for each metabolite, to cover the expected concentrations in plasma and urine. All working calibration curves were found to have a good correlation coefficient ($r^2 > 0.990$) in the tested ranges for both plasma and urine (see Table S1).

Metabolites at low concentration levels were linear in the range 1–250 ng/mL. By contrast, for high level metabolites, the upper quantification point was 12500 ng/mL, and above this the MS response was no longer linear. The exceptions were 3-hydroxykynurenine (3-OH-KYN) in urine, which was linear between 15–25,600 ng/mL, and homovanillic acid (HVA) in plasma, which was linear in the range of 156–25,000 ng/mL.

LOQs were in the order of a few ng/mL for low level metabolites, except for 2-aminophenol (2-AM) (78.1 ng/mL) and 3-hydroxyanthranilic acid (3-OH-AA) (31.2 ng/mL) in plasma, indole-3-acetonitrile (IACN) in urine (19.5 mg/mL) and 3-OH-KYN in both matrices (31.2 and 15.6 ng/mL in plasma and urine respectively). For high level metabolites, the LOQ was set as the lowest calibration point. Metabolites detected in negative ion mode (HVA, DOPAC and IS) displayed higher LOQs in both matrices.

2.3. Retention Time Stability

For both matrices, metabolite RT stability was addressed over a period of three weeks. Most of the metabolites showed a coefficient of variation lower than 1%, except for 2-AM (CV%: 2.10) and TYR-d4 (CV% 1.04) in plasma, and IS (CV% 1.09) in urine. See Table S1 for details on plasma and urine respectively.

2.4. Matrix Effects

Matrix effects (ME), evaluated with the matrix match calibration (MMC) approach, were minimal and in the range of 80–120% for most metabolites in both plasma and urine (Table S1). Ion suppression by the matrix component significantly affected quantification of the most polar metabolites: VAL, dopamine (DA), MET, and quinolinic acid (QA) were suppressed both in plasma and urine, while 2-AM and tyramine (TYRA) were affected only in urine. Quantification of GABA was significantly deviated in both matrices due to its poor retention with a C₁₈ analytical column.

2.5. Recovery, Intra- and Inter-Day Accuracy and Precision

At medium spiked concentration, metabolite recovery from plasma was over 85%, except for VAL (80.7%) and picolinic acid (PA) (82.8%). At low spiked concentration, recovery was over 80% for all metabolites except GABA (71.2%) and QA (76.5%). In urine, recovery at medium spiked concentration was over 80% for all metabolites. At low spiked concentration, several metabolites, such as DA, ILE, LEU, TYRA and 3-OH-KYN, had lower recovery, due to the fact that spiked values were close to the LOQ, so analytical error was greater. Recovery at the highest spiked concentration was slightly over 80% for all metabolites, except 3-OH-AA in urine and GABA in both matrices. All information on plasma and urine can be found in Table S2.

Accuracy at medium spiked concentration was excellent for all metabolites (CV<15%) in both plasma and urine (Table S2). At low concentrations, precision was lower than 20% for all metabolites in plasma, except for PA, 3-OH-KYN, 3-methoxy-p-tyramine (3-ME-TYRA), 3-OH-AA, DOPAC, 5-methoxytryptamine (5-ME-TRY), 5-hydroxyindole-acetic acid (5-OH-IAA) and TRP- methyl ester (TRPME). Accuracy at low spiked concentration was not calculated for the internal standard. At the highest concentration, accuracy was low for VAL in plasma and PHE, TYR, 3-OH-AA and TRP in urine. This was due to the fact that spiked amounts were above the detector linear response. Accuracy was unsatisfactory for GABA at all concentration levels and was not reported. We propose to use data on GABA to detect fold changes rather than to provide accurate quantitative data.

2.6. Carryover Effect and Phospholipid Removal

No carryover effect was observed within and between runs for either plasma or urine. Figure 3 shows the MRM transition of TRP (205.29 > 146.06; RT: 4.95 min) for a plasma sample spiked at the highest concentration (25,000 ng/mL) (panel A) and the blank, after the acquisition of 5 plasma samples spiked at the highest concentration (B). Similarly, (C) shows the MRM transition of kynurenic acid (KA) (190.09 > 149.99; RT: 5.45 min) at the highest calibration point, while (D) shows the MRM acquired in the following run after injection of acetonitrile (ACN). Column cleaning for 3 min at 100% B ensured complete elution of the tested metabolites, while the strong wash solvent ensured good needle cleaning.

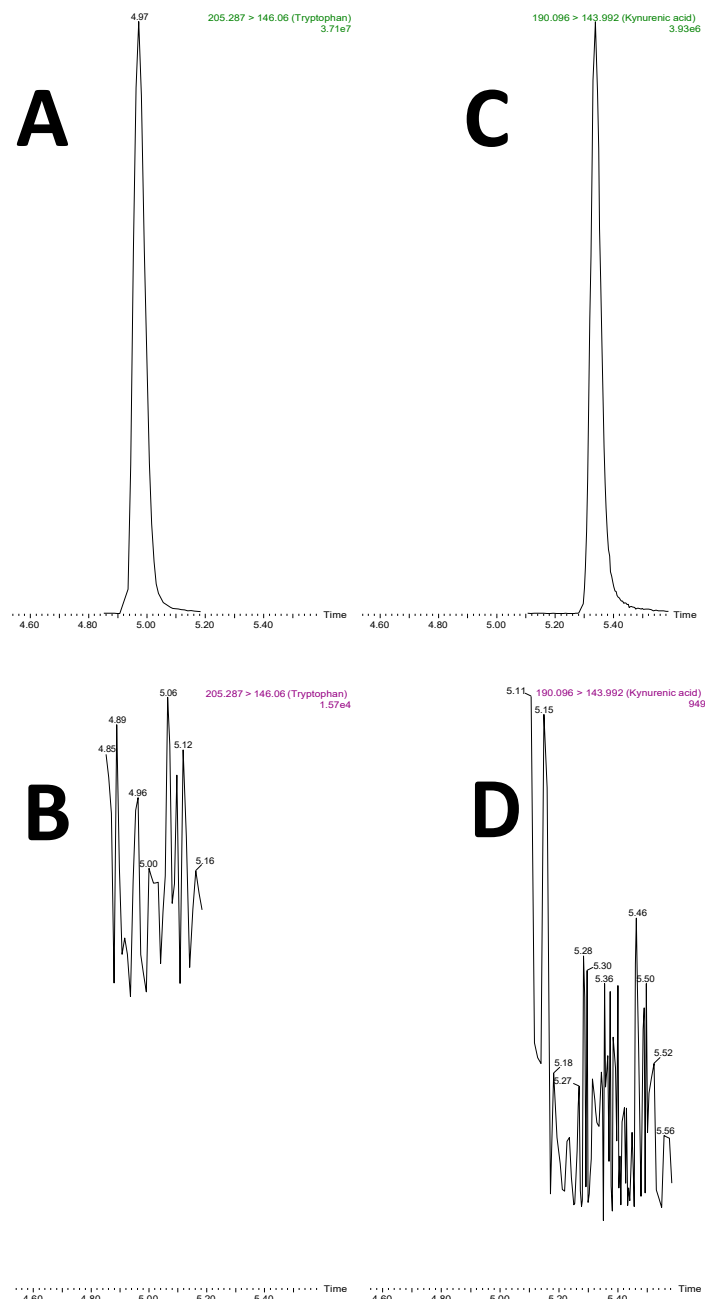


Figure 3. MRM of TRP (205.29 > 146.06) after injection of a plasma sample spiked at the highest concentration (panel A) and injection of ACN at the end of the entire batch ($n = 5$) (B). MRM of KA (190.09 > 143.99) at the highest point of calibration (C) and in the following run after injection of ACN (D).

Biological samples, particularly plasma, contain significant amounts of phospholipids, mainly phosphatidylcholine (PC), phosphatidylethanolamine (PE) and sphingomyelin (SM). All these matrix components can significantly affect compound ionization through ion enhancement/suppression effects. With our chromatographic setup, phospholipids eluted after 8.50 min, therefore well after the last eluting metabolite (IPA, RT: 8.06 min). Nevertheless, Ostro 96-well plates were also able to efficiently remove phospholipids from plasma, as demonstrated by the Precursor Ion Scan (PIS) of m/z 184.03 in crude plasma (Figure 4A) or plasma after sample clean up (B). Urine contained traces of PC and SM and 10-fold dilution did not affect the MS response (data not shown).

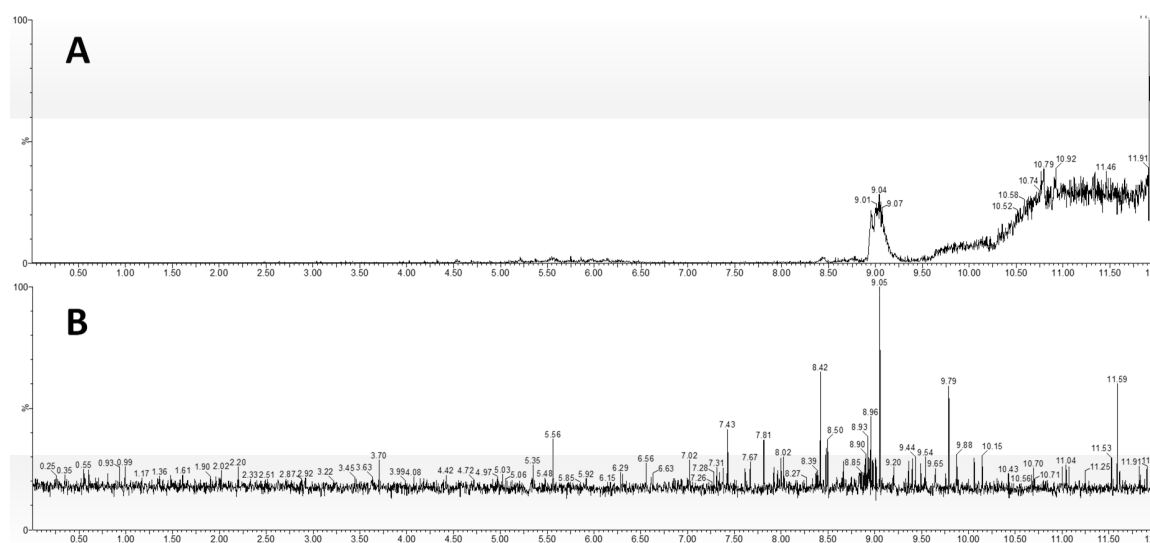


Figure 4. Panel A: Chromatogram of PIS of m/z 184.03 in untreated plasma, showing the signal generated by presence of PC and SM. Panel B: chromatogram of PIS of m/z 184.03 after plasma clean up on an Ostro 96-well plate, demonstrating the removal of interfering signal due to lipids eluting after 8.50 min

2.7. Method Application to Biological Samples

To demonstrate the applicability of the method, we analysed fasting samples of plasma ($n = 1000$) and 24-h urine samples ($n = 672$) from two independent populations. As the Rhineland Study did not collect 24-h urine and the DONALD study did not collect blood, no paired samples were available from the same individual. Samples were pseudonymised and randomised prior to extraction, and were extracted independently. Biological QCs were prepared by mixing equal volumes of sample. Twenty QCs were injected at the beginning of the acquisition sequence in order to stabilise the MS response and at intervals of 15 samples across the sequence in order to test MS stability. Calibration curves were acquired after the first 20 QCs, approximately every 300 samples, and at the end of each batch.

The method allowed quantification of 24 metabolites in plasma and 30 metabolites in urine: 23 metabolites were common to the two matrices; DOPAC was detected exclusively in plasma, while 8 metabolites were found exclusively in urine (Figure 5). The metabolites in our study resulting unique to urine were the neurotransmitter TYRA, the metabolite from methylation of DA, 3-ME-TYRA, the immediate precursor of 5-HT, 5-OH-TRP, the highly reactive neurotoxin 3-OH-KYN and the uremic toxin AA in the KP, as well as the β -arylamine neurotransmitter and microbial catabolite TRY and the intermediate of the indole-3-acetic acid (IAA) pathway indole-3-acetamide (IACT) (Figure 1).

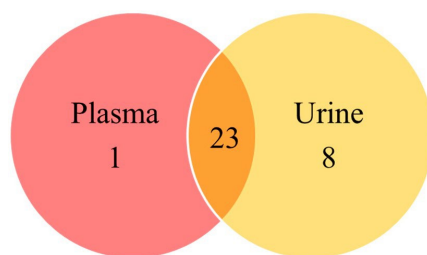


Figure 5. Venn diagram illustrating metabolites found exclusively in plasma (1), exclusively in urine (8) and in both matrices (23).

The minimum, median and maximum values detected in both matrices for the two German populations are reported in Table 2. Qualitatively, here we divided the metabolites into three categories according to the median value: low (median $< 1 \mu\text{M}$), medium (median $1 < x < 10$) and high (median > 10) level metabolites (Figure 6). In general, high level metabolites in plasma (VAL, ILE, LEU, MET, TYR, PHE and TRP) were also present in high concentrations in urine. Medium level metabolites (QA, KYN, IACN and IAA) were detected in higher concentrations in urine, except for IPA, which was found at a lower concentration. Of the low level metabolites in plasma, XA, KA, 5-OH-IAA and HVA were those excreted at the highest concentrations in urine. As expected, indole-3-carboxylic acid (ICA) was detected only in urine.

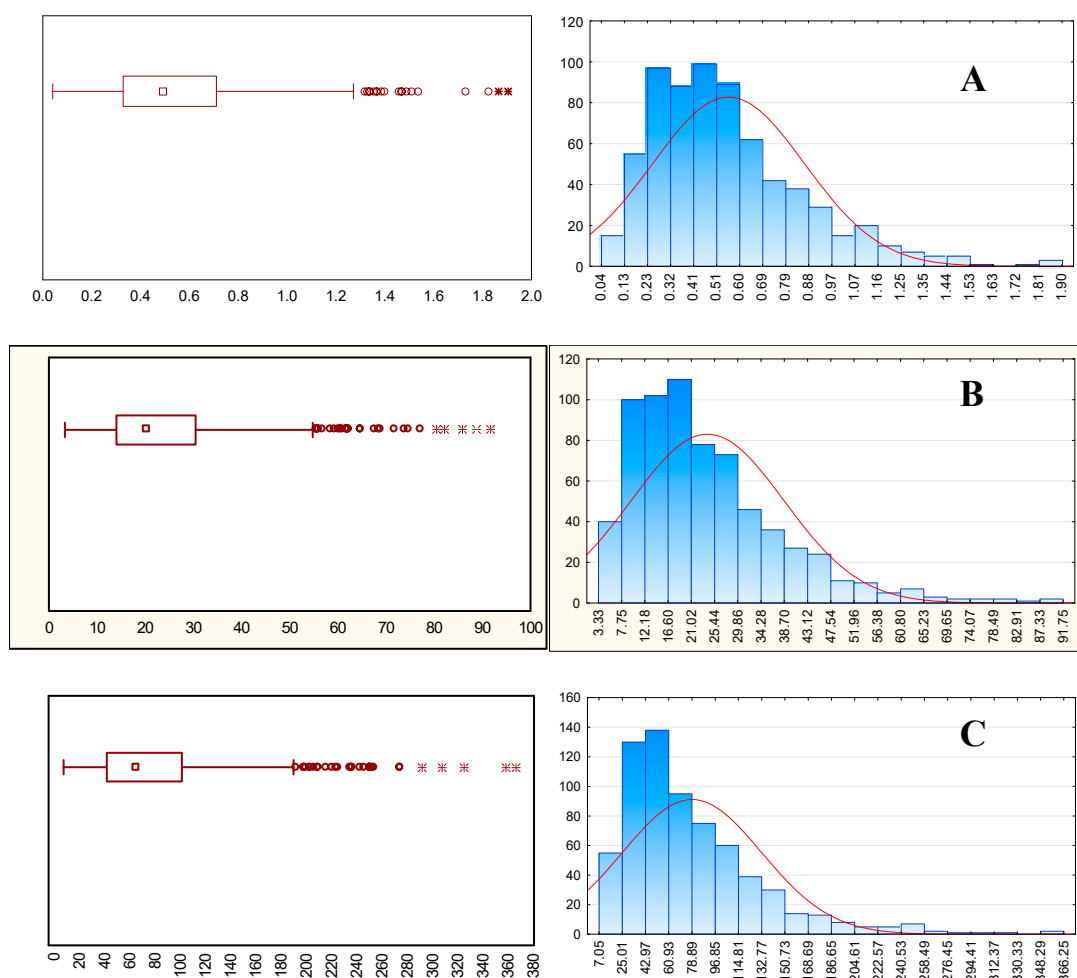


Figure 6. Box plots (90% confidence interval) and graphic distribution of metabolites with (A) low (5-HT, median $0.492 \mu\text{M}$), (B) medium (XA, median $5.424 \mu\text{M}$) and (C) high median (TRP, median $64.02 \mu\text{M}$) levels quantified in urine in the DONALD study ($n = 672$).

Table 2. Metabolite concentration ranges (μM) detected in plasma and urine. n.d.: not detected; n.a.: data not available.

Metabolite	Plasma (μM)			Urine (μM)		
	Min	Median	Max	Min	Median	Max
l-valine	12.09	62.12	130	1.678	29.15	94.71
picolinic acid	0.00179	0.0198	0.057	0.649	1.402	2.488
dopamine	0	0.0128	0.0718	0.29	2.089	8.029
methionine	3.09	11.45	25.10	0	2.158	36.23
2-aminophenol		n.d.			n.d.	
quinolinic acid	0.414	1.404	9.694	10.58	40.16	146
3-hydroxykynurenine		n.d.		0	0.357	3.870
tyrosine	6.721	27.86	71.30	6.013	136	849
l-isoleucine	4.924	26.46	77.95	0.106	12.69	55.82
tyramine		n.d.		0.197	4.518	139
l-leucine	10.71	57.07	120.0	1.763	33.05	158
serotonin	0	0.167	1.047	0.04	0.492	1.905
5-hydroxy-tryptophan		n.d.		0.0394	0.151	0.723
3-methoxy- <i>p</i> -tyramine		n.d.		0.0846	0.346	1.722
kynurenine	0.450	1.270	3.479	0.215	3.703	43.88
dl-phenylalanine	8.096	27.86	71.30	2.342	18.08	107
3-hydroxyanthranilic acid	0.177	0.203	0.322	0.0808	0.412	4.494
tryptophan	8.499	29.82	81.49	7.051	64.02	366
1-acetylisatin		n.d.			n.d.	
3,4-dihydroxyphenyl acetic acid	0	0.0477	73.7		n.d.	
xanthurenic acid	0.02	0.0661	0.183	0.561	5.424	36.10
kynurenic acid	0.00553	0.0185	0.167	3.334	20.38	91.75
tryptamine		n.d.		0.0272	0.449	2.467
5-methoxytryptamine		n.d.			n.d.	
5-hydroxyindole acetic acid	0.0164	0.0447	0.456	0.0268	19.68	89.54
<i>N</i> -acetyl-5-hydroxytryptamine		n.d.			n.d.	
tryptophan methyl ester		n.d.			n.d.	
homovanillic acid	0.0118	0.0782	1.0	9.313	35.58	136
indoxyl sulfate	0.0491	2.744	12.99		n.a.	
indole-3-acetamide		n.d.		0.0170	0.272	10.07
anthranilic acid		n.d.		0.0950	0.401	2.058
indole-3-lactic acid	0.0759	0.697	4.009	0.198	1.165	18.90
indole-3-carboxylic acid		n.d.		0.0305	0.0994	7.279
melatonin		n.d.			n.d.	
5-methoxyindole acetic acid		n.d.			n.d.	
indole-3-carboxaldehyde	0.0103	0.0494	0.186	0.00245	0.123	3.992
indole-3-acetonitrile	0.326	2.003	31.72	3.116	15.60	96.82
indole-3-acetic acid	0.292	1.51	23.01	6.114	30.09	205
indole-3-propionic acid	0	1.156	12.75	0.0187	0.0557	2.197

3. Discussion

3.1. Optimisation of MS Parameters and Analytical Specificity

The selection of Q and q ions was based on signal intensity, with Q ions being the most intense. In order to increase MS settling time, we selected just one qualifier ion per molecule and tried to avoid MRM transitions common to many metabolites when possible. Recently, Whiley et al. (2019) highlighted that the second transition of the TRP ¹³C-isotope shares the same MRM transition as XA (206.09 > 132.01), interfering with its quantification [51]. With our experimental setup, XA quantification was achieved by MRM transition (206.09 > 160.01) while the MRM (206.09 > 132.01) was used for qualitative purposes. Furthermore, the two peaks were chromatographically sufficiently separated, having TRP and XA RT of 4.94 and 5.03 min respectively. The MRM transition (206.09 > 160.01) was also common to ILA (RT: 6.96 min) and 5-methoxyindole-acetic acid (5-ME-IAA) (RT: 7.35 min), but the three molecules were well separated.

Similarly, *N*-acetyl-5-hydroxytryptamine (NA-5-HT) and the TRPME had the same MRM for quantification (219.2 > 160.0), but the two peaks were baseline separated, having an RT of 5.86 and 6.07 min respectively.

All the tested compounds except DOPAC and HVA contained nitrogen atoms and were easily detected as [M+H]⁺ in positive ion mode. IS contains both a nitrogen atom and a sulfate group, but a better response is obtained in negative ion mode. Therefore DOPAC, HVA and IS were detected as [M-H]⁻, by setting up polar switching within the chromatographic run.

Calibration accuracy was obtained with the use of 8 deuterated standards (Table 1). Since deuterated internal standards were not available for all the tested metabolites, and in order to limit the cost of the calibration, we opted for a) chemically related molecules (i.e., TYR-d4 for PHE, TRP-d5 for indole derivatives and DOPAC-d5 for HVA in negative ion mode) and b) molecules eluting nearby (i.e., MET-d4 for BCAAs).

3.2. Choice of Chromatographic Technique

Two analytical approaches were initially tested, based on Reversed-Phase (RP) chromatography on a Waters ACQUITY BEH C₁₈ 1.7 μm, 2.1 × 150 mm, and Hydrophilic Interaction Liquid Chromatography (HILIC) using a Waters ACQUITY BEH AMIDE 1.7 μm, 2.1 × 150 mm. HILIC was tested due to the high polarity of certain metabolites, such as GABA, VAL, ILE, LEU, TYR, MET, DA, among others. This column is widely considered to be suitable for the analysis of several other polar metabolites [52]. This column provided excellent efficiency and chromatographic resolution for separation of most polar compounds, but indole derivatives were poorly retained, hampering their separation and quantification (see Figure S1 for details).

HILIC RT stability was affected by slight pH modification and we noticed that RT shifts could appear during long acquisition sequences. Nevertheless, ammonium formate, present in both mobile phases, tends to stick on the orifice plate after desolvation, which increases the chance of source contamination and ion suppression. All these considerations made HILIC relatively less attractive for the analysis of TRP-derived metabolites in a large number of biological samples. At this point, RP chromatography was selected for further method optimisation and HILIC remained as a complementary tool for the separation of highly hydrophilic compounds.

3.3. Optimisation of Chromatography on C₁₈ Stationary Phase

Five different RP columns were tested using different elution programs: Waters ACQUITY BEH C₁₈ 1.7 μm, 2.1 × 150 mm; Waters ACQUITY HSST3 1.8 μm, 2.1 × 150 mm; Waters Cortecs UPLC C₁₈ 1.6 μm, 2.1 × 100 mm; Phenomenex Kinetex Polar C₁₈ 2.6 μm, 2.1 × 100 mm; and Phenomenex Kinetex EVO C₁₈ 2.6 μm, 2.1 × 100 mm (see Figure S2 for details).

Most polar compounds were poorly retained on 100 mm columns, even if the percentage of aqueous solvent was increased to 100%; therefore, these columns were not selected for further optimisation.

150 mm columns demonstrated the same separation efficiency, but the Waters HSST3 column was selected given that a) polar compounds are better retained, b) the critical couple of analytes ILE (RT: 2.25 min) and LEU (RT: 2.38 min) are baseline separated (Figure 2, panels A and B).

3.4. Comparison of Proposed Extraction Procedures and Analytical Performance: Efficiency and Efficacy

The efficiency and efficacy of Ostro 96-well plate and Liquid-Liquid Extraction (LLE) methods were first evaluated for an initial set of 21 key metabolites in plasma, by studying recovery and relative standard deviations (RSDs) (Table 3). The Ostro 96-well plate rapidly extracted and precipitated proteins using ice-cold ACN, containing 1% FA. To improve metabolite recovery, plates were shaken twice for 10 min before filtering; different ratios of water: ACN (1:1, *v/v*, 8:2, *v/v* and pure ACN), and the addition of FA were also tested as reconstitution solvents. According to the manufacturer's procedures, a mixture of water and MeOH were used to recover extracted metabolites. In our case, MeOH was replaced by ACN in order to a) increase retention and b) increase the selectivity and peak shapes of more polar compounds, especially those eluting in the first 3 min of the chromatographic run. Ultimately, water: ACN (8:2, *v/v*) 0.1% FA was a good compromise for metabolite recovery, peak shape and chromatographic selectivity. On the other hand, urine samples were simply diluted and filtered. In this context, the dilution factor was first studied. Urine samples were diluted five- and ten-fold in water with 0.1% FA. Five-fold dilution enabled the detection of metabolites present in low amounts as DA, but those present at high levels could saturate the detector, hampering quantification. Ten-fold dilution avoided detector saturation, while at the same time the presence of more water in the sample improved the retention of polar compounds and peak shapes.

Table 3. Recovery obtained from analysis of 21 pre-selected metabolites using LLE or Ostro 96-well plate. The selected metabolites were: GABA, 2-AM, VAL, MET, ILE, LEU, DA, 5-HT, PHE, TYR, 3-ME-TYRA, TRP, AA, 1-acetylisatin, 3-OH-AA, IACN, IAA, KA, XA, NA-5-HT, 5-OH-TRP and alpha-chloralose.

Recovery (Average = 5)	Extraction Methods	
	LLE	Ostro 96-Well plate
21 pre-selected metabolites		
<50	1	1
50–60	1	1
60–70	5	0
70–80	3	1
80–90	4	1
90–100	3	15
>100	4	2

LLE and Ostro 96-well plate methods were compared in terms of plasma recovery (Table 3). In this table, LLE and Ostro 96-well plate showed a suitable range of recovery, which in the vast majority of cases was over 60%. However, the LLE method showed relatively lower recovery rates compared to Ostro 96 well plate, ranging from 50% to 90%. Recovery was over 75% for LEU, ILE and VAL. By contrast, 5-OH-TRP and KA did not reach 65% recovery, and XA showed the lowest recovery. On the other hand, Ostro 96-well plate was able to adequately extract the selected metabolites, with 15 metabolites ranging from 90-100%, such as TRP, MET and KYN. More importantly, the recovery obtained was in an acceptable range and RSDs were below 20%. To sum up, data comparison showed that the Ostro 96-well plate method offered an appropriate range of recovery and low RSDs compared with LLE. It should be noted that this method is supposed to be routinely used within the HEALTHMARK project and thousands of samples from several clinical studies would be analysed. Therefore, in addition to the standard parameters required for a new method (sufficiently innovative and robust compared to other available methods for the intended application), here reproducibility, speed and accurate quantification are strongly required. For these reasons, the Ostro 96-well plate method was selected, since it was the most efficient and effective extraction procedure evaluated.

The combination of sample preparation with an Ostro 96-well plate and UHPLC separation with C₁₈ stationary phase was selected for further studies in order to extend the number of metabolites and validate the method.

3.5. Method Validation

The following parameters were studied for 40 metabolites related to TRP and TYR metabolism and BCAAs: linearity, LOQ, recovery, precision as repeatability and within-lab reproducibility, process efficiency and ME. Calibration curves were designed independently for plasma and urine to cover the expected metabolite concentration range according to available data, and changed accordingly after the analysis of biological samples, in order to precisely define the typical working range for each metabolite.

Linear dynamic ranges for both plasma and urine were acceptable, as the correlation coefficient was always adequate ($r^2 > 0.990$). For low level metabolites, the LOQ was in the range of a few ng/ml for both matrices, except for some compounds that behaved differently. As an example, 2-AM had a LOQ of 3.9 ng/mL in urine, while in plasma it went up to 78.1 ng/mL. For high level metabolites (BCAAs, TRP, TYR and PHE), it is not necessary to achieve an LOQ of few ng/mL and the value was set as the lowest calibration point falling within the linear range.

The use of Ostro 96-well plates with modifications enabled us to achieve satisfactory recovery, over 85% in plasma and 80% in urine spiked at low concentration. Similarly, accuracy at medium spiked concentration was excellent for both matrices, with CV being below 15%.

Several metabolites saw a decrease in recovery and poorer accuracy at low spiked concentration; this was due to the fact that spiked amounts were close to the LOQ, and analytical error may therefore be greater. The quantification of GABA was significantly deviated in both matrices. This is because GABA was not retained with our experimental setup and eluted with the chromatographic front.

We propose using data on GABA to detect fold changes rather than to provide absolute quantification. For better quantification of most polar metabolites, HILIC may still represent an appropriate method. The presence of co-eluting compounds may affect the ionization of the targeted metabolites producing ME. In this research, ME was negligible for most metabolites, ranging between 80–120% in both plasma and urine. Ion suppression by matrix components significantly affected quantification for VAL, DA, MET, QA and LEU in plasma, together with 2-AM and TYRA in urine. These metabolites are the most polar of those tested and were eluted at the beginning of the chromatographic run, before 2.5 min. Several attempts were made to improve chromatographic separation and MS response. For example, starting with 100% mobile phase A or keeping it isocratically at 95%A for a few minutes increased retention, but the peak shapes got worse, hampering integration and thus quantification. Phospholipids were efficiently removed from plasma by Ostro 96-well plates, while no significant effects were detected in urine.

Removal of matrix contaminant, together with splitting of the UHPLC flow to waste during non-acquisition time, along with good column cleaning, enabled us to acquire up to 300 samples per batch without any significant shift in RT and alteration in the MS response. This is very important in clinical applications, where simultaneous analysis of a large number of samples in the lowest number of separate batches is desirable.

3.6. Method Application

The availability of a large number of samples both for plasma (Rhineland Study) and urine (DONALD Study) allowed us to monitor the typical range of presence for each of these metabolites in two independent German populations. The method allowed the quantification of 24 out of 39 metabolites in plasma and 30 metabolites in urine (Table 2). In general, the results were in agreement with published results, despite some biological variation (Table S4).

This information is relevant for the analyst, since it allowed us to verify that the method allows quantitative analysis of 39 out of the 40 target metabolites (all of them except GABA). More detailed

analysis of multiple factors of variability influencing the concentration of these compounds is outside the scope of this paper and will be the subject of other publications.

3.7. Study Strengths and Limitations

Most of the studies available in the literature cover a limited number of metabolites related to TRP, TYR, BCAAs and gut-derived metabolites [49–51]. To achieve a full understanding of microbial metabolite–host interaction in homeostasis and diseases, we validated an analytical method for the separation and detection of 39 metabolites, targeting key branches of different metabolic pathways simultaneously, in particular those related to the microbiota-gut-brain axis [10], covering the different forms of TRP usage, simultaneously investigating serotonergic metabolism [25] and KP metabolism [22].

Our quantitative results suggest that the method is suitable for high-throughput applications in clinical studies, covering an unprecedented number of crucial metabolites in a single analysis. It represents the starting point for future research, and other metabolites of interest can be inserted as required.

The method was designed for low sample requirements, minimal sample handling and working steps, fast extraction, high sample throughput and fast instrumental analysis of 14 min per sample. Up to 384 samples (4 well plates) can be extracted by a single operator per day, and up to 96 samples can be acquired per day.

The method was independently validated on plasma and urine, in order to support multi-compartment studies, allowing direct comparison of metabolite concentrations in both biofluids.

One limitation of this study relates to pre-analytical sample management, from sample collection to handling and storage, which can affect sample quality. This issue was outside the scope of this work, but we are aware it is important for the final results [53–57]. For example, accurate measurement of 5-HT in the whole blood sample is affected by 5-HT instability and reflects platelet 5-HT [58–60]; inappropriate blood sample handling can lead to inaccurate results. To avoid these problems, we relied on standard laboratory practices to prepare samples, such as those highlighted in [57]. In this particular case, we selected fasting plasma; EDTA blood was collected and centrifuged within 10 min of collection, and aliquoted and stored at $-80\text{ }^{\circ}\text{C}$ within 2 h of collection. EDTA is commonly used as anticoagulants for the generation of platelet-free plasma [61].

Urine was collected as 24-h samples in order to obtain an overall picture of an individual's metabolic excretion and to eliminate the wide variability observed for spot urine collection. Urine pH can affect the final results; to avoid this problem urine pH was checked at sampling (pH range: 4.9–7.9) and all the samples fell within the desired range [62]. Furthermore, since the samples were stored at low temperature, urine pH was expected to be stable until the analytical phase [62].

The attention of researchers on complex interactions between gut bacteria and human brain has increased in recent years [15,16,22,25]. In 2013, the term “psychobiotics” was introduced to define beneficial bacteria that, when ingested in appropriate quantities (probiotics), exert positive effects in psychiatric patients by influencing the gut bacteria-brain-relationship [63]. This definition was then expanded to prebiotics, food components that support growth of intrinsic commensal bacteria, but this concept could be extended to any substance that “exerts a microbiome-mediated psychological effect” [64]. The psychobiotics treatment could be an interesting strategy to improve life of people suffering from psychiatric disorders but further studies are needed to facilitate its development [64,65]; our validated method can be a complementary tool to evaluate the direct effect of psychobiotics on TRP, TYR, BCAA and gut-derived metabolites.

4. Materials and Methods

4.1. Reagents and Chemicals

Gamma-aminobutyric acid (HMDB0000112), tryptamine (HMDB0000303) and l-tyrosine (HMDB0000158) were purchased from Fluka (Milan, Italy); 2-aminophenol (ChemSpider ID 5596;

PubChem CID 5801), 3,4-dihydroxyphenyl acetic acid (HMDB0001336), 3,4-dihydroxyphenyl acetic acid-d5, 3-hydroxykynurenine (HMDB0011631), 5-methoxyindole-3-acetic acid (HMDB0004096), 5-methoxytryptamine (HMDB0004095), indole-3-acetic acid (HMDB0000197), indole-3-carboxaldehyde (HMDB0029737), indole-3-carboxylic acid (HMDB0003320), indole-3-lactic acid (HMDB0000671), indole-3-propionic acid (HMDB0002302), indoxyl sulfate (HMDB0000682), kynurenine (HMDB0000684), melatonin (HMDB0001389), dl-phenylalanine (HMDB0000159), picolinic acid (HMDB0002243), tryptophan methyl ester (ChemSpider ID 70366, PubChem CID 77980) and tyramine (HMDB0000306) were purchased from Sigma (Milan, Italy); 1-acetylisatin (ChemSpider ID 10845, PubChem CID 11321), 3-hydroxyanthranilic acid (HMDB0001476), 3-methoxy-p-tyramine (HMDB0000022), 5-hydroxyindole-3-acetic acid (HMDB0000763), 5-hydroxyindole-3-acetic acid-d5, 5-hydroxy-tryptophan (HMDB0000472), anthranilic acid (HMDB0001123), dopamine (HMDB0000073), dopamine-d4, homovanillic acid (HMDB0000118), indole-3-acetamide (HMDB0029739), indole-3-acetonitrile (HMDB0006524), kynurenic acid (HMDB0000715), kynurenic acid-d5, l-isoleucine (HMDB0000172), l-leucine (HMDB0000687), l-valine (HMDB0000883), methionine (HMDB0000696), methionine-d4, N-acetyl-5-hydroxytryptamine (HMDB0001238), quinolinic acid (HMDB0000232), serotonin (HMDB0000259), serotonin-d4, l-tryptophan (HMDB0000929), l-tryptophan-d5, l-tyrosine-d4 and xanthurenic acid (HMDB0000881) were purchased from Spectra 2000 (Rome, Italy). Human citrated plasma was obtained from Sigma (Milan, Italy).

LC-MS grade acetonitrile (ACN), methanol (MeOH) and 2-propanol were purchased from Honeywell (Monza, Italy), LC-MS grade FA was purchased from Sigma (Milan, Italy). Ultrapure Milli-Q deionized water was obtained from Elix (Merck-Millipore, Milan, Italy). OSTRO 96-well plates (25 mg) were purchased from Waters (Milan, Italy). Human plasma was purchased from Sigma Aldrich (Milan, Italy).

4.2. Preparation of Stock Solution and Calibration Curves

Stock solutions (1000 mg/mL) were prepared by dissolving each standard in methanol except TYR, TYR-d4 and 3-OH-KYN, which were dissolved in 1 M HCl, KA-d5 in MeOH: DMSO 1:1 (*v/v*) and XA in DMSO. The concentration ranges are reported in Table S3.

4.3. Method Validation

4.3.1. Linearity and LOQs

Calibration standards were evaluated at 14 concentration levels, prepared with serial dilution in water with 0.1% FA. A linear polynomial model was employed with 1/X weighting factor. The method was considered linear in a specific concentration range if the correlation coefficient (r^2) was equal to or greater than 0.990. The calibration range was designed according to data available in literature, public databases (www.hmdb.ca) and from analysis of real plasma and urine samples. LOQs were calculated by estimating the calibration points with a signal-to-noise ratio (S/N) of 10.

4.3.2. Recovery, Intra- and Inter-Day Accuracy and Precision, and RT Stability

Analytical recovery was assessed by spiking standards in plasma and urine at low, medium and high concentrations according to the calibration ranges described above. The low and high concentration were set as 5-fold lower or higher than the medium values. As both matrices contained tested metabolites at a different concentration, the spiked concentration was calculated as the % of metabolite recovered compared to the spiked concentration after subtracting the average response from the blank (unspiked) sample. Calibration curves in water with 0.1% FA were used for recovery determination. See Tables S1 and S2 for further details.

Intra-day repeatability was assessed by analysing samples ($n = 5$) spiked at low, medium and high concentration for both plasma and urine within one day. Inter-day repeatability was assessed by analysing QC ($n = 5$), analysed on three separate days (1, 3 and 5). Precision is expressed as

the coefficient of the variation percentage (CV%) estimated for spiked QC, after subtracting the concentration of unspiked samples. For acceptance, CV was required to be within 15% at the medium and high concentration and within 20% at the low concentration.

4.3.3. RT Stability

RT stability was assessed by analysis of metabolites detected in 1000 plasma and 672 urine samples. For metabolites not detected in biological samples, the RT was obtained from analysis of QC spiked at medium standard concentration.

4.3.4. Analysis of Blank Samples and ME

Urine blanks (5X) were prepared as described in paragraph 4.4.1 by diluting 25 μL of sample in 225 μL of water with 0.1% FA. Plasma blanks (5X) were prepared as described in paragraph 4.4.1.2 by adding 20 μL of ACN 1% FA to 50 μL plasma instead of standard mix.

MEs were evaluated using a MMC approach. Solvent calibration slopes (SC) were compared with those obtained by fortifying the biological fluids and the deviation was calculated as follows: % of variation = (MMC slope/SC slope) \times 100. For plasma, 50 μL of sample and 20 μL of ACN 1% FA (MMC) were loaded into Ostro 96-well plates and extracted as described below. Dried samples were reconstituted in 100 μL of water/ACN (8:2, *v/v*), 0.1% FA at appropriate concentration levels. For urine, 25 μL of deionized water (SC) or urine (MMC) were diluted with 225 μL 0.1% FA spiked at appropriate levels.

4.3.5. Carryover Effect and Phospholipid Removal

The carryover effect was assessed by injecting neat ACN after the highest calibration points of SC and MMC and after the acquisition of each recovery batch.

Plasma clean up from phospholipids was addressed by performing a PIS in positive ion mode at *m/z* 184.03 (protonated phosphocholine), which is specific for PC and SM. 50 μL of plasma were directly mixed with 50 μL of water: ACN 8:2 (*v/v*), 0.1% FA in order to achieve the same dilution obtained after plasma extraction on Ostro 96-well plates. For urine, the comparison was conducted with undiluted and 10-fold diluted urine.

4.4. Extraction Procedures

4.4.1. Urine

Urine was thawed on ice and 25 μL aliquots were loaded into 96-well multfilter plates (Millipore) together with 225 μL of internal standard mix (500 ng/mL) in water with 0.1% FA. 96-well plates were shaken on a vortex for 15 sec, and subsequently filtered using a positive pressure-96 manifold (Waters). Samples were collected in 350 μL 96-well plates and kept at $-80\text{ }^{\circ}\text{C}$ until analysis.

Plasma

Plasma aliquots (50 μL) were loaded onto an Ostro 96-well plate (Waters, Milan, Italy) and 20 μL of internal standard mix in ACN 1% FA (500 ng/mL) were added. Protein precipitation and metabolite extraction were performed by adding 150 μL of ice-cold ACN 1% FA. Plates were covered, vortexed for 15 sec and placed on an Eppendorf shaker for 10 min at 500 rpm (Eppendorf, Milan, Italy), then filtered using a positive pressure-96 manifold (Waters). The extraction procedure was repeated by adding 150 μL of ice-cold ACN 1% FA. Extracts were brought to dryness with a gentle stream of nitrogen at $37\text{ }^{\circ}\text{C}$ using a Techne Dr-block DB 3D heater, re-dissolved in 100 μL of water: ACN 8:2 0.1 % FA and transferred into 350 μL 96-well plates, kept at $-80\text{ }^{\circ}\text{C}$ until analysis.

LLE of Urine and Plasma

100 μ L of plasma or urine were extracted using 200 μ L of ice-cold ACN containing internal standards. The mixtures were first shaken for 30 min at 500 rpm (5 °C). Then, mixtures were stored 1 h at -20 °C to improve protein precipitation and then centrifuged at 17,968 g (14000 rpm) for 15 min at 4 °C. Afterwards, the supernatants were collected and stored at -80 °C until analysis. The supernatants were directly injected.

4.5. Ultra High Performance Liquid Chromatography-Electrospray Ionization-Triple Quadrupole-Mass Spectrometry (UHPLC-ESI-QqQ-MS)

Detection was performed on a Waters[®] Xevo TQ MS Triple Quadrupole equipped with ESI source and coupled online with an Acquity UHPLC (Waters, Milford, MA, USA). The MS operated in positive ionization mode, setting the capillary at 270 °C, the source at 300 °C and source voltage at 3 kV. Detection of IS, DOPAC, DOPAC-d5 and HVA were performed in negative ion mode in the same run by setting polarity switching. Ultra-high purity argon was used as collision gas. MS and MS/MS conditions were optimised via software (Intellistart, Waters, Milford, MA, USA) by infusing analytical standards.

4.5.1. RP C₁₈ Chromatography

Chromatographic separation was performed using a Water UPLC HSST3 (1.8 μ m, 2.1 \times 150 mm, 100 A pore diameter) purchased from Waters (Milan, Italy). Mobile phase A was water with 0.1% FA, B was ACN 0.1% FA. The gradient started with 5% B and was maintained for 0.5 min; then % B was increased to 10% at 2.5 min, 15% at 3.5 min, 25% at 4.5 min, 35% at 5.5 min, 45% at 6.5 min, 55% at 7 min and then to 100%B at 7.5 min. Final conditions were retained for 3 min and the column was re-equilibrated to the initial conditions for 4 min. The total run time including column re-equilibration was 14 min. The flow rate was 0.3 mL/min, the injection volume was 2 μ L and the column oven was set at 40 °C. The weak and strong solvent washes were water: MeOH (9:1, *v/v*) and water: ACN: MeOH: 2-propanol (1:1:1:1, *v/v/v/v*) respectively. Data were acquired and processed with Mass Lynx 4.1 software (Waters).

4.5.2. HILIC Chromatography

A Waters ACQUITY BEH AMIDE 1.7 μ m, 2.1 \times 150 mm analytical column was used. The mobile phases consisted of (A) 10 mM ammonium formate and 0.2% FA in water: ACN (1:1, *v/v*), and (B) 10 mM ammonium formate and 0.2% FA in water: ACN (5:95, *v/v*). A multi-step elution gradient was developed as follows, at a flow rate of 0.5 mL/min: at 0.0 min, 100% B a gradient up to 4.0 min, 90% B; then %B was decreased to 70% at 8.0 min, 60% at min 9.0, 50% at min 9.5 and maintained isocratically until min 11.0. Lastly, a reconditioning period up to 1.5 min at 100% B was used. The sample injection volume was 5 μ L and the autosampler temperature was kept at 5 °C. The weak and strong solvent washes were water: ACN: MeOH: 2-propanol (1:1:1:1, *v/v/v/v*) and water: MeOH (9:1, *v/v*) respectively.

4.6. Method Application to Biological Samples

This analysis was carried out as part of the European Joint Programming Initiative, “A Healthy Diet for a Healthy Life” Metabolic HEALTH through Nutrition, Microbiota and Tryptophan bioMARKers (HEALTHMARK) project. The project aims to investigate the complex associations between microbiota and microbiota-derived bioactives of the TRP metabolism, diet and metabolic health. The applicability of the method was assessed by analysis of 24-h urine ($n = 672$, mean age of 16 years with 50.5% males and 49.5% females) collected within the DONALD study and of plasma samples ($n = 1000$) obtained from adults (age ≥ 30 years) collected within the Rhineland study. Data were analysed using Statistica v. 13.3 (TIBCO Software Inc., Palo Alto, CA, USA).

4.6.1. The DONALD Study

The DONALD study is an ongoing, open cohort study conducted in Dortmund, Germany by the Unit of Nutritional Epidemiology, Department of Nutrition and Food Sciences, University of Bonn, Bonn, Germany. This study has collected data on the diet, growth, development and metabolism of apparently healthy children and adolescents since 1985. Children are enrolled at 3 months of age. The collection of 24-h urine samples is part of the annual assessments as soon as the children can provide the samples. The pre-analytical urine pH range was between 4.9 and 7.9, therefore suitable for metabolite quantification [62]. All samples were stored at $-22\text{ }^{\circ}\text{C}$ without the addition of preservatives or chemicals and then at $-80\text{ }^{\circ}\text{C}$ until laboratory analysis. Further details on the DONALD study [66] and urine collection and storage [67] have been described elsewhere. The DONALD study was approved by the Ethics Committee of the University of Bonn according to the guidelines of the Declaration of Helsinki (approval number 098/06). Written consent was obtained from parents and later on from study participants.

4.6.2. The Rhineland Study

The Rhineland Study is an ongoing community-based cohort study in which all inhabitants of two geographically defined areas in the city of Bonn, Germany aged 30–100 years are being invited to participate. Persons living in these areas are predominantly German with Caucasian ethnicity. Participation in the study is possible by invitation only. The only exclusion criterion is insufficient German language skills to give informed consent. Approval to undertake the study was obtained from the ethics committee of the University of Bonn, Medical Faculty (approval number 338/15). All participants gave written informed consent.

Fasting blood was collected from all participants between 7:00 and 9:30 am, including $2 \times 10\text{ mL}$ EDTA blood (EDTA Vacutainer K2), an anticoagulant commonly used for the generation of platelet-free plasma. Plasma is centrifuged for 10 min at $2000 \times g$ at $20\text{ }^{\circ}\text{C}$ within 10 min of blood collection; centrifuge brake is set on off to avoid platelet activation. Automated aliquoting of the plasma takes place within less than 35 min after centrifugation into $500\text{ }\mu\text{L}$ aliquots (Hamilton Microlab Star). All aliquots are directly cooled ($10\text{ }^{\circ}\text{C}$) during the process and are placed into a chest freezer ($-80\text{ }^{\circ}\text{C}$) within less than 45 min after aliquoting. Time points of blood withdrawal, centrifugation, aliquoting and freezing time are documented in the laboratory information management system (LIMS).

5. Conclusions

A UHPLC-ESI-QqQ-MS method was developed for high-throughput, accurate quantification of 39 metabolites related to TRP, TYR, BCAAs and several gut-derived metabolites. The inclusion of a large number of known metabolites, whose concentration is driven by microbial metabolite–host interaction, provided a new metabolomic profiling method suitable for supporting clinical investigation of several important biological questions and opening up new possibilities for nutritional studies aimed at understanding and preventing disease.

Metabolite extraction from plasma was designed on Ostro 96-well plates in order to ensure protein precipitation, lipid removal and good metabolite recovery. For urine, we opted for filtration and 10-fold dilution in order to ensure the simultaneous analysis of metabolites present in different concentration ranges.

The new method was then tested on a large number of real human plasma and urine samples obtained from two main observational and epidemiological studies across the lifespan. This allowed us to estimate the typical working concentration range for each analyte, and to verify that application of the method to real samples representative of Central Europe subpopulations falls within the validation conditions of the method.

Supplementary Materials: The following are available online at <http://www.mdpi.com/2218-1989/9/11/261/s1>. Table S1: Calibration curve range of linearity, coefficient of correlation, limit of quantification, LOQ, matrix effect and retention time stability in plasma and urine; Table S2: Recovery and precision at low, medium and high spiked concentrations in plasma and urine; Table S3: stock solution and spiked concentrations (low, medium and high) used for recovery and precision assays in plasma and urine. Table S4: Metabolite concentration ranges detected in plasma and urine compared to reference data. Figure S1: Chromatogram of 13 standard compounds obtained with RP and HILIC chromatography. Figure S2: Chromatogram of the most polar metabolites obtained on five different C₁₈ analytical columns.

Author Contributions: Individual contributions to this manuscript are as follows: responsible for the study design: F.M. (metabolomics); U.N. (DONALD Study); M.M.B.B. (Rhineland Study); conceptualization (metabolomics): A.A. and J.R.; (DONALD Study): K.O.; (Rhineland Study) X.O.-R.; methodology: A.A. (RP chromatography), J.R. (HILIC) and F.M.; data analysis A.A.; data interpretation; A.A., J.R., K.O., X.O.-R., U.N., M.M.B.B. and F.M.; writing-original draft preparation: A.A., J.R., F.M.; writing- review and editing, final approval: A.A., J.R., K.O., X.O.-R., U.N., M.M.B.B. and F.M.; project administration: U.M., M.M.B.B. and F.M.; funding acquisition: U.M., M.M.B.B. and F.M.

Funding: This work was supported through the JPI HDHL on “Biomarkers for Nutrition and Health”, ‘HEALTHMARK’; by the following national funding organisations: Ministry of Education, University and Research (MIUR), Italy (CUP D43C17000100006), Federal Ministry of Education and Research, Germany (grant numbers 01EA1705A and 01EA1705B) and Diet-Body-Brain (DietBB) the Competence Cluster in Nutrition Research funded by the Federal Ministry of Education and Research (FKZ 01EA1809C).

Acknowledgments: We thank Vivienne Frankell for English editing.

Conflicts of Interest: The authors declare no conflict of interest. The funders had no role in the design of the study, the collection, analysis or interpretation of data, the writing of the manuscript or the decision to publish the results.

References

- Carey, M.; Small, H.; Yoong, S.L.; Boyes, A.; Bisquera, A.; Sanson-Fisher, R. Prevalence of comorbid depression and obesity in general practice: A cross-sectional survey. *Br. J. Gen. Pract.* **2014**, *64*, e122–e127. [[CrossRef](#)]
- Jantaratnotai, N.; Mosikanon, K.; Lee, Y.; McIntyre, R.S. The interface of depression and obesity. *Obes. Res. Clin. Pract.* **2017**, *11*, 1–10. [[CrossRef](#)] [[PubMed](#)]
- O’Mahony, S.M.; Marchesi, J.R.; Scully, P.; Codling, C.; Ceolho, A.-M.; Quigley, E.M.M.; Cryan, J.F.; Dinan, T.G. Early Life Stress Alters Behavior, Immunity, and Microbiota in Rats: Implications for Irritable Bowel Syndrome and Psychiatric Illnesses. *Biol. Psychiatry* **2009**, *65*, 263–267. [[CrossRef](#)]
- Lee, S.P.; Sung, I.-K.; Kim, J.H.; Lee, S.-Y.; Park, H.S.; Shim, C.S. The effect of emotional stress and depression on the prevalence of digestive diseases. *J. Neurogastroenterol. Motil.* **2015**, *21*, 273–282. [[CrossRef](#)]
- Walter, F.M.; Emery, J.D.; Mendonca, S.; Hall, N.; Morris, H.C.; Mills, K.; Dobson, C.; Bankhead, C.; Johnson, M.; Abel, G.A.; et al. Symptoms and patient factors associated with longer time to diagnosis for colorectal cancer: Results from a prospective cohort study. *Br. J. Cancer* **2016**, *115*, 533–541. [[CrossRef](#)]
- Mosher, C.E.; Winger, J.G.; Given, B.A.; Helft, P.R.; O’Neil, B.H. Mental health outcomes during colorectal cancer survivorship: A review of the literature. *Psychooncology* **2016**, *25*, 1261–1270. [[CrossRef](#)]
- Walker, J.; Hansen, C.H.; Martin, P.; Symeonides, S.; Ramessur, R.; Murray, G.; Sharpe, M. Prevalence, associations, and adequacy of treatment of major depression in patients with cancer: A cross-sectional analysis of routinely collected clinical data. *Lancet Psychiatry* **2014**, *1*, 343–350. [[CrossRef](#)]
- Gigic, B.; Boeing, H.; Toth, R.; Böhm, J.; Habermann, N.; Scherer, D.; Schrotz-King, P.; Abbenhardt-Martin, C.; Skender, S.; Brenner, H.; et al. Associations between dietary patterns and longitudinal quality of life changes in colorectal cancer patients: The colocale study. *Nutr. Cancer* **2018**, *70*, 51–60. [[CrossRef](#)]
- Song, M.; Garrett, W.S.; Chan, A.T. Nutrients, Foods, and Colorectal Cancer Prevention. *Gastroenterology* **2015**, *148*, 1244–1260.e16. [[CrossRef](#)]
- Yano, J.M.; Yu, K.; Donaldson, G.P.; Shastri, G.G.; Ann, P.; Ma, L.; Nagler, C.R.; Ismagilov, R.F.; Mazmanian, S.K.; Hsiao, E.Y. Indigenous bacteria from the gut microbiota regulate host serotonin biosynthesis. *Cell* **2015**, *161*, 264–276. [[CrossRef](#)]
- Bellono, N.W.; Bayrer, J.R.; Leitch, D.B.; Castro, J.; Zhang, C.; O’Donnell, T.A.; Brierley, S.M.; Ingraham, H.A.; Julius, D. Enterochromaffin Cells Are Gut Chemosensors that Couple to Sensory Neural Pathways. *Cell* **2017**, *170*, 185–198.e16. [[CrossRef](#)] [[PubMed](#)]

12. Marchesi, J.R.; Adams, D.H.; Fava, F.; Hermes, G.D.A.; Hirschfield, G.M.; Hold, G.; Quraishi, M.N.; Kinross, J.; Smidt, H.; Tuohy, K.M.; et al. The gut microbiota and host health: A new clinical frontier. *Gut* **2016**, *65*, 330–339. [[CrossRef](#)] [[PubMed](#)]
13. Kaelberer, M.M.; Buchanan, K.L.; Klein, M.E.; Barth, B.B.; Montoya, M.M.; Shen, X.; Bohórquez, D.V. A gut-brain neural circuit for nutrient sensory transduction. *Science* **2018**, *361*. [[CrossRef](#)] [[PubMed](#)]
14. Golubeva, A.V.; Joyce, S.A.; Moloney, G.; Burokas, A.; Sherwin, E.; Arbolea, S.; Flynn, I.; Khochanskiy, D.; Moya-Pérez, A.; Peterson, V.; et al. Microbiota-related Changes in Bile Acid & Tryptophan Metabolism are Associated with Gastrointestinal Dysfunction in a Mouse Model of Autism. *EBioMedicine* **2017**, *24*, 166–178. [[CrossRef](#)]
15. Dinan, T.G.; Cryan, J.F. Gut-brain axis in 2016: Brain-gut-microbiota axis-mood, metabolism and behaviour. *Nat. Rev. Gastroenterol. Hepatol.* **2017**, *14*, 69–70. [[CrossRef](#)]
16. Dinan, T.G.; Cryan, J.F. The Microbiome-Gut-Brain Axis in Health and Disease. *Gastroenterol. Clin. N. Am.* **2017**, *46*, 77–89. [[CrossRef](#)]
17. Kelly, J.R.; Borre, Y.; O’ Brien, C.; Patterson, E.; El Aidy, S.; Deane, J.; Kennedy, P.J.; Beers, S.; Scott, K.; Moloney, G.; et al. Transferring the blues: Depression-associated gut microbiota induces neurobehavioural changes in the rat. *J. Psychiatr. Res.* **2016**, *82*, 109–118. [[CrossRef](#)]
18. Agus, A.; Planchais, J.; Sokol, H. Review Gut Microbiota Regulation of Tryptophan Metabolism in Health and Disease. *Cell Host Microbe* **2018**, *23*, 716–724. [[CrossRef](#)]
19. Valles-Colomer, M.; Falony, G.; Darzi, Y.; Tigchelaar, E.F.; Wang, J.; Tito, R.Y.; Schiweck, C.; Kurilshikov, A.; Joossens, M.; Wijnemga, C.; et al. The neuroactive potential of the human gut microbiota in quality of life and depression. *Nat. Microbiol.* **2019**, *4*, 623–632. [[CrossRef](#)]
20. Cervenka, I.; Agudelo, L.Z.; Ruas, J.L. Kynurenines: Tryptophan’s metabolites in exercise, inflammation, and mental health. *Science* **2017**, *357*. [[CrossRef](#)]
21. Nikolaus, S.; Schulte, B.; Al-Massad, N.; Thieme, F.; Schulte, D.M.; Bethge, J.; Rehman, A.; Tran, F.; Aden, K.; Häslér, R.; et al. Increased Tryptophan Metabolism Is Associated with Activity of Inflammatory Bowel Diseases. *Gastroenterology* **2017**, *153*, 1504–1516.e2. [[CrossRef](#)] [[PubMed](#)]
22. Kennedy, P.J.; Cryan, J.F.; Dinan, T.G.; Clarke, G. Kynurenine pathway metabolism and the microbiota-gut-brain axis. *Neuropharmacology* **2017**, *112*, 399–412. [[CrossRef](#)] [[PubMed](#)]
23. Badawy, A.A.B. Kynurenine pathway of tryptophan metabolism: Regulatory and functional aspects. *Int. J. Tryptophan Res.* **2017**, *10*. [[CrossRef](#)] [[PubMed](#)]
24. Crotti, S.; D’ Angelo, E.; Bedin, C.; Fassan, M.; Pucciarelli, S.; Nitti, D.; Bertazzo, A.; Agostini, M. Tryptophan metabolism along the kynurenine and serotonin pathways reveals substantial differences in colon and rectal cancer. *Metabolomics* **2017**, *13*. [[CrossRef](#)]
25. O’Mahony, S.M.; Clarke, G.; Borre, Y.E.; Dinan, T.G.; Cryan, J.F. Serotonin, tryptophan metabolism and the brain-gut-microbiome axis. *Behav. Brain Res.* **2015**, *277*, 32–48. [[CrossRef](#)]
26. Zhang, L.S.; Davies, S.S. Microbial metabolism of dietary components to bioactive metabolites: Opportunities for new therapeutic interventions. *Genome Med.* **2016**, *8*, 1–18. [[CrossRef](#)]
27. Bansal, T.; Alaniz, R.C.; Wood, T.K.; Jayaraman, A. The bacterial signal indole increases epithelial-cell tight-junction resistance and attenuates indicators of inflammation. *Proc. Natl. Acad. Sci. USA* **2010**, *107*, 228–233. [[CrossRef](#)]
28. Shimada, Y.; Kinoshita, M.; Harada, K.; Mizutani, M.; Masahata, K.; Kayama, H.; Takeda, K. Commensal bacteria-dependent indole production enhances epithelial barrier function in the colon. *PLoS ONE* **2013**, *8*, e80604. [[CrossRef](#)]
29. Dou, L.; Jourde-Chiche, N.; Faure, V.; Cerini, C.; Berland, Y.; Dignat-George, F.; Brunet, P. The uremic solute indoxyl sulfate induces oxidative stress in endothelial cells. *J. Thromb. Haemost.* **2007**, *5*, 1302–1308. [[CrossRef](#)]
30. Lin, C.J.; Chen, H.H.; Pan, C.F.; Chuang, C.K.; Wang, T.J.; Sun, F.J.; Wu, C.J. P-Cresylsulfate and Indoxyl Sulfate Level At Different Stages of Chronic Kidney Disease. *J. Clin. Lab. Anal.* **2011**, *25*, 191–197. [[CrossRef](#)]

31. Chyan, Y.-J.; Poeggeler, B.; Omar, R.A.; Chain, D.G.; Frangione, B.; Ghiso, J.; Pappolla, M.A. Potent Neuroprotective Properties against the Alzheimer β -Amyloid by an Endogenous Melatonin-related Indole Structure, Indole-3-propionic Acid. *J. Biol. Chem.* **1999**, *274*, 21937–21942. [[CrossRef](#)] [[PubMed](#)]
32. Venkatesh, M.; Mukherjee, S.; Wang, H.; Li, H.; Sun, K.; Benechet, A.P.; Qiu, Z.; Maher, L.; Redinbo, M.R.; Phillips, R.S.; et al. Symbiotic Bacterial Metabolites Regulate Gastrointestinal Barrier Function via the Xenobiotic Sensor PXR and Toll-like Receptor 4. *Immunity* **2014**, *41*, 296–310. [[CrossRef](#)] [[PubMed](#)]
33. Dodd, D.; Spitzer, M.H.; Van Treuren, W.; Merrill, B.D.; Hryckowian, A.J.; Higginbottom, S.K.; Le, A.; Cowan, T.M.; Nolan, G.P.; Fischbach, M.A.; et al. A gut bacterial pathway metabolizes aromatic amino acids into nine circulating metabolites. *Nature* **2017**, *551*, 648–652. [[CrossRef](#)] [[PubMed](#)]
34. Aragozzini, F.; Ferrari, A.; Pacini, N.; Gualandris, R. Indole-3-lactic acid as a tryptophan metabolite produced by *Bifidobacterium* spp. *Appl. Environ. Microbiol.* **1979**, *38*, 544–546.
35. Manna, S.K.; Patterson, A.D.; Yang, Q.; Krausz, K.W.; Idle, J.R.; Fornace, A.J.; Gonzalez, F.J. UPLC-MS-based urine metabolomics reveals indole-3-lactic acid and phenyllactic acid as conserved biomarkers for alcohol-induced liver disease in the Ppara-null mouse model. *J. Proteome Res.* **2011**, *10*, 4120–4133. [[CrossRef](#)]
36. Zelante, T.; Iannitti, R.G.; Cunha, C.; DeLuca, A.; Giovannini, G.; Pieraccini, G.; Zecchi, R.; D'Angelo, C.; Massi-Benedetti, C.; Fallarino, F.; et al. Tryptophan catabolites from microbiota engage aryl hydrocarbon receptor and balance mucosal reactivity via interleukin-22. *Immunity* **2013**, *39*, 372–385. [[CrossRef](#)]
37. Nie, C.; He, T.; Zhang, W.; Zhang, G.; Ma, X. Branched chain amino acids: Beyond nutrition metabolism. *Int. J. Mol. Sci.* **2018**, *19*, 954. [[CrossRef](#)]
38. Shoaie, S.; Ghaffari, P.; Kovatcheva-Datchary, P.; Mardinoglu, A.; Sen, P.; Pujos-Guillot, E.; De Wouters, T.; Juste, C.; Rizkalla, S.; Chilloux, J.; et al. Quantifying Diet-Induced Metabolic Changes of the Human Gut Microbiome. *Cell Metab.* **2015**, *22*, 320–331. [[CrossRef](#)]
39. Baranyi, A.; Amouzadeh-Ghadikolai, O.; von Lewinski, D.; Rothenhäusler, H.-B.; Theokas, S.; Robier, C.; Mange, H.; Reicht, G.; Hlade, P.; Meinitzer, A. Branched-Chain Amino Acids as New Biomarkers of Major Depression – A Novel Neurobiology of Mood Disorder. *PLoS ONE* **2016**, *11*, e0160542. [[CrossRef](#)]
40. Delphan, M.; Lin, T.; Liesenfeld, D.B.; Nattenmüller, J.; Böhm, J.T.; Gigic, B.; Habermann, N.; Zielske, L.; Schrotz-King, P.; Schneider, M.; et al. Associations of branched-chain amino acids with parameters of energy balance and survival in colorectal cancer patients: results from the ColoCare study. *Metabolomics* **2018**, *14*. [[CrossRef](#)]
41. Morita, I.; Kawamoto, M.; Hattori, M.; Eguchi, K.; Sekiba, K.; Yoshida, H. Determination of tryptophan and its metabolites in human plasma and serum by high-performance liquid chromatography with automated sample clean-up system. *J. Chromatogr. B Biomed. Sci. Appl.* **1990**, *526*, 367–374. [[CrossRef](#)]
42. Huang, Y.; Louie, A.; Yang, Q.; Massenkoff, N.; Xu, C.; Hunt, P.W.; Gee, W. A simple LC-MS/MS method for determination of kynurenine and tryptophan concentrations in human plasma from HIV-infected patients. *Bioanalysis* **2013**, *5*, 1397–1407. [[CrossRef](#)] [[PubMed](#)]
43. Chen, J.; Hou, W.; Han, B.; Liu, G.; Gong, J.; Li, Y.; Zhong, D.; Liao, Q.; Xie, Z. Target-based metabolomics for the quantitative measurement of 37 pathway metabolites in rat brain and serum using hydrophilic interaction ultra-high-performance liquid chromatography-tandem mass spectrometry. *Anal. Bioanal. Chem.* **2016**, *408*, 2527–2542. [[CrossRef](#)] [[PubMed](#)]
44. Fuertig, R.; Ceci, A.; Camus, S.M.; Bezar, E.; Luippold, A.H.; Hengerer, B. LC-MS/MS-based quantification of kynurenine metabolites, tryptophan, monoamines and neopterin in plasma, cerebrospinal fluid and brain. *Bioanalysis* **2016**, *8*, 1903–1917. [[CrossRef](#)]
45. Hu, L.J.; Li, X.F.; Hu, J.Q.; Ni, X.J.; Lu, H.Y.; Wang, J.J.; Huang, X.N.; Lin, C.X.; Shang, D.W.; Wen, Y.G. A Simple HPLC-MS/MS method for determination of tryptophan, kynurenine and kynurenic acid in human serum and its potential for monitoring antidepressant therapy. *J. Anal. Toxicol.* **2017**, *41*, 37–44. [[CrossRef](#)]
46. Torii, Y.; Kawano, Y.; Sato, H.; Fujimori, T.; Sasaki, K.; Kawada, J.I.; Takikawa, O.; Lim, C.K.; Guillemain, G.J.; Ohashi, Y.; et al. Metabolome analysis reveals the association between the kynurenine pathway and human herpesvirus 6 encephalopathy in immunocompetent children. *Metabolomics* **2017**, *13*, 1–10. [[CrossRef](#)]

47. Miller, D.; Tan, L.; Dorshorst, D.; Morrissey, K.; Mahrus, S.; Milanowski, D.; McKnight, J.; Cape, S.; Dean, B.; Liang, X. A validated surrogate analyte LC-MS/MS assay for quantitation of endogenous kynurenine and tryptophan in human plasma. *Bioanalysis* **2018**, *10*, 1307–1317. [[CrossRef](#)]
48. Wang, W.; Zhuang, X.; Liu, W.; Dong, L.; Sun, H.; Du, G.; Ye, L. Determination of kynurenine and tryptophan, biomarkers of indoleamine 2,3-dioxygenase by LC-MS/MS in plasma and tumor. *Bioanalysis* **2018**, *10*, 1335–1344. [[CrossRef](#)]
49. Zhu, W.; Stevens, A.P.; Dettmer, K.; Gottfried, E.; Hoves, S.; Kreutz, M.; Holler, E.; Canelas, A.B.; Kema, I.; Oefner, P.J. Quantitative profiling of tryptophan metabolites in serum, urine, and cell culture supernatants by liquid chromatography-tandem mass spectrometry. *Anal. Bioanal. Chem.* **2011**, *401*, 3249–3261. [[CrossRef](#)]
50. Marcos, J.; Renau, N.; Valverde, O.; Aznar-Laín, G.; Gracia-Rubio, I.; Gonzalez-Sepulveda, M.; Pérez-Jurado, L.A.; Ventura, R.; Segura, J.; Pozo, O.J. Targeting tryptophan and tyrosine metabolism by liquid chromatography tandem mass spectrometry. *J. Chromatogr. A* **2016**, *1434*, 91–101. [[CrossRef](#)]
51. Whiley, L.; Nye, L.C.; Grant, I.; Andreas, N.; Chappell, K.E.; Sarafian, M.H.; Misra, R.; Plumb, R.S.; Lewis, M.R.; Nicholson, J.K.; et al. Ultrahigh-Performance Liquid Chromatography Tandem Mass Spectrometry with Electrospray Ionization Quantification of Tryptophan Metabolites and Markers of Gut Health in Serum and Plasma—Application to Clinical and Epidemiology Cohorts. *Anal. Chem.* **2019**, *91*, 5207–5216. [[CrossRef](#)] [[PubMed](#)]
52. Gika, H.G.; Theodoridis, G.A.; Vrhovsek, U.; Mattivi, F. Quantitative profiling of polar primary metabolites using hydrophilic interaction ultrahigh performance liquid chromatography-tandem mass spectrometry. *J. Chromatogr. A* **2012**, *1259*, 121–127. [[CrossRef](#)] [[PubMed](#)]
53. Guder, W.G. Preanalytical factors and their influence on analytical quality specifications. *Scand. J. Clin. Lab. Investig.* **1999**, *59*, 545–549. [[CrossRef](#)] [[PubMed](#)]
54. Zhang, A.; Sun, H.; Wang, P.; Han, Y.; Wang, X. Recent and potential developments of biofluid analyses in metabolomics. *J. Proteomics* **2012**, *75*, 1079–1088. [[CrossRef](#)] [[PubMed](#)]
55. Yin, P.; Peter, A.; Franken, H.; Zhao, X.; Neukamm, S.S.; Rosenbaum, L.; Lucio, M.; Zell, A.; Häring, H.U.; Xu, G.; et al. Preanalytical aspects and sample quality assessment in metabolomics studies of human blood. *Clin. Chem.* **2013**, *59*, 833–845. [[CrossRef](#)]
56. Lima-Oliveira, G.; Volanski, W.; Lippi, G.; Picheth, G.; Guidi, G.C. Pre-analytical phase management: A review of the procedures from patient preparation to laboratory analysis. *Scand. J. Clin. Lab. Investig.* **2017**, *77*, 153–163. [[CrossRef](#)]
57. Ulaszewska, M.M.; Weinert, C.H.; Trimigno, A.; Portmann, R.; Andres Lacueva, C.; Badertscher, R.; Brennan, L.; Brunius, C.; Bub, A.; Capozzi, F.; et al. Nutrimetabolomics: An Integrative Action for Metabolomic Analyses in Human Nutritional Studies. *Mol. Nutr. Food Res.* **2019**, *63*, 1–38. [[CrossRef](#)]
58. Kema, I.P.; De Vries, E.G.E.; Schellings, A.M.J.; Postmus, P.E.; Muskiet, F.A.J. Improved diagnosis of carcinoid tumors by measurement of platelet serotonin. *Clin. Chem.* **1992**, *38*, 534–540.
59. Xiao, R.; Beck, O.; Hjemdahl, P. On the accurate measurement of serotonin in whole blood. *Scand. J. Clin. Lab. Investig.* **1998**, *58*, 505–510. [[CrossRef](#)]
60. Carling, R.S.; Degg, T.J.; Allen, K.R.; Bax, N.D.S.; Barth, J.H. Evaluation of whole blood serotonin and plasma and urine 5-hydroxyindole acetic acid in diagnosis of carcinoid disease. *Ann. Clin. Biochem.* **2002**, *39*, 577–582. [[CrossRef](#)]
61. Bowen, R.A.R.; Remaley, A.T. Interferences from blood collection tube components on clinical chemistry assays. *Biochem. Med.* **2014**, *24*, 31–44. [[CrossRef](#)]
62. Cook, J.D.; Strauss, K.A.; Caplan, Y.H.; LoDico, C.P.; Bush, D.M. Urine pH: The effects of time and temperature after collection. *J. Anal. Toxicol.* **2007**, *31*, 486–496. [[CrossRef](#)]
63. Dinan, T.G.; Stanton, C.; Cryan, J.F. Psychobiotics: A novel class of psychotropic. *Biol. Psychiatry* **2013**, *74*, 720–726. [[CrossRef](#)]
64. Sarkar, A.; Lehto, S.M.; Harty, S.; Dinan, T.G.; Cryan, J.F.; Burnet, P.W.J. Psychobiotics and the Manipulation of Bacteria–Gut–Brain Signals. *Trends Neurosci.* **2016**, *39*, 763–781. [[CrossRef](#)]
65. Cheng, L.H.; Liu, Y.W.; Wu, C.C.; Wang, S.; Tsai, Y.C. Psychobiotics in mental health, neurodegenerative and neurodevelopmental disorders. *J. Food Drug Anal.* **2019**, *27*, 632–648. [[CrossRef](#)]

66. Buyken, A.E.; Alexy, U.; Kersting, M.; Remer, T. Die DONALD Kohorte: Ein aktueller Überblick zu 25 Jahren Forschung im Rahmen der Dortmund Nutritional and Anthropometric Longitudinally Designed Study. *Bundesgesundheitsblatt Gesundheitsforsch. Gesundheitsschutz* **2012**, *55*, 875–884. [[CrossRef](#)]
67. Remer, T.; Neubert, A.; Maser-Gluth, C. Anthropometry-based reference values for 24-h urinary creatinine excretion during growth and their use in endocrine and nutritional research. *Am. J. Clin. Nutr.* **2002**, *75*, 561–569. [[CrossRef](#)]



© 2019 by the authors. Licensee MDPI, Basel, Switzerland. This article is an open access article distributed under the terms and conditions of the Creative Commons Attribution (CC BY) license (<http://creativecommons.org/licenses/by/4.0/>).

3.3 Association of abdominal MRI visceral and subcutaneous adipose tissue with cardiometabolic risk markers and their comparison with anthropometric measurements (Submitted)

Ximena Orozco-Ruiz¹, Santiago Estrada^{1,2}, Martin Reuter^{2,3,4}, Monique M.B. Breteler^{1,4,5}

¹ Population Health Sciences, German Center for Neurodegenerative Diseases (DZNE), Bonn, Germany.

² Image analysis, German Center for Neurodegenerative Diseases (DZNE), Bonn, Germany.

³ A.A. Martinos Center for Biomedical Imaging, Massachusetts General Hospital, Boston MA, USA.

⁴ Department of Radiology, Harvard Medical School, Boston MA, USA.

⁵ Institute for Medical Biometry, Informatics and Epidemiology (IMBIE), Faculty of Medicine, University of Bonn, Bonn, Germany.

Keywords: Visceral adipose tissue, subcutaneous adipose tissue, magnetic resonance imaging, anthropometric measurements, cardiometabolic risk markers.

Corresponding Author:

Monique M.B. Breteler, MD, PhD

German Center for Neurodegenerative Diseases (DZNE)

Venusberg Campus 1/ 99, 53127 Bonn

Tel: +49-22843302-929

Mail: monique.breteler@dzne.de

Abstract

Objective: This study aimed to assess the relationships of subcutaneous and visceral adipose tissue (aSAT and aVAT) with anthropometric measurements and compare their respective associations with cardiometabolic risk markers.

Methods: We included 3350 participants from the population-based Rhineland Study. Volumes of aSAT and aVAT were assessed with magnetic resonance imaging. Anthropometric measurements included body mass index (BMI), waist circumference (WC), waist-to-hip ratio (WHR), and waist-to-height ratio (WHtR). We used markers of blood lipids, glucose metabolism, inflammation, and systolic blood pressure (SBP) to assess cardiometabolic risk.

Results: Among anthropometric measurements, BMI had the strongest correlation with aSAT and WC with aVAT. Larger aVAT had a stronger association with cardiometabolic risk markers than aSAT in women ($P < 0.001$), except for SBP. In men, the associations of aVAT were significantly weaker than in women and not different from aSAT, except for insulin. The associations of anthropometric measurements with cardiometabolic risk markers largely improved by adding aVAT.

Conclusions: In women, larger aVAT volumes are more metabolically detrimental than larger aSAT. In men, aSAT and aVAT are associated with cardiometabolic risk markers to a similar extent. Although WC is higher correlated with aVAT than BMI, aVAT was the best predictor of cardiometabolic risk markers

Introduction

Obesity is one of the major risk factors for cardiovascular diseases (CVD) and mortality (1) and its prevalence is increasing worldwide (2). The World Health Organization (WHO) defines obesity as an excessive fat accumulation in the adipose tissue that impairs health. Obesity is traditionally evaluated using body mass index (BMI) (3). However, BMI can neither distinguish between fat mass and fat-free mass, nor can it differentiate body fat distributions (4). Therefore, the sole use of BMI to estimate the prevalence of obesity and to assess the effects of excess adiposity on disease burden may result in biased estimations. Indeed, a large overlap in mortality risk between individuals with high and low BMI has been reported (5–7). Abdominal fat is the hallmark of obesity that is associated with the highest risk of cardiometabolic diseases (8,9). Within abdominal fat, one can distinguish between abdominal subcutaneous adipose (aSAT) and abdominal visceral adipose tissue (aVAT) (10). These fat depots have different structural and metabolic characteristics (11) that result in inconsistent associations with CVD reported across studies. For instance, aSAT in contrast with aVAT has been associated with a decreased risk for insulin resistance (12), and longitudinally, did not show an association with incidence CVD and cancer (13). Other studies, however, have shown that high volumes of both aVAT and aSAT are significantly associated with different cardiometabolic risk factors (14–17).

Imaging methods such as Magnetic Resonance Imaging (MRI) and computerized axial tomography (CT) are considered “gold standard” techniques to quantify abdominal adipose tissue. However, because of the radiation exposure of CT scanning, MRI measurements are preferred (18). However, MRI imaging is not always available in clinical practice, and the manual quantification of abdominal fat on MR images is very time-consuming. Therefore, other proxies of obesity such as WC, WHR, and WHtR are commonly used as surrogates for abdominal fat. Several systematic reviews, meta-analyses (19–22), and epidemiological studies (7,23) have compared the performance of anthropometric measurements in predicting cardiometabolic risk and mortality. However, results are inconsistent concerning the superiority of any of these measures. Whereas some studies found that WHtR outperforms BMI and WC in the association with certain cardiometabolic risk factors (20–22), a large longitudinal study showed that WC, WHR,

and BMI, used individually or combined, did not improve the prediction of CVD risk over some of the Framingham risk score covariates (23).

Whether and to what extent anthropometric measurements are accurate surrogates of abdominal fat measurements is an important question. Whereas some smaller studies suggested WC to correlate best with MRI aSAT (24) or aVAT (25,26), it remains unclear to what extent anthropometric measures can capture additional aspects of cardiovascular risk. Therefore, in a large population study, we examined the relationship between anthropometric measurements and aSAT and aVAT as measured on MRI, and their differential association with cardiometabolic risk markers. Moreover, we investigated whether anthropometric measurements can provide additional information beyond what is offered by aSAT and aVAT measurements, and vice versa.

Methods

Study population

This analysis was based on the first 5000 participants who participated in the baseline examination of the population-based Rhineland Study between May 2016 and February 2020. The Rhineland Study is a community-based prospective cohort study in two geographically defined areas in the city of Bonn, Germany (27). Names and addresses of all inhabitants of these areas were obtained from the municipality, and people were invited to participate via direct mailing. Inclusion criteria are being aged 30 years or older and having sufficient command of the German language to provide written informed consent. We excluded participants with any serious illness, metallic fragments, or implants, as were pregnant or lactating women for the MRI examinations. The population structure in our target areas is conformed by participants predominantly German with Caucasian ethnicity. The study was conducted following the Declaration of Helsinki guidelines and approved by the Medical Faculty Ethics Committee of the University of Bonn.

From the 5000 participants, a total of 3503 participants had complete data on abdominal MRI and anthropometric measurements. Of those, we excluded 42 underweight participants ($\text{BMI} \leq 18.5$) and 111 persons with extreme outliers in cardiometabolic risk markers. Thus, the overall sample size for analysis was 3350 participants.

Anthropometric measurements

Anthropometric measurements were collected by trained study technicians. All measurements were performed on participants wearing light underwear, without shoes, socks, jewelry, watches, or belts. Body height and weight were measured with the wireless measuring station SECA 285 device in an upright position with the feet in a slightly V-shaped open side by side, keeping the end of the external auditory canal on an imaginary horizontal line at the level of the yoke arch ("Frankfurt Line"). WC and hip circumferences were measured with an ergonomic measuring tape (SECA 201) to the nearest 0.1 cm. The tape was placed at the middle point between the lowest rib and the iliac crest to measure WC and around the widest portion of the buttocks for hip circumference (28). During the measurements, participants were asked to stand upright with their legs open at hip-width breathing normally not retracting the abdomen. WHR was calculated dividing WC by the hip circumference and WHtR by dividing WC by body height. Finally, BMI was calculated as weight in kilograms divided by the square of height in meters.

Imaging and Abdominal fat segmentation

To quantify aSAT and aVAT volumes, abdominal MR Dixon images were acquired using 3T Siemens MAGNETOM Prisma MR Scanners (Siemens Healthcare, Erlangen, Germany). We computed the region of interest (ROI) defined from the lower bound of the twelfth thoracic vertebra to the lower bound of the fifth lumbar vertebrae.

The ROI, fat tissue segmentation, and quantification (aSAT and aVAT volumes) were obtained using FatSegNet, a fully automated and validated postprocessing pipeline (29). The quality of the FatSegNet outputs were manually assessed in a subset of 1040 segmentation maps. This subset was selected based on image quality flags (i.e. motion artifacts, water-fat swaps, etc.), examination warnings, and 10% of random cases.

Cardiometabolic risk markers

Seated systolic blood pressure (SBP) and diastolic blood pressure (DBP) were measured three times with 10 minutes intervals in a temperature controlled room. We used the mean of the last two measurements in our analysis.

Fasting plasma samples were collected and stored at -80° C until analysis. Glucose, glycated hemoglobin (HbA1c), insulin, triglycerides, high-density lipoprotein (HDL-C), and low-density lipoprotein (LDL-C) cholesterol were measured according to standard

procedures at University Hospital Bonn. Additionally, C-reactive protein was measured by high-sensitivity assay (Dimension Vista® System, Siemens Healthcare Diagnostics GmbH). TNFA and IL-6 were quantified using the Single-Molecule Assay (SIMOA) bead-based technology in an HD-1 device (Qanterix, USA).

Other covariates

Age, biological sex, smoking status, menopause status, medication (lipid-lowering, diabetes, and antihypertensive medication) and hormone therapy used were assessed through self-report. Women who indicated they underwent bilateral oophorectomy or had no menstruation for more than a year not due to pregnancy, breastfeeding, or contraception, and women above the age of 60 years were classified as postmenopausal.

Smoking status at baseline was evaluated with a self-administered questionnaire and classified as non-smoking and current smoking. Missing information in smoking status was imputed based on blood cotinine level, measured with a metabolomics platform (Metabolon, Durham, UK). For this, we first identified the 97.5th percentile of cotinine levels in non-smokers and set it as a cut-off value. Participants above this cut-off were classified in the current smoking group.

Statistical analysis.

Clinical and demographic characteristics were compared between sexes using analysis of covariance (ANCOVA) adjusting for age. Fasting glucose, insulin, triglycerides, hs-CRP, IL-6, and TNFA levels were log-transformed before analysis due to their skewed distributions. For concentrations of glucose and lipid related cardiometabolic risk markers, we defined outliers as values above or below 3 times the interquartile range (IQR). For inflammatory markers, we defined outliers as values above or below 5 standard deviations (SD) from the mean values. All anthropometric measurements and cardiometabolic risk markers were standardized to a mean of 0 and SD of 1 to facilitate the comparison of effect sizes. Because of the reported sex differences in body fat distribution and cardiometabolic risk markers (30), we stratified all analyses by sex. To assess the relationship of anthropometric measurements with aSAT and aVAT, we used sex-specific partial correlation, adjusted for age and ROI height of the abdominal MRI fat segmentation.

To evaluate the relationship between aSAT and aVAT (independent variables) with cardiometabolic risk markers (dependent variables), we used sex-specific multivariable linear regression models. The initial model (model 1) was adjusted for age, smoking (non-smoking used as the reference group), menopause status and hormone therapy (women only), medication and ROI height. We tested statistical differences in the standardized effect sizes between aSAT and aVAT with the equation of Clogg et al (31). To statistically test for sex differences, we also ran the models including both men and women, adjusting for sex and with a sex-interaction term added. Further, we assessed the independent relationship of aSAT with cardiometabolic risk markers while accounting for aVAT, and vice versa, by including both aSAT and aVAT simultaneously in the models. To examine the relations of aSAT and aVAT with cardiometabolic risk markers independently of the anthropometric measurements, we next ran additional multivariable linear regression models where we separately added either BMI, WC, WHR, or WHtR as covariates.

Finally, we used the Akaike information criterion (AIC) to compare the fit across all the different regression models linking anthropometric measures and aSAT and aVAT with cardiometabolic risk markers, to assess which measurement(s) best predicted cardiometabolic risk (a lower AIC value indicating a better model fit). All statistical analyses were conducted with the software package R version 1.1.463 (32). A *P* value < 0.05 was considered statistically significant.

Results

The demographic and clinical characteristics of the study participants are depicted in Table 1. Overall, this study included 1942 women (58%) and 1408 men (42%). There were no differences in mean age between women and men (55 ± 13.3 vs. 54 ± 13.8 , $p=0.095$). Independently of age, men had higher mean values for anthropometric measurements, aVAT, and total abdominal adipose tissue (TAAT) than women. However, women showed larger aSAT volumes than men (3.3 ± 1.7 vs. 2.8 ± 1.2 liters, $p<0.001$). We also observed that men on average had a less favorable cardiometabolic risk profile than women.

Table 1 Demographic and clinical characteristics of the study participants.

	Women (n=1942)	Men (n=1408)	<i>P</i> -adjusted
Age, years (SD)	55 (13.3)	54 (13.8)	0.095
Current smokers, n (%)	240 (12.4)	183 (13)	0.669
Non smokers, n (%)	686 (37.4)	560 (41.1)	
Menopause, n (%)	1142 (63.6)		
Abdominal adipose tissue			
aVAT, L [IQ range]	0.8 [0.4, 1.5]	2.1 [1.1, 3.2]	<0.001
aSAT, L (SD)	3.3 (1.7)	2.8 (1.2)	<0.001
TAAT, L (SD)	4.4 (2.4)	5.1 (2.3)	<0.001
Anthropometric measurements			
BMI, kg/m ² (SD)	25.1 (4.6)	26.1 (3.4)	<0.001
WC, cm (SD)	81.9 (11.5)	93.4 (10.5)	<0.001
WHR (SD)	0.8 (0.07)	0.9 (0.07)	<0.001
WHtR (SD)	0.5 (0.07)	0.5 (0.06)	<0.001
Cardiometabolic risk markers			
Triglycerides, mg/dL [IQ range]	84 [65, 111]	106 [78, 150]	<0.001
HDL-C, mg/dL (SD)	70.4 (16.9)	54.1 (14.2)	<0.001
LDL-C, mg/dL (SD)	126.5 (36.8)	128.8 (34.4)	0.027
Glucose, mg/dL [IQ range]	87 [82, 93.6]	92 [86.2, 99]	<0.001
Insulin, mU/L [IQ range]	7.3 [5.3, 10.4]	8.8 [5.9, 12.9]	<0.001
HbA1c, % (SD)	5.4 (0.4)	5.4 (0.4)	0.219
hs-CRP, mg/L (SD)	0.8 [0.5, 1.9]	0.8 [0.4, 1.6]	0.042
TNFA, pg/mL [IQ range]	2.3 [1.8, 2.7]	2.4 [2.05, 2.9]	<0.001
IL-6, pg/mL [IQ range]	1.2 [0.8, 1.9]	1.2 [0.8, 1.9]	0.006
SBP, mmHg (SD)	123.4 (17.1)	129.6 (13.4)	<0.001

Abbreviations: aVAT, visceral adipose tissue; aSAT, subcutaneous adipose tissue; TAAT, total abdominal adipose tissue; BMI, body mass index; WC, waist circumference; WHR, Waist-to-hip ratio; WHtR, waist-to-height ratio; HDL-C, high-density lipoprotein cholesterol; LDL-C, low-density lipoprotein cholesterol; TNFA, Tumor necrosis factor alpha; IL-6, Interleukin 6; SBP, systolic blood pressure.

Note. Data are presented as mean (SD) for normally distributed variables and median [25th, 75th percentiles] for not normally distributed variables and as a percentage (%) for proportions. Clinical characteristics were compared using ANCOVA test adjusting for age.

The sex-specific correlation of anthropometric measurements with aSAT and aVAT adjusted for age and ROI height is depicted in Table 2. Among the anthropometric measurements, BMI had the highest correlation with aSAT ($r=0.905$, $P <0.001$; $r=0.818$, $P <0.001$) and WC had the highest correlation with aVAT ($r =0.814$, $P <0.001$; $r=0.815$, $P <0.001$) in both, women and men respectively. However, in women, the correlation of BMI with aSAT was considerably superior to the correlation of WC with aVAT

Table 2 Sex-specific partial correlation of anthropometric measurements with abdominal MRI-fat variables.

	Women			Men		
	aSAT	aVAT	aTAT	aSAT	aVAT	aTAT
BMI	0.905 (0.90, 0.91)	0.757 (0.74, 0.78)	0.910 (0.90, 0.92)	0.818 (0.80, 0.83)	0.737 (0.71, 0.76)	0.858 (0.84, 0.87)
WC	0.879 (0.87, 0.89)	0.814 (0.80, 0.83)	0.909 (0.90, 0.92)	0.811 (0.79, 0.83)	0.815 (0.80, 0.83)	0.898 (0.89, 0.91)
WHR	0.506 (0.47, 0.54)	0.619 (0.59, 0.65)	0.573 (0.54, 0.60)	0.546 (0.51, 0.58)	0.736 (0.71, 0.76)	0.708 (0.68, 0.73)
WHtR	0.857 (0.84, 0.87)	0.798 (0.78, 0.81)	0.888 (0.88, 0.90)	0.768 (0.75, 0.79)	0.804 (0.78, 0.82)	0.868 (0.85, 0.88)

Abbreviations: aSAT, abdominal subcutaneous adipose tissue; aVAT, abdominal visceral adipose tissue; aTAT, abdominal total adipose tissue; BMI, body mass index; WC, waist circumference; WHR, Waist-to-hip ratio; WHtR, waist-to-height ratio.

Note: Partial correlation was adjusted by age and height of the ROI. (95% confidence interval). All correlations were statistically significant ($p <0.001$).

Table 3 shows the associations of aSAT and aVAT volumes with cardiometabolic risk markers with and without adjusting for one another. In the initial models, we observed that both larger aSAT and aVAT were associated with cardiometabolic risk markers, in both women and men. However, in women, aVAT was significantly stronger associated with cardiometabolic risk markers than aSAT ($P_{aSAT \text{ vs. } aVAT} <0.001$), except for SBP (aSAT $\beta =0.14$; aVAT $\beta =0.20$, $P_{aSAT \text{ vs. } aVAT} = 0.102$). In men, the effects of aVAT and aSAT on cardiometabolic risk markers were of similar magnitude, except for insulin levels that more strongly depended on aSAT than aVAT levels (aSAT $\beta =0.71$; aVAT $\beta =0.62$, $P_{aSAT \text{ vs. } aVAT} =0.024$).

When aSAT and aVAT were entered simultaneously in the model, the effect sizes of aSAT mostly became much smaller. Independently of aVAT, aSAT remained only significantly associated in women with levels of glucose, insulin, hs-CRP, and IL-6, and with SBP; and in men with levels of insulin, hs-CRP, TNFA, and IL-6, and with SBP. The associations of aVAT with cardiometabolic risk markers, on the other hand, did not change or changed only slightly when adjusted for aSAT, and remained statistically significant for all cardiometabolic risk markers, except SBP, for both men and women. When we tested for sex differences, we found statistically significant sex interaction effects in the association of aVAT with all cardiometabolic risk markers, with larger volumes of aVAT being consistently more strongly associated with a more adverse cardiometabolic risk profile in women than in men. For aSAT, we only observed statistically significant sex differences in its association with triglycerides and insulin levels, with larger aSAT volume being more strongly associated with higher concentrations of triglycerides and insulin levels in men than in women.

Table 3 Sex-specific multivariable linear regression models estimating changes of 1-SD on cardiometabolic risk markers per SD in aSAT and aVAT volumes.

	Women (n=1942)			Men (n=1408)			
	Model 1		Model 1 + aSAT and aVAT	Model 1		Model 1 + aSAT and aVAT	<i>P</i> value ^b
	β (95% CI)	<i>P</i> value ^a	β (95% CI)	β (95% CI)	<i>P</i> value ^a	β (95% CI)	
Triglycerides, (mg/dL)							
aSAT	0.27 (0.23 to 0.30)	<0.001	0.01 (-0.04 to 0.06)	0.40 (0.33 to 0.47)	0.083	0.02 (-0.07 to 0.10)	0.001
aVAT	0.63 (0.57 to 0.69)		0.62 (0.57 to 0.74)	0.47 (0.42 to 0.52)		0.46 (0.40 to 0.53)	<0.001
HDL-C, (mg/dL)							
aSAT	-0.28 (-0.32 to -0.24)	<0.001	-0.02 (-0.08 to 0.03)	-0.25 (-0.31 to -0.20)	0.148	-0.01 (-0.08 to 0.05)	0.774
aVAT	-0.64 (-0.71 to -0.58)		-0.62 (-0.72 to -0.52)	-0.30 (-0.34 to -0.26)		-0.30 (-0.35 to -0.24)	<0.001
LDL-C, (mg/dL)							
aSAT	0.14 (0.10 to 0.18)	<0.001	-0.01 (-0.07 to 0.05)	0.20 (0.14 to 0.26)	0.728	0.08 (0.00 to 0.16)	0.323
aVAT	0.33 (0.26 to 0.41)		0.34 (0.24 to 0.45)	0.19 (0.14 to 0.24)		0.15 (0.08 to 0.21)	<0.001
Glucose, (mg/dL)							
aSAT	0.25 (0.21 to 0.29)	<0.001	0.09 (0.03 to 0.14)	0.25 (0.18 to 0.31)	0.870	0.07 (-0.01 to 0.14)	0.799
aVAT	0.50 (0.43 to 0.57)		0.39 (0.29 to 0.49)	0.25 (0.21 to 0.30)		0.22 (0.16 to 0.28)	<0.001
Insulin, (mU/L)							
aSAT	0.43 (0.39 to 0.29)	<0.001	0.17 (0.12 to 0.22)	0.71 (0.65 to 0.77)	0.024	0.34 (0.27 to 0.41)	<0.001
aVAT	0.84 (0.78 to 0.90)		0.63 (0.54 to 0.71)	0.62 (0.58 to 0.67)		0.45 (0.39 to 0.51)	<0.001
HbA1c, (%)							
aSAT	0.06 (0.02 to 0.10)	<0.001	-0.06 (-0.11 to -0.00)	0.11 (0.05 to 0.18)	0.364	-0.02 (-0.10 to 0.06)	0.252
aVAT	0.21 (0.14 to 0.27)		0.28 (0.18 to 0.38)	0.15 (0.10 to 0.20)		0.16 (0.09 to 0.22)	0.043
hs-CRP, (mg/dL)							
aSAT	0.46 (0.42 to 0.50)	<0.001	0.28 (0.22 to 0.33)	0.43 (0.37 to 0.49)	0.080	0.22 (0.15 to 0.30)	0.341
aVAT	0.79 (0.72 to 0.86)		0.42 (0.33 to 0.53)	0.36 (0.31 to 0.40)		0.25 (0.19 to 0.31)	<0.001
TNFA, (pg/mL)							
aSAT	0.19 (0.14 to 0.23)	<0.001	0.05 (-0.02 to 0.11)	0.20 (0.14 to 0.27)	0.608	0.09 (0.01 to 0.17)	0.645
aVAT	0.39 (0.32 to 0.47)		0.32 (0.21 to 0.44)	0.18 (0.13 to 0.23)		0.14 (0.08 to 0.20)	<0.001
IL-6, (pg/mL)							
aSAT	0.28 (0.24 to 0.32)	<0.001	0.13 (0.08 to 0.19)	0.31 (0.25 to 0.37)	0.071	0.19 (0.11 to 0.28)	0.595
aVAT	0.52 (0.45 to 0.59)		0.35 (0.24 to 0.45)	0.24 (0.19 to 0.29)		0.14 (0.08 to 0.20)	<0.001
SBP, (mmHg)							
aSAT	0.14 (0.09 to 0.18)	0.102	0.11 (0.05 to 0.17)	0.17 (0.12 to 0.23)	0.152	0.12 (0.05 to 0.19)	0.656
aVAT	0.20 (0.13 to 0.28)		0.06 (-0.04 to 0.16)	0.12 (0.08 to 0.16)		0.06 (0.00 to 0.12)	<0.001

Values are beta coefficients (95% confidence interval). Model 1, multivariable linear regression model adjusted for age, smoking, menopause status and medication use and ROI height. Additionally, model 1 was adjusted aSAT and aVAT simultaneously.

Abbreviations: aVAT, abdominal visceral adipose tissue; aSAT, abdominal subcutaneous adipose tissue; SBP, systolic blood pressure; HDL-C, high-density lipoprotein cholesterol; LDL-C, low-density lipoprotein cholesterol; TNFA, Tumor necrosis factor alpha; IL-6, Interleukin 6. ^a *P* value for differences in the standardized effect sizes between aSAT and aVAT. ^b *P* value for sex interaction terms in model 1.

The associations of aSAT and aVAT with cardiometabolic risk markers with additional adjustment for anthropometric measurements are shown in Figures 1a and 1b. For both women and men, the associations of aSAT with cardiometabolic risk markers became weaker and partly no longer statistically significant after adjusting for anthropometric measurements, whereas the associations of aVAT with cardiometabolic risk markers remained statistically significant, and mostly only slightly changed, except for SBP.

When considered separately, anthropometric measurements were associated with cardiometabolic risk markers. However, these relations attenuated and were no longer statistically significant for most of the cardiometabolic risk markers after accounting for aSAT and aVAT. In women, however, WC, WHR and WHtR remained statistically associated with lower HDL-C and higher insulin levels. In men, the effect size of all anthropometric measurements with SBP remained without change and statistically significant after adding aSAT and aVAT to the models. Furthermore, WHR remained weakly but significantly associated with higher triglycerides, insulin, IL-6 levels and low HDL-C. BMI and WHtR also remained significantly associated with higher insulin levels in women and men (supplementary Figure 1).

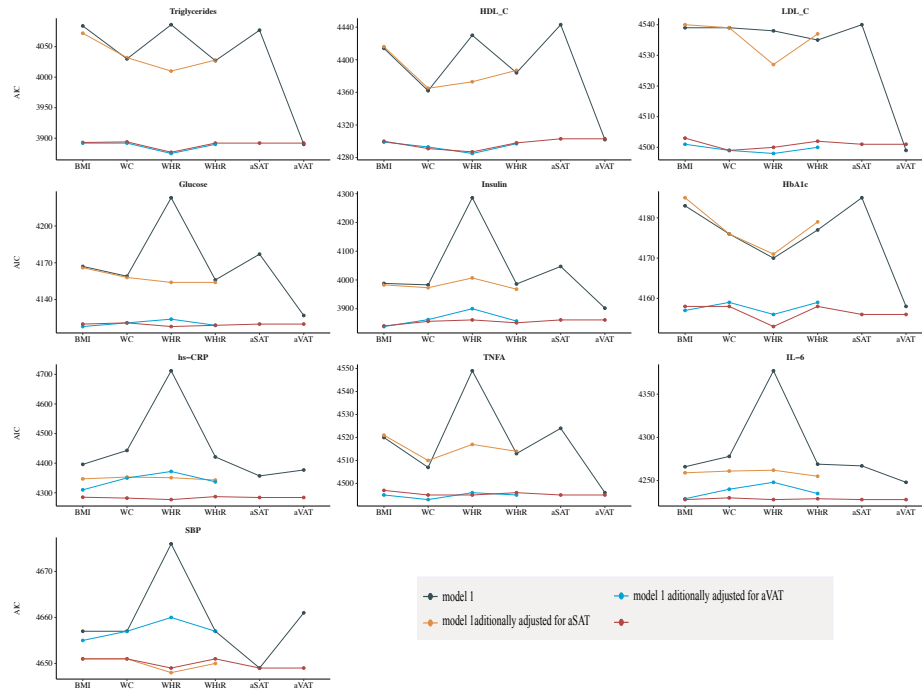
Figure 2 shows the comparison of the ability of the various anthropometric, aSAT, aVAT to predict cardiometabolic risk markers levels, without and with additional adjustment for aSAT, aVAT, or both. When evaluated separately, aVAT best predicted all cardiometabolic risk factors in both women and men, except for SBP (in both women and men), hs-CRP (in women), IL-6 (in men). For these immune markers, aSAT and aVAT performed approximately equally when considered separately, and the model improved when both were added simultaneously. SBP was best predicted by aSAT in women, and by WC in men. Adding aVAT to the models of the anthropometric measures significantly improved the prediction of all other cardiometabolic risk factors. Moreover, combined models including aSAT and aVAT did not or hardly outperform the models that only contained aVAT. Interestingly, when comparing the performance of the various anthropometric measurements, patterns were different between women and men. In women, WHR was the poorest single predictor of most cardiometabolic risk markers. In men, on the contrary, WHR was the best single predictor of several risk markers, including levels of triglycerides, HDL-C, HbA1c, and IL-6, while BMI and aSAT most poorly predicted several of these and other risk markers (Figure 2).



Figure 1 Multivariable linear regression models estimating the change of 1-SD increase of cardiometabolic risk markers per SD increase in aSAT and aVAT in 1a) women and 1b) men.

Note. Shapes represent beta coefficients of the different models. Black and orange stars represent the effect size of aSAT (black) and aVAT (orange) from multivariable linear regression models adjusted for age, medication use, smoking, hormone replacement therapy, and menopause status and height of ROI. Squares, circles, diamonds, and triangles shapes represent the effect sizes of aVAT (black) and aSAT (orange) after additionally adjusting for BMI, WC, WHR, and WHtR respectively. The vertical lines crossing the shapes represent the 95% confidence interval.

a) Women



b) Men

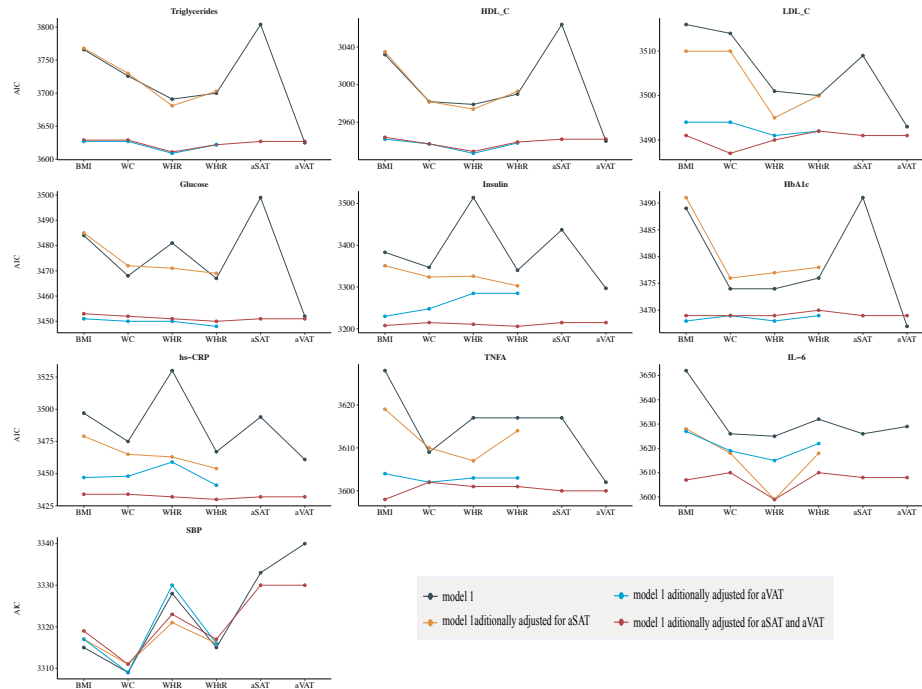
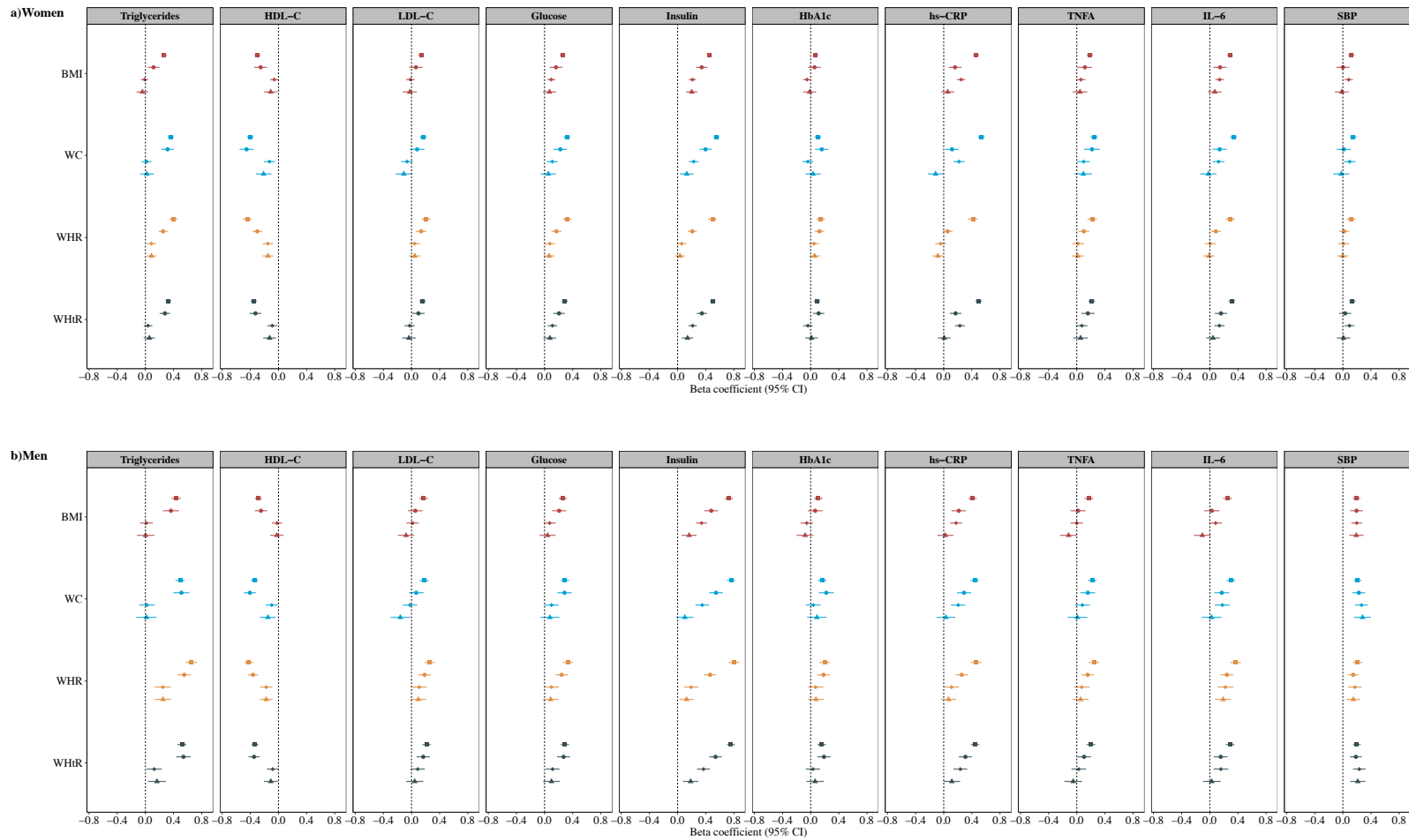


Figure 2 Change in model fit (AIC) estimating cardiometabolic risk markers after accounting for aVAT and aSAT in 1a) women and 1b) men.

Note. Dots in the figure are positioned in the AIC value from model 1 (grey), adjusted for age, medication use, smoking, hormone replacement therapy, and menopause status and height of ROI, and models additionally adjusted for aSAT (yellow), aVAT (blue), or aVAT and aSAT simultaneously (red)

All multivariable linear regression models were adjusted for age, medication use, smoking, hormone replacement therapy, and menopause status.



Supplementary Figure 1 Multivariable linear regression models estimating the change of 1-SD increase of cardiometabolic risk markers per SD increase in BMI (red), WC (blue), WHR (orange), and WHtR (black).

Note. Shapes represent beta coefficients of the different models. Squares represent the effect size of anthropometric measurements from multivariable linear regression models adjusted for age, medication use, smoking, hormone replacement therapy, and menopause status. Circles, diamonds, and triangles represent the effect size of anthropometric measurements after further adjustment for SAT, VAT, or VAT and SAT simultaneously. The horizontal lines crossing the shapes represent the 95% confidence interval.

Discussion:

In this population-based study, we showed that among commonly used anthropometric measurements, BMI had the highest correlation with aSAT, and WC with aVAT in both sexes. However, the correlation of WC with aVAT outperformed in women compared to men.

In line with previous studies we found that aVAT is more metabolically detrimental than aSAT in women (33–36). However, our study identified a different pattern in men, from whom aSAT and aVAT were associated with cardiometabolic risk markers to a similar extent. The strength of the association of aVAT with cardiometabolic risk markers was not significantly modified after adjustment for anthropometric measurements in either women or men. However, associations of aSAT were attenuated and remained significant for only some of the cardiometabolic risk markers.

Correlation of anthropometric measurements with aSAT and aVAT

Since many large epidemiological studies merely rely on anthropometric measurements to classify obesity, we compared the correlations of BMI, WC, WHR, and WHtR with MRI measured aSAT and aVAT. BMI had the strongest correlation with aSAT, whereas WC had the strongest correlation with aVAT. Some smaller studies (≤ 120 participants) reported only weak correlations of anthropometric measurements with aVAT, especially in comparison to correlations with aSAT and aTAT (24,25,37). However, our findings concur however with a study based on the German EPIC cohort, which showed that among a range of anthropometric measures, WC showed the highest correlation with VAT (25) and expanded those findings by identifying a higher correlation of WC with aVAT in women compared to men.

Associations of aSAT and aVAT with cardiometabolic risk markers

Earlier studies reported aVAT rather than aSAT to be associated with cardiometabolic risk markers (16, 34–36). We confirmed that observation in women but not in men, for whom aSAT and aVAT had similar effects on cardiometabolic risk markers, except for insulin (larger aSAT volumes were more strongly associated with higher insulin levels than aVAT). Remarkably, we observed associations of aVAT volume with levels of blood lipids, markers of glucose metabolism and inflammation markers, but not with SBP. Many observational studies have shown obesity, primarily measured by BMI, to be associated with high blood pressure. Indeed, in our data we found that BMI and WC best

predicted SBP in both women and men, with some improvement of the prediction in women by taking aSAT into account. This suggests that the association of high BMI with increased blood pressure is might not primarily a consequence of increasing aVAT accumulation but rather general adiposity.

The heterogenous associations of aSAT and aVAT with cardiometabolic risk could be explained by the metabolic differences of the adipocytes in these fat compartments. Hypertrophic adipocytes are a hallmark of dysfunctional adipose tissue, particularly in aVAT, because they have a higher rate of lipolysis which increases the release of free fatty acids (FFAs) (38). The FFAs from aVAT are drained directly to the liver through the portal vein (11), increasing the hepatic storage (39) and circulating levels of triglycerides (40). Furthermore, hypertrophic adipocytes from aVAT are more insulin-resistant, have a stronger association with lipid impairment markers, and secrete higher concentrations of pro-inflammatory cytokines than aSAT adipocytes (41,42).

Our results show that although men had higher aVAT volumes, the effects of larger aVAT were more metabolically detrimental in women. Previously, one study showed that particularly in women, the proportion of hepatic FFAs delivery from the aVAT was higher than in men (43). Other explanations of the sex differences in distribution and cardiometabolic effects of adipose tissue may involve sex-specific adipose tissue provoked immune responses (44) and sex-specific genetic factors (45). However, this requires further research.

Associations of aSAT and aVAT with cardiometabolic risk markers independently of anthropometric measurements

In our study, aVAT was significantly associated with all the cardiometabolic risk markers, except for SBP, independently of any of the anthropometric measurements. This corroborates and extends findings from prior studies which showed significant associations of aVAT with certain cardiometabolic risk markers independently of BMI (15,17) and WC (33). For aSAT, the strength of the relations with cardiometabolic risk markers usually attenuated to a greater or lesser extent upon adjustment for anthropometric measures. In contrast, anthropometric measurements were weakly or no longer associated with cardiometabolic risk markers once we accounted for aSAT and aVAT, with one big exception for SBP in men, in which the effect sizes of anthropometric measurements did

not change after accounting for aSAT and aVAT. Indeed, when we compared different measures of obesity, aVAT was the single best predictor of cardiometabolic risk markers (lowest AIC), except for SBP, with little or no model improvement when other obesity markers were added.

Strengths and limitations

The main strengths of our study include the use of a large community-based sample with a broad age range, the accurate quantification of aSAT and aVAT from multi-slice MR images with a validated method, and the exploration of a broad number of cardiometabolic risk markers and anthropometric measurements. This is the first study that compares the performance of several commonly used anthropometric measurements with aVAT and aSAT predicting cardiometabolic risk markers.

A limitation is that, due to the resolution of our fast Dixon MRI sequence, we were not able to differentiate between superficial (SSAT) and deep SAT (DSAT), which are considered two metabolic different fat compartments. Furthermore, we did not assess fat accumulation in other anatomical parts. For instance, gluteofemoral fat mass accumulation can be a strong determinant for a decreased cardiovascular risk. Our results warrant future research elucidating the physiology and mechanisms implicated in the metabolic sex differences in the association of abdominal adipose tissue and cardiometabolic risk markers.

Conclusion

In conclusion, larger aVAT volumes were more metabolically detrimental in women, whereas in men, aSAT and aVAT were associated with cardiometabolic risk markers to a similar extent. Our results support that, principally in women WC could be the closest surrogate measure of aVAT for epidemiological studies that merely rely on anthropometric measurements. However, none of the anthropometric measurements outperformed aVAT alone in predicting cardiometabolic risk markers nor added further information.

Funding statement: This work was supported by by the Federal Ministry of Education

and Research (BMBF), Germany, through the Diet-Body-Brain Competence Cluster in Nutrition Research (FKZ: 01EA1809C); and the JPI HDHL on Biomarkers for Nutrition and Health 'HEALTHMARK' (grant number: 01EA1705B); and by the Deutsche Forschungsgemeinschaft (DFG, German Research Foundation) under Germany's Excellence Strategy (EXC 2151–390873048) and through SFB1454 – project number 432325352.

Conflict of interest: The authors declare no conflict of interest.

Author Contributions: O.R.X contributed to the study concept and design, analysis and interpretation of the data, drafting and revising the manuscript. S.E implemented the segmentation and quantification of aVAT and aSAT, contributed to the critical revision of the manuscript for important intellectual content. M.R designed the plan of the MRI experiment and contributed to the critical revision of the manuscript for important intellectual content.

M.M.B.B. contributed to the study concept and design, interpretation of data, revision of the manuscript, funding, and supervision. All the authors have accepted responsibility for the entire content of this submitted manuscript and approved the final version of the manuscript for submission.

References

1. Afshin A, Forouzanfar MH, Reitsma MB, et al. Health effects of overweight and obesity in 195 countries over 25 years. *N Engl J Med*. 2017;377(1):13–27.
2. Chooi YC, Ding C, Magkos F. The epidemiology of obesity. *Metabolism*. 2019;92:6–10.
3. Consultation WH. Obesity: preventing and managing the global epidemic. World Health Organization technical report series. 2000;894:1–253.
4. Sommer I, Teufer B, Szelag M, et al. The performance of anthropometric tools to determine obesity: a systematic review and meta-analysis. *Sci Rep*. 2020;10(1):1–12.
5. Song X, Jousilahti P, Stehouwer CDA, et al. Cardiovascular and all-cause mortality in relation to various anthropometric measures of obesity in Europeans.

- Nutr Metab Cardiovasc Dis.* 2015;25(3):295–304.
6. Flegal KM, Kit BK, Orpana H, Graubard BI. Association of all-cause mortality with overweight and obesity using standard body mass index categories a systematic review and meta-analysis. *JAMA.* 2013;309(1):71–82.
 7. Rost S, Freuer D, Peters A, et al. New indexes of body fat distribution and sex-specific risk of total and cause-specific mortality: A prospective cohort study. *BMC Public Health.* 2018;18(1):1–12.
 8. Després JP. Body fat distribution and risk of cardiovascular disease: An update. *Circulation.* 2012;126(10):1301–13.
 9. Neeland IJ, Ross R, Després JP, et al. Visceral and ectopic fat, atherosclerosis, and cardiometabolic disease: a position statement. *Lancet Diabetes Endocrinol.* 2019;7(9):715–25.
 10. Shen W, Wang ZM, Punyanita M, et al. Adipose tissue quantification by imaging methods: A proposed classification. *Obes Res.* 2003;11(1):5–16.
 11. Ibrahim MM. Subcutaneous and visceral adipose tissue: structural and functional differences. *Obes Rev.* 2010;11(1):11–8.
 12. McLaughlin T, Lamendola C, Liu A, Abbasi F. Preferential fat deposition in subcutaneous versus visceral depots is associated with insulin sensitivity. *J Clin Endocrinol Metab.* 2011;96(11).
 13. Britton KA, Massaro JM, Murabito JM, Kreger BE, Hoffmann U, Fox CS. Body fat distribution, incident cardiovascular disease, cancer, and all-cause mortality. *J Am Coll Cardiol.* 2013;62(10):921–5.
 14. Preis SR, Massaro JM, Robins SJ, et al. Abdominal subcutaneous and visceral adipose tissue and insulin resistance in the framingham heart study. *Obesity.* 2010;18(11):2191–8.
 15. Abraham TM, Pedley A, Massaro JM, Hoffmann U, Fox CS. Association between visceral and subcutaneous adipose depots and incident cardiovascular disease risk factors. *Circulation.* 2015;132(17):1639–47.
 16. Fox CS, Massaro JM, Hoffmann U, et al. Abdominal visceral and subcutaneous adipose tissue compartments: Association with metabolic risk factors in the framingham heart study. *Circulation.* 2007;116(1):39–48.
 17. Liu J, Fox CS, Hickson DMA, et al. Impact of abdominal visceral and

- subcutaneous adipose tissue on cardiometabolic risk factors: The Jackson Heart Study. *J Clin Endocrinol Metab.* 2010;95(12):5419–26.
18. Cornier MA, Després JP, Davis N, et al. Assessing adiposity: A scientific statement from the American Heart Association. *Circulation.* 2011;124(18):1996–2019.
 19. Huxley R, Mendis S, Zheleznyakov E, Reddy S, Chan J. Body mass index, waist circumference and waist:hip ratio as predictors of cardiovascular risk—a review of the literature. *Eur J Clin Nutr.* 2010;64(1):16–22.
 20. Ashwell M, Gunn P, Gibson S. Waist-to-height ratio is a better screening tool than waist circumference and BMI for adult cardiometabolic risk factors: systematic review and meta-analysis. *Obes Rev.* 2012;13(3):275–86.
 21. Lee CMY, Huxley RR, Wildman RP, Woodward M. Indices of abdominal obesity are better discriminators of cardiovascular risk factors than BMI: a meta-analysis. *Journal of Clinical Epidemiology.* 2008;61(7):646–53.
 22. Czernichow S, Kengne AP, Stamatakis E, Hamer M, Batty GD. Body mass index, waist circumference and waist-hip ratio: Which is the better discriminator of cardiovascular disease mortality risk? Evidence from an individual-participant meta-analysis of 82864 participants from nine cohort studies. *Obes Rev.* 2011;12(9):680–7.
 23. The Emerging Risk Factors Collaboration. Separate and combined associations of body-mass index and abdominal adiposity with cardiovascular disease: collaborative analysis of 58 prospective studies. *Lancet.* 2011;377(9771):1085–95.
 24. Ludescher B, Machann J, Eschweiler GW, et al. Correlation of fat distribution in whole body MRI with generally used anthropometric data. *Invest Radiol.* 2009;44(11):712–9.
 25. Neamat-Allah J, Wald D, Hüsing A, et al. Validation of Anthropometric Indices of Adiposity against Whole-Body Magnetic Resonance Imaging – A Study within the German European Prospective Investigation into Cancer and Nutrition (EPIC) Cohorts. Randeve HS, editor. *PLoS One.* 2014;9(3):e91586.
 26. Valsamakis G, Chetty R, Anwar A, Banerjee AK, Barnett A, Kumar S. Association of simple anthropometric measures of obesity with visceral fat and the metabolic syndrome in male Caucasian and Indo-Asian subjects. *Diabet Med.*

- 2004;21(12):1339–45.
27. Breteler MMB, Stöcker T, Pracht E, Brenner D, Stirnberg R. MRI in the Rhineland Study: a Novel Protocol for Population Neuroimaging. *Alzheimer's Dement.* 2014;10:P92–P92.
 28. Nishida C, Ko GT, Kumanyika S. Body fat distribution and noncommunicable diseases in populations: Overview of the 2008 WHO Expert Consultation on Waist Circumference and Waist-Hip Ratio. *Eur J Clin Nutr.* 2010;64(1):2–5.
 29. Estrada S, Lu R, Conjeti S, et al. FatSegNet: A fully automated deep learning pipeline for adipose tissue segmentation on abdominal dixon MRI. *Magn Reson Med.* 2020;83(4):1471–83.
 30. Lew J, Sanghavi M, Ayers CR, et al. Sex-Based Differences in Cardiometabolic Biomarkers. *Circulation.* 2017;135(6):544–55.
 31. Clogg CC, Petkova E, Haritou A. Statistical Methods for Comparing Regression Coefficients Between Models. *Am J Sociol.* 1995;100(5):1261–93.
 32. R Core Team. R: A language and environment for statistical computing. *R Foundation for Statistical Computing, Vienna, Austria.* 2018.
 33. Fox CS, Massaro JM, Hoffmann U, et al. Abdominal visceral and subcutaneous adipose tissue compartments: Association with metabolic risk factors in the framingham heart study. *Circulation.* 2007;116(1):39–48.
 34. Abraham TM, Pedley A, Massaro JM, Hoffmann U, Fox CS. Association between visceral and subcutaneous adipose depots and incident cardiovascular disease risk factors. *Circulation.* 2015;132(17):1639–47.
 35. Elffers TD, De Mutsert R, Lamb HJ, et al. Body fat distribution, in particular visceral fat, is associated with cardiometabolic risk factors in women with obesity. *PLoS One.* 2017;12(9):e0185403.
 36. De Mutsert R, Gast K, Widya R, et al. Associations of Abdominal Subcutaneous and Visceral Fat with Insulin Resistance and Secretion Differ between Men and Women: The Netherlands Epidemiology of Obesity Study. *Metab Syndr Relat Disord.* 2018;16(1):54–63.
 37. Browning LM, Mugridge O, Dixon AK, Aitken SW, Prentice AM, Jebb SA. Measuring Abdominal Adipose Tissue: Comparison of Simpler Methods with MRI. *Obes Facts.* 2011;4(1):9–15.

38. Smith U, Kahn BB. Adipose tissue regulates insulin sensitivity: role of adipogenesis, de novo lipogenesis and novel lipids. *J Intern Med.* 2016;280(5):465–75.
39. Ferrara D, Montecucco F, Dallegri F, Carbone F. Impact of different ectopic fat depots on cardiovascular and metabolic diseases. *J Cell Physiol.* 2019;234(12):21630–41.
40. Ebbert JO, Jensen MD. Fat depots, free fatty acids, and dyslipidemia. *Nutrients.* 2013;5(2):495–508.
41. Ye RZ, Richard G, Gévy N, Tchernof A, Carpentier AC. Fat Cell Size: Measurement Methods, Pathophysiological Origins, and Relationships With Metabolic Dysregulations. *Endocr Rev.* 2022;43(1):35–60.
42. Kranendonk MEG, van Herwaarden JA, Stupkova T, et al. Inflammatory characteristics of distinct abdominal adipose tissue depots relate differently to metabolic risk factors for cardiovascular disease: Distinct fat depots and vascular risk factors. *Atherosclerosis.* 2015;239(2):419–27.
43. Nielsen S, Guo ZK, Johnson CM, Hensrud DD, Jensen MD. Splanchnic lipolysis in human obesity. *J Clin Invest.* 2004;113(11):1582–8.
44. Vasanthakumar A, Chisanga D, Blume J, et al. Sex-specific adipose tissue imprinting of regulatory T cells. *Nature.* 2020;579(7800):581–5.
45. Sung YJ, Pérusse L, Sarzynski MA, et al. Genome-wide association studies suggest sex-specific loci associated with abdominal and visceral fat. *Int J Obes.* 2016;40(4):662–74.

3.4 Branched-chain and aromatic amino acids related to visceral adipose tissue impact metabolic health risk markers.

The Journal of Clinical Endocrinology & Metabolism, 2022, 107, e2896–e2905
<https://doi.org/10.1210/clinem/dgac160>
 Advance access publication 23 March 2022
 Clinical Research Article



Branched-Chain and Aromatic Amino Acids Related to Visceral Adipose Tissue Impact Metabolic Health Risk Markers

Ximena Orozco-Ruiz,^{1, ID} Andrea Anesi,^{2, ID} Fulvio Mattivi,^{2,3, ID} and Monique M. B. Breteler^{1,4, ID}

¹Population Health Sciences, German Center for Neurodegenerative diseases (DZNE), 53127 Bonn, Germany

²Department of Food Quality and Nutrition, Research and Innovation Centre, Fondazione Edmund Mach (FEM), 38010 San Michele all'Adige, Italy

³University of Trento, Department of Cellular, Computational and Integrative Biology (CIBIO), 38123 Povo, Italy

⁴Institute for Medical Biometry, Informatics and Epidemiology (IMBIE), Faculty of Medicine, University of Bonn, 53127 Bonn, Germany.

Correspondence: Monique M. B. Breteler, MD PhD, German Center for Neurodegenerative Diseases (DZNE), Venusberg Campus 1/99, 53127 Bonn, Germany.
 Email: monique.breteler@dzne.de

Abstract

Context: Visceral (VAT) and subcutaneous adipose tissue (SAT) function as endocrine organs capable of influencing metabolic health across adiposity levels.

Objective: We aimed to investigate whether metabolites associated with VAT and SAT impact metabolic health through metabolite concentrations.

Methods: Analyses are based on 1790 participants from the population-based Rhineland Study. We assessed plasma levels of methionine (Met), branched-chain amino acids (BCAA), aromatic amino acids (AAA), and their metabolic downstream metabolites with liquid chromatography-mass spectrometry. VAT and SAT volumes were assessed by magnetic resonance imaging (MRI). Metabolically healthy and unhealthy phenotypes were defined using Wildman criteria.

Results: Metabolically unhealthy participants had higher concentrations of BCAA than metabolically healthy participants ($P < 0.001$). In metabolically unhealthy participants, VAT volumes were significantly associated with levels of L-isoleucine, L-leucine, indole-3-lactic acid, and indole-3-propionic acid (in log SD units: $\beta = 0.16$, $P = 0.003$; $\beta = 0.12$, $P = 0.038$; $\beta = 0.11$, $P = 0.035$ and $\beta = -0.16$, $P = 0.010$, respectively). Higher concentrations of certain BCAA and AAA-downstream metabolites significantly increased the odds of cardiometabolic risk markers. The relation between VAT volume and cardiometabolic risk markers was mediated by BCAA (indirect effects 3.7%–11%, $P = 0.02$ to < 0.0001), while the effect of VAT on systemic inflammation was mediated through higher kynurenine concentrations (indirect effect 6.4%, $P < 0.0001$).

Conclusion: Larger volumes of VAT in metabolically unhealthy individuals are associated with altered concentrations of circulating BCAA and AAA-downstream metabolites, increasing the odds of cardiometabolic risk markers. This suggests that these metabolites are involved in the mechanisms that underlie the relationship of abdominal VAT with metabolic health.

Key Words: branched-chain amino acids, aromatic amino acids, metabolites, cardiometabolic risk markers, visceral adipose tissue, subcutaneous adipose tissue

Abbreviations: 3-IAA, indole-3-acetic acid; 5-HIAA, 5-hydroxyindole-3-acetic acid; 5-HT, serotonin; AAA, aromatic amino acid; BCAA, branched-chain amino acid; BMI, body mass index; DA, dopamine; HDL-C, high-density lipoprotein cholesterol; HOMA-IR, homeostasis model assessment of insulin resistance; hsCRP, high-sensitivity C-reactive protein; I3A, indole-3-carboxaldehyde; ILA, indole-3-lactic acid; IPA, indole-3-propionic acid; Kyn, kynurenine; KYNA, kynurenic acid; OR, odds ratio; Phe, phenylalanine; ROI, region of interest; SAT, subcutaneous adipose tissue; T2D, type 2 diabetes; Trp, tryptophan; Tyr, tyrosine; VAT, visceral adipose tissue; XA, xanthurenic acid.

Obesity is worldwide one of the major risk factors for cardiovascular diseases, type 2 diabetes (T2D), different types of cancer, and a high rate of mortality (1, 2). However, there is a growing awareness that obesity is a heterogeneous condition, and that risk profiles for metabolic and cardiovascular disease vary widely among individuals with the same body mass index (BMI). Thus, risk stratification of individuals according to their metabolite profile, that is, grouping according to similarities in metabolic profile, becomes crucial (3, 4). Among individuals with high BMI, a subset can be considered metabolically healthy as they have a healthy metabolic profile characterized by high insulin sensitivity, favorable lipid profile, low

pro-inflammatory cytokine levels, and normal blood pressure. Conversely, there are also individuals who are metabolically unhealthy despite a low BMI (5, 6). The variation of metabolic health across obesity groups is mainly due to differences in abdominal fat distribution (7) such as visceral (VAT) and subcutaneous abdominal adipose tissues (SAT) (8). Larger SAT and VAT have been associated with future conversion to metabolically unhealthy from a healthy phenotype (9). One important mechanism by which VAT and SAT are involved in the progression from a metabolically healthy to a metabolically unhealthy phenotype is by changes in the functionality of the adipocytes through their ability to expand (10). Hypertrophic

Received: 14 October 2021. Editorial Decision: 11 March 2022. Corrected and Typeset: 19 April 2022

© The Author(s) 2022. Published by Oxford University Press on behalf of the Endocrine Society. All rights reserved. For permissions, please e-mail: journals.permissions@oup.com

adipocytes are characteristic of an unhealthier mechanism of adipocyte expansion. They cause a cascade of metabolic dysfunction by promoting insulin resistance and glucose intolerance and they induce inflammation by secreting high levels of pro-inflammatory cytokines (11, 12). Furthermore, the higher release of free fatty acids by hypertrophic adipocytes leads to hepatic lipid accumulation and hypertriglyceridemia (13). Nevertheless, the connection between abdominal fat and metabolically unhealthy phenotype is yet not totally understood and could be explained by other factors such as metabolomic biomarkers. Metabolomics has emerged as a powerful tool for assessing perturbations in metabolic pathways and for determining biomarkers that are associated with specific health conditions or diseases. Metabolomic biomarkers are a measure of exposure and susceptibility to specific outcomes and allow us to classify at-risk/diseased individuals (14). It has been shown that there are differences in circulating levels of branched-chain amino acids (BCAA) and aromatic amino acids (AAA) across metabolic phenotypes (15-17). Furthermore, BCAA and AAA have been associated with metabolic abnormalities and obesity in cross-sectional studies (18, 19), and could predict the development of diabetes (20, 21) and cardiovascular diseases in longitudinal studies (22).

Evidence from animal and human adipose tissue studies suggests that the adipose tissue is an important determinant of BCAA and AAA oxidation and metabolism (23-25).

In particular, the route of tryptophan (Trp) catabolism through the kynurenine (Kyn) pathway degrades Trp into several metabolites with toxic and inflammatory effects. The kynurenine pathway can be upregulated in the adipose tissue by activating indoleamine 2,3-dioxygenase (IDO) (24, 25), a rate-limiting enzyme that breaks down Trp into downstream products such as Kyn, kynurenic acid (KYNA) and xanthurenic acid (XA) (26). Thus, increased activity of the kynurenine pathway in the adipose tissue is reflected in the higher circulation of toxic Trp-derived metabolites. On the other hand, gene expression of enzymes involved in the catabolism of BCAA in the adipocytes (23, 27, 28) reportedly decreases mainly in VAT compartments (23), which leads to a significant increase in circulating levels of BCAA in persons with high levels of VAT.

To our knowledge, few studies have investigated the relationship between abdominal adipose tissue and methionine (Met). Two animal studies showed that a diet restricted on Met was associated with a reduction of VAT accumulation and hepatic triglyceride synthesis. Furthermore, in the VAT adipocytes, lipogenesis and fatty acid oxidation increased, and there was an improvement in insulin sensitivity (29, 30). Similar results were further replicated in humans with metabolic syndrome (31). Additionally, some authors showed that the uptake of Met was diminished in the VAT of obese subjects, reflecting an increased release of Met in the circulation (32, 33). Therefore, circulating metabolites could constitute the biological link between adiposity and metabolic diseases.

Thus, we aimed to understand whether known metabolites associated with VAT and SAT impact metabolic health and how they are involved in the link between abdominal VAT and SAT with cardiometabolic risk markers.

Methods

Study Population

We selected the first 2000 participants from the Rhineland Study, who participated between March 2016 to April 2019

and for whom blood samples and abdominal MRI data were available, for further metabolomic analysis as described below.

The Rhineland Study is an ongoing community-based cohort study in Bonn, Germany, that started in 2016. One of its central aims is to find biomarkers and multimodal biomarker profiles to identify individuals at risk for neurodegenerative and other age-related diseases. Participants in the Rhineland Study are recruited from 2 municipal districts in Bonn and are primarily Caucasians of European descent. Inclusion criteria are age of 30 years or older and sufficient command of the German language to provide written informed consent.

At baseline examination, participants completed an 8-hour in-depth multidomain phenotypic assessment of anthropometry, physical activity and fitness, cardiovascular health, brain imaging, cognitive testing, neurologic functioning, ophthalmologic health and functioning, and other sensory systems. No financial incentives were offered for study participation (34). The study was approved by the Medical Faculty Ethics Committee of the University of Bonn and conducted following the Declaration of Helsinki. We obtained informed written consent from all the participants before they underwent any of the examinations.

Blood Samples

Overnight fasting plasma samples were collected in 2 × 10 mL EDTA tubes from all participants between 7:00 and 9:30 a.m. and directly processed. The plasma was centrifuged within less than 10 minutes after blood withdrawal for 10 minutes at 2000g at 20 °C (brake of the centrifuge set off to avoid platelet activation). Automated aliquoting (Hamilton Microlab Star) of the plasma was done within less than 35 minutes after centrifugation into 500-µL aliquots. All aliquots were directly cooled (10 °C) during the process. The aliquots were placed into a chest freezer (-80 °C) within less than 45 minutes after aliquoting.

Targeted Metabolomics

For metabolomics analysis, frozen plasma samples were shipped on dry ice to Fondazione Edmund Mach (FEM), in Trento Italy. Metabolomics analyses were done in 2 batches, with a 7-month time difference between batches.

Liquid chromatography-tandem mass spectrometry (LC-MS/MS) targeted analyses were performed on 2000 frozen plasma samples; all samples were thawed at 4 °C. An aliquot of 50 µL was loaded on 96-well plates Oströ (Water) and 20 µL of an internal standard mix in methanol were added (tryptophan-d5, tyrosine-d4, methionine-d4, serotonin-d4, kynurenic acid-d5, 5-hydroxyindole-acetic acid-d5 and dopamine-d5 at 2.5 ppm; final concentration in the extracted and recovered sample: 0.5 ppm).

Ultra-High Performance Liquid Chromatography-Electrospray Ionization-Triple-Quadrupole-Mass Spectrometry Analysis

The detection was performed on a Waters Xevo Triple Quadrupole-mass spectrometer (MS) equipped with electrospray ionization (ESI) source and coupled on-line with an Acquity UHPLC (Waters). The MS operated in positive and negative ion modes. Separations were performed on a Water UPLC HSST3 (150 × 2.1 mm I.D., 1.8 µm particle size, 100 Å pore diameter) purchased from Waters. Mobile phase A was water containing 0.1% formic acid, mobile phase B was acetonitrile with 0.1% formic acid. The gradient started

at 5% B and was maintained for 0.5 minutes; then %B was increased to 10% at 2.5 minutes, to 15% at 3.5 minutes, to 25% at 4.5 minutes, to 35% at 5.5 minutes, to 45% at 6.5 minutes, to 55% at 7 minutes and then to 100% B at 7.5 minutes. Final conditions were kept for 3 minutes and then the column was re-equilibrated for 4 minutes. The flow rate was 0.3 mL/min, the injection volume was 2 μ L, the column oven was set at 40 °C and the sample tray temperature was 5 °C. With this method, we are able to quantify 3 BCAAs, L-valine (Val), L-isoleucine (Ile), and L-leucine (Leu); as well as 13 aromatic amino acids and their metabolic downstream products; 5-hydroxyindole-3-acetic acid (5-HIAA), serotonin (5-HT), indole-3-acetic acid (3-IAA), indole-3-carboxaldehyde (I3A), indole-3-lactic acid (ILA), indole-3-propionic acid (IPA), kynurenic acid (KYNA), kynurenine (Kyn), xanthurenic acid (XA), L-tryptophan (Trp), L-phenylalanine (Phe), L-tyrosine (Tyr), dopamine (DA), and L-methionine (Met). Further details of the methods are described elsewhere (35).

Biochemical and Clinical Measurements

Fasting insulin, high-density lipoprotein cholesterol (HDL-C), triglycerides, glucose, and high-sensitivity C-reactive protein (hsCRP) were measured on the day of blood withdrawal according to standard procedures at the University Hospital Bonn (UKB). HsCRP was measured by high-sensitivity assay (Dimension Vista System, Siemens Healthcare Diagnostics GmbH).

We used the homeostatic model assessment to calculate insulin resistance (HOMA-IR), as glucose levels (mmol/L) \times insulin levels (mU/L)/22.5.

Systolic and diastolic blood pressure were measured 3 times in sitting position, with 10 minutes intervals, in a resting and quiet environment. The mean of the blood pressure was obtained from the mean of the last 2 measurements.

Metabolic Health Classification

Metabolic health was defined using Wildman et al criteria (5), which include 6 cardiometabolic risk markers defined as follow: 1) elevated blood pressure: systolic/diastolic blood pressure \geq 130/85 mm Hg or antihypertensive medication use; 2) elevated triglyceride level: fasting triglyceride level \geq 150 mg/dL; 3) low HDL-C level: HDL-C level $<$ 40 mg/dL in men or $<$ 50 mg/dL in women or lipid-lowering medication use; 4) systemic inflammation: hsCRP level $>$ 0.1 mg/L; 5) elevated glucose level: fasting glucose level \geq 100 mg/dL or antidiabetic medication use; 6) insulin resistance: HOMA-IR $>$ 5.13. Metabolically unhealthy phenotype was defined when participants had \geq 2 of the above cardiometabolic risk markers, and metabolically healthy when $<$ 2 cardiometabolic risk markers were present.

Abdominal Fat Segmentation

Abdominal MR image acquisition was performed using a 2-point Dixon sequence at 2 different sites, both with identical 3T Siemens MAGNETOM Prisma MR scanners (Siemens Healthcare, Erlangen, Germany). Data were acquired during a single breath-hold in a supine position with arms at the sides.

Abdominal MRI-fat variables were extracted from the predicted segmentation maps of the Fat-SegNet pipeline, a fully automated deep learning pipeline that accurately segments VAT and SAT inside a consistent anatomically defined abdominal region (36).

The segmented area was defined from the lower bound of the twelfth thoracic vertebra to the lower bound of the fifth lumbar vertebra. We calculated the height of the region of interest segmented (height of ROI) measuring the segmented slices on the Z-axis.

Total Energy and Protein Intake

We assessed dietary intake with a self-administered semi-quantitative food frequency questionnaire (FFQ) (37). To calculate protein and energy intakes, we used an algorithm developed by The Institute of Nutritional and Food Sciences at the University of Bonn, utilizing as reference the German Food Code and Nutrient Data Base (version 3.02).

Statistical Analysis

We compared differences in the adjusted mean concentration of metabolites and clinical characteristics between metabolically healthy and metabolically unhealthy participants with analysis of covariance (ANCOVA) adjusting for age, sex, and additionally, BMI.

For further analyses, all metabolite concentrations were log-transformed to obtain approximately normal distributions. We applied rank-based inverse normal transformed due to skewness of the metabolite residuals. Outliers in metabolites were identified as concentrations above or below 3 times the interquartile range (IQR) before the rank-based inverse normal transformation.

We used multivariable linear regression to assess the association of VAT and SAT with metabolite concentrations, independent of BMI. In every model, we considered single metabolites as the dependent variable, and VAT and SAT as the main independent variables, adjusting for BMI, age, sex, batch effect, and height of the ROI. In additional analyses, we further adjusted the linear regression models for dietary total energy and protein intake. To account for multiple comparisons, we adjusted *P* values for multiple testing using the Benjamini-Hochberg method (38). We evaluated whether the association of VAT and SAT with metabolite concentrations differed between sexes by including sex-VAT and sex-SAT interaction terms in the models.

To analyze the association of metabolite concentration with presence of cardiometabolic risk markers we used logistic regression models. We first adjusted for age, sex, BMI, batch effect, and smoking. Subsequently, we additionally included VAT and SAT to evaluate whether the associations of metabolites with cardiometabolic risk markers were independent of abdominal adiposity. In additional analyses, we further adjusted the logistic regression models for dietary total energy and protein intake.

To investigate whether the effects of metabolites on cardiometabolic risk markers differed between sexes, we added sex-metabolite interaction terms to our models.

The effect sizes from the linear and logistic regression models (beta coefficients and odds ratio [OR]) can be interpreted as standardized effect sizes due to the inverse rank normalization (1-SD increased in log standardized units of metabolites). All models were adjusted for age, sex, BMI, batch effect, smoking, VAT, SAT, and the height of the ROI.

Mediation Analysis

To investigate whether the association of abdominal fat with cardiometabolic risk markers is mediated through circulating metabolites, we performed a causal mediation analysis.

Since VAT rather than SAT is strongly associated with higher odds of cardiometabolic risk markers, we considered VAT as the main independent variable to calculate the direct and indirect effect. All models were adjusted for sex, age, BMI, batch effect, and SAT. To evaluate the indirect effect, which depicts how much of the effect of VAT on cardiometabolic risk markers is mediated through metabolite concentration, we applied the product method (39). We used bootstrapping to assess whether the mediation effect was statistically significant (different from zero) (40).

Results

From the 2000 study participants with metabolomics analyses, we excluded participants with extreme values in metabolite concentration ($n = 152$) and cardiometabolic risk markers ($n = 44$), as well as those participants without valid data on abdominal MRI-fat segmentation ($n = 14$), leaving 1790 participants who were included in the analyses. Table 1 shows the descriptive characteristics of the participants stratified by metabolic health phenotypes. Independently of age and sex, metabolically unhealthy participants had significantly higher concentrations of Val, Leu, Ile, Tyr, Phe, Kyn, Kyn/Trp, KYNA, I3A, and lower concentrations of IPA. When we further adjusted the mean differences for BMI, only concentrations of Val, Ile, and Leu remained statistically significantly higher in metabolically unhealthy compared with metabolically healthy participants.

Figure 1 depicts the association of VAT and SAT volumes with metabolite concentration in metabolic health phenotypes, independently of age, sex, and BMI. We observed significant associations of VAT with Ile, Leu, ILA, and IPA (in log standard deviation units per L increase in VAT: $\beta = 0.16$, $P = 0.002$; $\beta = 0.12$, $P = 0.02$; $\beta = 0.11$, $P = 0.02$; $\beta = -0.16$, $P = 0.005$, respectively), only in metabolically unhealthy participants. Findings were also similar after adjustment for total diet energy and protein intake (data not shown).

The association of circulating metabolites with the presence of cardiometabolic risk markers without and with adjustment for VAT and SAT are shown in Fig. 2A and Fig. 2B. We observed a considerable reduction of the strength of the associations of metabolites with cardiometabolic risk markers after accounting for abdominal fat and BMI in the models. However, levels of some of the BCAA metabolites, such as Ile and Leu, remained statistically significantly associated with an increased odds of hypertriglyceridemia (OR per 1 SD increase in concentration = 1.39 [95% CI, 1.19-1.62]; OR = 1.34 [95% CI, 1.15-1.56]), low HDL-cholesterol (OR = 1.25 [95% CI, 1.08-1.45]; OR = 1.19 [95% CI, 1.03-1.37]), glucose impairment (OR = 1.32 [95% CI, 1.13-1.54]; OR = 1.23 [95% CI, 1.06-1.42]), and insulin resistance (OR = 1.95 [95% CI, 1.50-2.58]; OR = 1.74 [95% CI, 1.33-2.28]).

After adjusting for BMI and abdominal fat, higher levels of Tyr and Phe were associated with a significantly increased odds of insulin resistance (OR = 1.83 [95% CI, 1.42-2.36; OR = 1.42 [95% CI, 1.10-1.83]), whereas only Trp breakdown products (Kyn, Kyn/Trp, and ILA) were significantly associated with higher odds of systemic inflammation. Higher levels of ILA were associated with an increased odds of hypertriglyceridemia (OR = 1.26 [95% CI, 1.07-1.49]), insulin resistance (OR = 1.38 [95% CI, 1.04-1.82]) and systemic inflammation (OR = 1.26 [95% CI, 1.10-1.44]), but with lower odds of low HDL-cholesterol (OR = 0.81 [95%

CI, 0.69-0.95]). We further observed that higher IPA levels were associated with lower odds of glucose impairment (OR = 0.80 [95% CI, 0.69-0.92]). Findings were also similar after adjustment for total diet energy and protein intake (data not shown).

We found no significant sex effects except for the relation between 5-HT and hypertriglyceridemia ($P_{sex \times interaction} < 0.001$), where per SD increase 5-HT concentration the odds of having hypertriglyceridemia decreased with 29% ($P = 0.002$) in women but increased by 24% ($P = 0.027$) in men.

Table 2 shows the associations where we found a significant mediation effect of metabolite concentrations in the relationship between VAT and cardiometabolic risk markers. Ile and Leu were the main metabolites with significant mediation effects for hypertriglyceridemia, low HDL-C, glucose impairment, and insulin resistance. For systemic inflammation, Kyn was the only metabolite that showed a statistically significant mediation effect, with 6.4% of the effect of VAT volumes on the increased risk of systemic inflammation being mediated through increases in concentrations of Kyn levels.

Discussion

We found that levels of BCAA metabolites differ between metabolically unhealthy and metabolically healthy participants, regardless of BMI. Moreover, in metabolically unhealthy participants, VAT rather than SAT was implicated in altered metabolism of some of the BCAA and AAA metabolites. We further observed that independently of abdominal and general adiposity, higher circulating concentrations of BCAA and AAA-downstream metabolites were associated with a greater likelihood of the presence of cardiometabolic risk markers, especially of insulin resistance. Causal analysis revealed that several of these metabolites partly mediated the link between abdominal VAT and cardiometabolic risk markers.

Some previous studies in smaller samples have evaluated how metabolites differ across metabolic phenotypes in obese individuals, using different criteria of metabolic syndrome (41, 42) and metabolically health definition (15, 43) to classify healthy and unhealthy status. One study including 78 women showed that metabolically unhealthy obese participants had higher concentrations of BCAA, Tyr, and Phe compared with obese metabolically healthy (41). Likewise, metabolically unhealthy overweight/obese subjects showed significantly higher Kyn levels and Kyn/Trp ratio in comparison with healthy individuals (42). Other studies, however, found no differences in BCAA, Phe, and Tyr levels between metabolically healthy and metabolically unhealthy obese subjects (15). Furthermore, those metabolites were similarly associated with the odds of metabolically healthy and unhealthy phenotypes in obesity (43). Our study extended the prior work by demonstrating that BCAA metabolites levels are significantly higher in metabolically unhealthy individuals independently of adiposity levels in a large cohort study.

We found a significantly stronger effect of VAT than SAT on abnormal plasma metabolite levels. This is in line with previous studies, performed in 40 to maximally 491 healthy individuals, showing that VAT rather than SAT was associated with plasma BCAA and AAA levels (44-46). Moreover, it fits with findings from a longitudinal study of diet-induced weight loss, which reported that a decreased

Table 1. Characteristics of the study population.

	Metabolically healthy (n = 1017)	Metabolically unhealthy (n = 773)	Adjusted for age and sex ^a		Adjusted for age, sex, and BMI ^a	
			Mean difference [95% CI]	P value	Mean difference [95% CI]	P value
Women, n (%)	621 (58.0)	341 (44.1)	-0.7 [-0.9 to -0.6]	<0.001	-0.7 [-0.9 to -0.5]	<0.001
Age, years (SD)	50.1 (12.4)	60.1 (13.7)	10.3 [9.0 to 11.5]	<0.001	10.7 [9.3 to 12.0]	<0.001
BMI, kg/m ² (SD)	24.0 (3.4)	27.5 (4.1)	3.6 [3.2 to 4.0]	<0.001	3.6 [3.2 to 4.0]	<0.001
VAT, L (SD)	1.0 (0.8)	2.3 (1.2)	1.0 [0.9 to 1.1]	<0.001	0.4 [0.4 to 0.5]	<0.001
SAT, L (SD)	2.6 (1.3)	3.7 (1.6)	1.3 [1.2 to 1.5]	<0.001	0.2 [0.1 to 0.3]	<0.001
Total energy intake, kcal/day (SD)	2507 (821)	2545 (859)	-18.9 [-99 to 61.1]	0.642	-7.2 [-95.4 to 81]	0.873
Protein intake, g (SD)	79.5 (24)	81.4 (26)	0.9 [-1.5 to 3.3]	0.461	0.8 [-1.8 to 3.4]	0.552
Met, Umol (SD)	11.5 (2.78)	11.5 (2.8)	-0.02 [-0.3 to 0.3]	0.87	-0.04 [-0.3 to 0.3]	0.79
Val, Umol (SD)	50.7 (21.3)	54.7 (22.9)	4.6 [2.4 to 6.8]	<0.001	2.9 [0.5 to 5.4]	0.02
Leu, Umol (SD)	56.9 (13.8)	62.3 (15.4)	4.3 [2.9 to 5.6]	<0.001	2.5 [1.03 to 3.9]	0.001
Ile, Umol (SD)	27.1 (7.2)	30.3 (8.2)	2.6 [1.9 to 3.3]	<0.001	1.7 [0.9 to 2.4]	<0.001
Tyr, Umol (SD)	32.4 (8.9)	36.2 (9.8)	2.6 [1.6-3.5]	<0.001	0.9 [-0.1 to 1.9]	0.09
Phe, Umol (SD)	32.5 (8.0)	34.3 (8.4)	1.1 [0.3 to 1.9]	0.01	0.1 [-0.7 to 1.0]	0.77
DA, Umol (SD)	0.02 (0.01)	0.02 (0.01)	-0.0 [-0.0 to 0.0]	0.58	-0.0 [-0.0 to 0.0]	0.27
XA, Umol (SD)	0.3 (0.07)	0.3 (0.07)	0.0 [0.0 to 0.01]	0.16	0.0 [-0.01 to 0.01]	0.54
Trp, Umol (SD)	30.7 (7.5)	31.4 (7.5)	0.6 [-0.1 to 1.4]	0.10	0.2 [-0.6 to 1.0]	0.63
Kyn, Umol (SD)	1.5 (0.6)	1.7 (0.6)	0.09 [0.03 to 0.2]	0.002	0.01 [-0.05 to 0.08]	0.71
Kyn/Trp, Umol (SD)	0.04 (0.01)	0.05 (0.02)	0.0 [0.0 to 0.0]	0.01	-0.0 [-0.0 to 0.0]	0.88
KYNA, Umol (SD)	0.03 (0.01)	0.03 (0.02)	0.002 [0.0006 to 0.003]	0.007	-0.0 [-0.0 to 0.0]	0.82
IPA, Umol (SD)	1.4 (0.9)	1.2 (0.8)	-0.2 [-0.3 to -0.1]	<0.001	-0.9 [-0.2 to 0.01]	0.07
ILA, Umol (SD)	0.8 (0.3)	0.9 (0.4)	0.03 [-0.0 to 0.06]	0.08	0.0 [-0.03 to 0.04]	0.81
I3A, Umol (SD)	0.05 (0.02)	0.05 (0.02)	0.0 [0.0 to 0.0]	0.01	0.0 [-0.0 to 0.0]	0.11
3-IAA, Umol (SD)	2.02 (1.0)	2.1 (1.2)	-0.03 [-0.1 to 0.08]	0.62	-0.03 [-0.1 to 0.09]	0.58
5-HT, Umol (SD)	0.1 (0.07)	0.1 (0.06)	-0.0 [-0.01 to 0.0]	0.27	0.0 [-0.01 to 0.01]	0.98
5-HIAA, Umol (SD)	0.02 (0.01)	0.02 (0.01)	-0.0 [-0.0 to 0.0]	0.12	-0.0 [-0.0 to 0.0]	0.12
<i>Prevalence of cardiometabolic risk factors</i>						
Hypertension, N (%)	248 (24.4%)	656 (84.8%)				
Hypertriglyceridemia, N (%)	25 (2.6%)	294 (38.7%)				
Low HDL-C, N (%)	35 (3.4%)	290 (37.5%)				
Glucose impairment, N (%)	34 (3.3%)	279 (36.1%)				
Insulin resistance, N (%)	0 (0%)	103 (13.8%)				
Systemic inflammation, N (%)	197 (20.5%)	550 (72.5%)				

Data are presented as mean (SD) or frequencies (%). Characteristics and mean metabolite concentrations were compared using an ANCOVA test.

^aWhen applicable.

Abbreviations: 3-IAA, indole-3-acetic acid; 5-HIAA, 5-hydroxyindole-3-acetic acid; 5-HT, serotonin; DA, dopamine; I3A, indole-3-carboxaldehyde; IPA, indole-3-propionic acid; ILA, indole-3-lactic acid; Ile, L-isoleucine; Kyn, kynurenine; Kyn/Trp, kynurenine/tryptophan ratio; KYNA, kynurenic acid; Leu, L-leucine; Met, L-methionine; Phe, L-phenylalanine; SAT, subcutaneous adipose tissue; Trp, L-tryptophan; Tyr, L-tyrosine; Val, L-valine; VAT, visceral adipose tissue; XA, xanthurenic acid.

VAT mass was significantly associated with a reduction in BCAA levels independently of weight loss after 2 years of follow-up (47).

Some studies have investigated abdominal fat tissue-specific differences in the up/downregulation of the metabolism of BCAA and AAA (23-25). They concluded that mainly in VAT, the expression of catabolizing enzymes for BCAA and certain AAA is altered. Piro et al (33) reported that pathologically obese people had lower concentrations of BCAA in the VAT tissue than healthy participants but had increased production of BCAA catabolites. That suggests that an impaired BCAA catabolism in VAT boosts higher plasma circulation of these

metabolites. Moreover, the functionality of adipose tissue can also differ across metabolic health phenotypes. Genes related to BCAA catabolism reportedly are more downregulated in the abdominal adipose tissue of metabolically unhealthy obese compared to metabolically healthy obese individuals (15, 48). Thus, in the metabolically healthy phenotype, the abdominal adipose tissue is characterized by the maintenance of mitochondrial function and absence of inflammation, while in the metabolically unhealthy phenotype the adipose tissue is more dysfunctional (48). Our results could complement this approach in a large population-based study since we found that only in metabolically unhealthy participants,

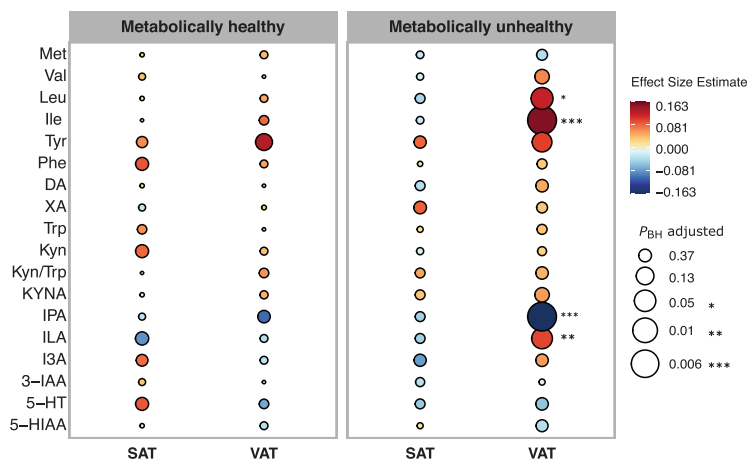


Figure 1. Association of VAT and SAT with metabolite concentrations stratified by metabolic health phenotypes. Models were adjusted for age, sex, BMI, batch effect, height of the ROI, VAT, and SAT simultaneously. Multiple testing was performed using the Benjamini and Hochberg method to adjust *P* values. Abbreviations: 3-IAA, indole-3-acetic acid; 5-HT, serotonin; 5-HIAA, 5-hydroxyindole-3-acetic acid; DA, dopamine; I3A, indole-3-carboxaldehyde; IPA, indole-3-propionic acid; ILA, indole-3-lactic acid; Ile, L-isoleucine; Kyn, kynurenine; Kyn/Trp, kynurenine/tryptophan ratio; KYNA, kynurenic acid; Leu, L-leucine; Met, L-methionine; Phe, L-phenylalanine; SAT, subcutaneous adipose tissue; Trp, L-tryptophan; Tyr, L-tyrosine; Val, L-valine; VAT, visceral adipose tissue; XA, xanthurenic acid.

larger VAT was associated with an increased level of several circulating metabolites.

We found that BCAA, AAA, and AAA-downstream metabolites were strongly associated with higher odds of cardiometabolic risk markers, independently of the well-known effects of VAT and SAT. The strongest effects were for insulin resistance, mainly by high concentrations of BCAA, Tyr, Trp, and XA metabolites. BCAA and certain AAA-downstream metabolites have been largely associated with insulin resistance in some population studies (20-22), suggesting that high concentrations of these metabolites are strong markers of an early manifestation of T2D.

To further elucidate possible mechanisms, an animal study showed that BCAAs lead to insulin resistance by activation of the mechanistic target of rapamycin (mTOR) and P70-S6 kinase 1 (S6K-1) in exposure to a high-fat diet (49), resulting in insulin resistance through the phosphorylation of insulin receptor substrate 1 (IRS-1) (50). On the other hand, in a human study, it was observed that elevated concentrations of BCAA could induce insulin resistance in human skeletal muscle by the direct inhibition of muscle glucose transport and/or phosphorylation with a subsequent reduction in rates of glycogen synthesis (51). Furthermore, the accumulation of toxic intermediates from the BCAA oxidation and impairment of mitochondria functionality may also be involved in the association between BCAA and insulin resistance (50). Moreover, few studies have investigated the mechanisms linking AAA with insulin resistance. One study showed that beta-cell function is affected by oral Tyr and its derived breakdown metabolites such as DA (52). Certain Trp downstream metabolites such as XA and KYNA have been associated with an impaired production, release, and biological activity of insulin. One intermediate pathway of Trp metabolism is the Kyn-nicotinamide adenine dinucleotide (NAD). Downregulation of the NAD pathway leads to the production of XA and KYNA and a decreased formation of NAD leads to inhibition of synthesis and secretion of insulin and the death of pancreatic beta cells (53).

In addition to insulin resistance, prior epidemiological studies have also evaluated a wider number of cardiometabolic risk markers as outcomes of impaired metabolite concentrations (54, 55). For instance, circulating levels of BCAA and AAA metabolites were associated with dyslipidemia, high blood pressure (54), and with a higher odds ratio of T2D, metabolic syndrome, and dyslipidemia after a 4-year follow-up period (55). This fits our observations that higher circulating concentrations of BCAA, AAA, and AAA-downstream metabolites were not only associated with insulin resistance, but also with the presence of other cardiometabolic risk markers, albeit to a lesser extent.

We found no sex differences for the associations between metabolite concentrations and cardiometabolic risk markers, except for the association of 5-HT levels with the odds of having hypertriglyceridemia. Higher 5-HT levels were associated with a significantly lower likelihood of hypertriglyceridemia in women, and a significantly increased likelihood in men. Serotonin (5-HT) is a metabolite from the hydroxylation pathway of Trp catabolism associated with energy homeostasis, appetite regulation, and depressive symptoms. Furthermore, 5-HT also participates in the regulation of hepatic lipid balance (56) and induces lipolysis of stored triacylglycerol increasing plasma levels of free fatty acids and glycerol (57). To the best of our knowledge, there are no population-based studies showing sex differences on the association of 5-HT levels with hypertriglyceridemia. One possible explanation, however, could lie in the different genetic architecture of 5-HT between men and women which may impact the variation on susceptibility to different phenotypes (58). Nonetheless, research on the molecular mechanism by which 5-HT associates with cardiometabolic risk markers in men and women is scarce. Therefore, we can not completely exclude that our finding of a sex-dependent association of 5-HT with hypertriglyceridemia, could have been spurious.

We observed that although BCAA had an abdominal fat-independent effect on the odds of some of the cardiometabolic risk markers, Ile and Leu partially mediate the association

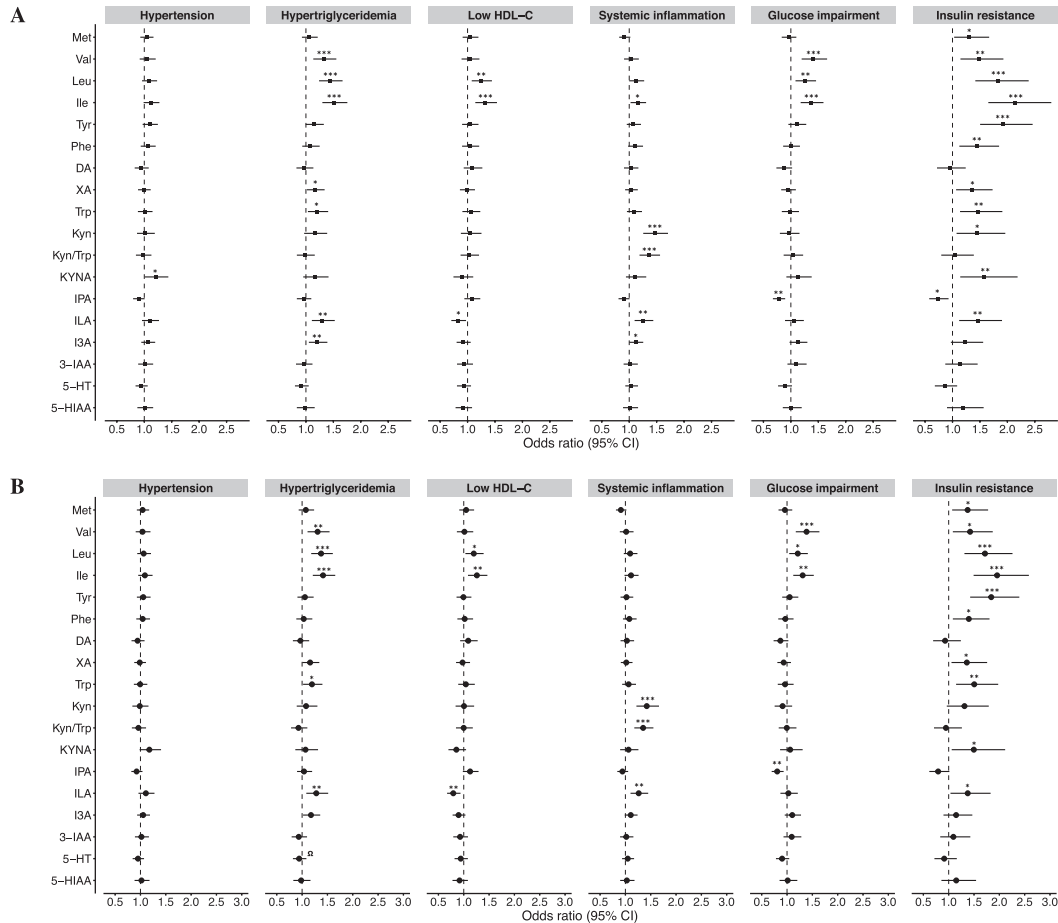


Figure 2. Odds ratio of cardiometabolic risk markers per increase in metabolite concentration. A) Logistic regression model adjusted for age, sex, smoking status, batch effect, and BMI. B) Additionally, models were adjusted for VAT, SAT, and height of the ROI. The horizontal lines crossing the squares and circles shapes represent the 95% CI. Abbreviations: 3-IAA, indole-3-acetic acid; 5-HT, serotonin; 5-HIAA, 5-hydroxyindole-3-acetic acid; DA, dopamine; I3A, indole-3-carboxaldehyde; IPA, indole-3-propionic acid; ILA, indole-3-lactic acid; Ile, L-isoleucine; Kyn, kynurenine; Kyn/Trp, kynurenine/tryptophan ratio; KYNA, kynurenic acid; Leu, L-leucine; Met, L-methionine; Phe, L-phenylalanine; SAT, subcutaneous adipose tissue; Trp, L-tryptophan; Tyr, L-tyrosine; Val, L-valine; VAT, visceral adipose tissue; XA, xanthurenic acid. * P value < 0.05, ** P value < 0.01, *** P value < 0.001. Ω P value for sex-interaction < 0.001.

of VAT with hypertriglyceridemia, low HDL-C, glucose impairment, and insulin resistance. These results suggest that BCAA are associated with metabolic health in 2 ways; acting as mediators between the connection of high VAT accumulation and cardiometabolic risk markers, and having an individual contribution for a higher odds of cardiometabolic risk markers. We also observed that Kyn was the only metabolite that partly mediated the association of VAT with systemic inflammation. Menni et al (59) analyzed the mediation effect of VAT in the association of BCAA with insulin resistance and showed that 19.4% to 46.6% of the variance of HOMA-IR explained by BCAA metabolites was through high VAT mass. Our results, however, support the hypothesis that altered metabolite concentrations are a consequence of a disrupted metabolism in adipocytes, and biologically, they could mediate the relationship between VAT and cardiometabolic risk markers.

Several limitations of this study should be considered. First, we based our analysis on cross-sectional data, which does not allow us to draw causal conclusions on whether high VAT volumes are the cause of disruptions in metabolite concentrations and whether metabolites have a causal effect on higher odds of cardiometabolic risk markers. Second, we identified metabolites in plasma and did not have tissue-specific information to draw more precise inferences on the effects of VAT and SAT metabolism. As a strength of our study, we consider the large and homogenous study population, including men and women from a broad spectrum of ages. Second, the targeted metabolomic approach performed in our study allowed us to quantify a large number of known metabolites with high sensitivity and accuracy. In a sensitivity analysis, we found neither influence of total energy and total protein intake on the associations of VAT and SAT with metabolites concentration, nor in the association of

Table 2. Mediation effect of metabolites in the relation of VAT with cardiometabolic risk factors.

Cardiometabolic risk markers	Metabolite	Direct effect (95% CI)	Indirect effect (95% CI)	Proportion mediated, % (95% CI)	<i>P</i> value
Hypertriglyceridemia	Ile	0.053 (0.04 – 0.06)	0.004 (0.002 – 0.01)	6.5 (3.1 – 11.0)	<0.001
	Leu	0.054 (0.05 – 0.06)	0.002 (0.0008 – 0.001)	4.03 (1.6 – 8.0)	<0.001
	ILA	0.055 (0.05 – 0.06)	0.009 (0.00007 – 0.002)	1.7 (0.3 – 4.0)	0.02
Low HDL-C	Ile	0.044 (0.03 – 0.05)	0.003 (0.001 – 0.01)	6.7 (2.0 – 14.0)	0.002
	Leu	0.045 (0.003 – 0.08)	0.002 (0.0001 – 0.004)	3.7 (0.2 – 9.0)	0.02
Systemic inflammation	Kyn	0.037 (0.02 – 0.04)	0.002 (0.0007 – 0.005)	6.4 (2.0 – 11.0)	<0.001
Glucose impairment	Ile	0.036 (0.02 – 0.05)	0.003 (0.002 – 0.01)	8.8 (3.2 – 18.0)	<0.001
	Leu	0.037 (0.02 – 0.05)	0.002 (0.0003 – 0.001)	4.6 (0.7 – 11.0)	0.02
	IPA	0.036 (0.02 – 0.05)	0.002 (0.0007 – 0.001)	6.3 (1.9 – 13.0)	0.004
Insulin resistance	Ile	0.009 (0.006 – 0.013)	0.001 (0.0005 – 0.002)	11.0 (5.8 – 18.0)	<0.001
	Leu	0.010 (0.008 – 0.013)	0.0007 (0.0002 – 0.001)	6.5 (2.5 – 12.0)	0.002
	ILA	0.011 (0.007 – 0.015)	0.0003 (0.00002 – 0.001)	2.5 (0.2 – 6.0)	0.02
	Tyr	0.010 (0.007 – 0.013)	0.0008 (0.0003 – 0.002)	7.8 (3.2 – 14.0)	<0.001
	Phe	0.011 (0.007 – 0.01)	0.0003 (0.00002 – 0.001)	2.6 (0.4 – 6.0)	0.02

Models for mediation analysis were adjusted for age, sex, BMI, VAT, SAT, height of ROI, and batch effect.

metabolite concentration with the odds of cardiometabolic risk markers (data not shown).

This is the first large-scale study highlighting the importance to include the simultaneous analysis in human plasma, by liquid chromatography–tandem mass spectrometry, of the metabolites belonging to Trp, BCAA, and AAA pathways. Several of these, as depicted in Fig. 1, emerged as potentially useful clinical markers to understand the link between the abdominal VAT and metabolic health risk markers. We also used a validated method to accurately quantify abdominal fat from MRI images that enable us to compare the metabolic activities of VAT and SAT volumes as different fat compartments. We considered as outcomes different cardiometabolic risk markers (prior state of disease) that allow identifying individuals before the onset of a disease. This study incites the further integration of genetic and lifestyle information to help to elucidate causal effects of metabolites on cardiometabolic risk markers and to understand the mechanism behind changes in VAT metabolism impact circulating metabolites.

Conclusion

In summary, we have shown that in metabolically unhealthy individuals, VAT is associated with an altered BCAA and AAA metabolism, as reflected in circulating concentrations. BCAA, AAA, and AAA-downstream metabolites are important biomarkers in metabolic health abnormalities, and

they are also partial mediators in the connection between VAT and cardiometabolic risk markers. Thus, these metabolites may provide a better insight into the biological mechanisms that underlie the relationship of abdominal VAT with metabolic health.

Financial Support

This work was supported by grants from the JPI HDHL on “Biomarkers for Nutrition and Health”, “HEALTHMARK”, by the Federal Ministry of Education and Research, Germany (grant number 01EA1705B), and the Italian Ministry of Education, University and Research, MIUR, (grant number CUP D43C17000100006); the “Competence Cluster Nutrition Research” funded by the Federal Ministry of Education and Research (FKZ: 01EA1809C); and the Deutsche Forschungsgemeinschaft (DFG, German Research Foundation) under Germany’s Excellence Strategy (EXC 2151–390873048) and through SFB1454—project number 432325352.

Author Contributions

O.R.X. contributed to the study concept and design, analysis, and interpretation of the data, drafting and revising the manuscript. A.A. implemented the metabolomic analysis, contributed to the interpretation of data, and critical revision of the

manuscript for important intellectual content. F.M. designed the plan of the experiment, supervised the metabolomic analyses, and contributed to the critical revision of the manuscript for important intellectual content. M.M.B.B. contributed to the study concept and design, interpretation of data, revision of the manuscript, funding, and supervision. All the authors have accepted responsibility for the entire content of this submitted manuscript and approved the final version of the manuscript for submission.

Disclosure

The authors have nothing to disclose.

Data Availability

Some or all datasets generated during and/or analyzed during the current study are not publicly available but are available from the corresponding author on reasonable request.

References

- GBD 2015 Obesity Collaborators, Afshin A, Forouzanfar MH, et al. Health effects of overweight and obesity in 195 countries over 25 years. *N Engl J Med*. 2017;377(1):13-27.
- Sung H, Siegel RL, Torre LA, et al. Global patterns in excess body weight and the associated cancer burden. *CA Cancer J Clin*. 2018;68(2):88-112.
- Riedl A, Wawro N, Gieger C, et al. Identification of comprehensive metabolites associated with cardiometabolic diseases in the population-based KORA study. *Mol Nutr Food Res*. 2018;62(16):1-9.
- Urpi-Sarda M, Almanza-Aguilera E, Llorach R, et al. Non-targeted metabolomic biomarkers and metabolotypes of type 2 diabetes: A cross-sectional study of PREDIMED trial participants. *Diabetes Metab*. 2019;45(2):167-174.
- Wildman RP, Muntner P, Reynolds K, et al. The obese without cardiometabolic risk factor clustering and the normal weight with cardiometabolic risk factor clustering prevalence and correlates of 2 phenotypes among the US population (NHANES 1999-2004). *Arch Intern Med*. 2008;168(15):1617-1624.
- Stefan N, Häring HU, Hu FB, Schulze MB. Metabolically healthy obesity: epidemiology, mechanisms, and clinical implications. *Lancet Diabetes Endocrinol*. 2013;1(2):152-162.
- Stefan N, Schick F, Häring HU. Causes, characteristics, and consequences of metabolically unhealthy normal weight in humans. *Cell Metab*. 2017;26(2):292-300.
- Neeland IJ, Poirier P, Després JP. Cardiovascular and metabolic heterogeneity of obesity: clinical challenges and implications for management. *Circulation*. 2018;137(13):1391-1406.
- Hwang YC, Hayashi T, Fujimoto WY, et al. Visceral abdominal fat accumulation predicts the conversion of metabolically healthy obese subjects to an unhealthy phenotype. *Int J Obes*. 2015;39(9):1365-1370.
- Stefan N. Causes, consequences, and treatment of metabolically unhealthy fat distribution. *Lancet Diabetes Endocrinol*. 2020;8(7):616-627.
- Chait A, den Hartigh LJ. Adipose Tissue Distribution, Inflammation and Its Metabolic Consequences, Including Diabetes and Cardiovascular Disease. *Front Cardiovasc Med*. 2020;7:22. doi:10.3389/fcvm.2020.00022
- Smith U, Kahn BB. Adipose tissue regulates insulin sensitivity: role of adipogenesis, de novo lipogenesis and novel lipids. *J Intern Med*. 2016;280(5):465-475.
- Ebbert JO, Jensen MD. Fat depots, free fatty acids, and dyslipidemia. *Nutrients*. 2013;5(2):495-508.
- Wild CP. Complementing the genome with an “exposome”: The outstanding challenge of environmental exposure measurement in molecular epidemiology. *Cancer Epidemiol Biomarkers Prev*. 2005;14(8):1847-1850.
- Badouf F, Lam KP, Dibattista A, et al. Serum and adipose tissue amino acid homeostasis in the metabolically healthy obese. *J Proteome Res*. 2014;13(7):3455-3466.
- Batch BC, Shah SH, Newgard CB, et al. Branched chain amino acids are novel biomarkers for discrimination of metabolic wellness. *Metabolism*. 2013;62(7):961-969.
- Chen HH, Tseng YJ, Wang SY, et al. The metabolome profiling and pathway analysis in metabolic healthy and abnormal obesity. *Int J Obes*. 2015;39(8):1241-1248.
- Yin X, Subramanian S, Willinger CM, et al. Metabolite signatures of metabolic risk factors and their longitudinal changes. *J Clin Endocrinol Metab*. 2016;101(4):1779-1789.
- Cusotto S, Delgado I, Anesi A, et al. Tryptophan metabolic pathways are altered in obesity and are associated with systemic inflammation. *Front Immunol*. 2020;11(2020):557.
- Wang TJ, Larson MG, Vasan RS, et al. Metabolite profiles and the risk of developing diabetes. *Nat Med*. 2011;17(4):448-453.
- Chen T, Zheng X, Ma X, et al. Tryptophan Predicts the Risk for Future Type 2 Diabetes. *PLoS One*. 2016;11(9):e0162192. doi:10.1371/journal.pone.0162192
- Magnusson M, Lewis GD, Ericson U, et al. A diabetes-predictive amino acid score and future cardiovascular disease. *Eur Heart J*. 2013;34(26):1982-1989.
- Boulet MM, Chevrier G, Grenier-Larouche T, et al. Alterations of plasma metabolite profiles related to adipose tissue distribution and cardiometabolic risk. *Am J Physiol Endocrinol Metab*. 2015;309(8):E736-E746.
- Wolowczuk I, Hennart B, Leloire A, et al. Tryptophan metabolism activation by indoleamine 2,3-dioxygenase in adipose tissue of obese women: An attempt to maintain immune homeostasis and vascular tone. *Am J Physiol Regul Integr Comp Physiol*. 2012;303(2):135-143.
- Favennec M, Hennart B, Caiazzo R, et al. The kynurenine pathway is activated in human obesity and shifted toward kynurenine monooxygenase activation. *Obesity*. 2015;23(10):2066-2074.
- Badawy AAB. Kynurenine pathway of tryptophan metabolism: Regulatory and functional aspects. *Int J Tryptophan Res*. 2017;10:1178646917691938. doi:10.1177/1178646917691938
- Herman MA, She P, Peroni OD, Lynch CJ, Kahn BB. Adipose tissue branched chain amino acid (BCAA) metabolism modulates circulating BCAA levels. *J Biol Chem*. 2010;285(15):11348-11356.
- Wiklund P, Zhang X, Pekkala S, et al. Insulin resistance is associated with altered amino acid metabolism and adipose tissue dysfunction in normoglycemic women. *Sci Rep*. 2016;6(1):1-11.
- Malloy VL, Krajcik RA, Bailey SJ, Hristopoulos G, Plummer JD, Orentreich N. Methionine restriction decreases visceral fat mass and preserves insulin action in aging male Fischer 344 rats independent of energy restriction. *Aging Cell*. 2006;5(4):305-314.
- Zhou X, He L, Wan D, et al. Methionine restriction on lipid metabolism and its possible mechanisms. *Amino Acids*. 2016;48(7):1533-1540.
- Plaisance EP, Greenway FL, Boudreau A, et al. Dietary methionine restriction increases fat oxidation in obese adults with metabolic syndrome. *J Clin Endocrinol Metab*. 2011;96(5):836-840.
- Hanzu FA, Vinaixa M, Papageorgiou A, et al. Obesity rather than regional fat depots marks the metabolomic pattern of adipose tissue: An untargeted metabolomic approach. *Obesity*. 2014;22(3):698-704.
- Piro MC, Tesauro M, Lena AM, et al. Free-amino acid metabolic profiling of visceral adipose tissue from obese subjects. *Amino Acids*. 2020;52(8):1125-1137.
- Breteler MMB, Stöcker T, Pracht E, Brenner D, Stirnberg R, Iq-P-165: MRI in the Rhineland Study: a novel protocol for population neuroimaging. *Alzheimers Dement*. 2014;10:P92-P92.

35. Anesi A, Rubert J, Oluwagbemigun K, *et al.* Metabolic profiling of human plasma and urine, targeting tryptophan, tyrosine and branched chain amino acid pathways. *Metabolites*. 2019;9(11):261.
36. Estrada S, Lu R, Conjeti S, *et al.* FatSegNet: A fully automated deep learning pipeline for adipose tissue segmentation on abdominal Dixon MRI. *Magn Reson Med*. 2020;83(4):1471-1483.
37. Kroke A, Klipstein-Grobusch K, Voss S, *et al.* Validation of a self-administered food-frequency questionnaire administered in the European Prospective Investigation into Cancer and Nutrition (EPIC) Study: comparison of energy, protein, and macronutrient intakes estimated with the doubly labeled water. *Am J Clin Nutr*. 1999;70(4):439-447.
38. Benjamini Y, Hochberg Y. Controlling the FDR: A practical and powerful approach to multiple testing. *J R Stat Soc Ser B*. 1995;57(1):289-300.
39. VanderWeele TJ. Mediation analysis: a practitioner's guide. *Annu Rev Public Health*. 2016;37:17-32.
40. Zhao X, Lynch JG, Chen Q. Reconsidering Baron and Kenny: myths and truths about mediation analysis. *J Consum Res*. 2010;37(2):197-206.
41. Wiklund PK, Pekkala S, Autio R, *et al.* Serum metabolic profiles in overweight and obese women with and without metabolic syndrome. *Diabetol Metab Syndr*. 2014;6(1):1-9.
42. Mangge H, Summers KL, Meinitzer A, *et al.* Obesity-related dysregulation of the Tryptophan-Kynurenine metabolism: Role of age and parameters of the metabolic syndrome. *Obesity*. 2014;22(1):195-201.
43. Bagheri M, Farzadfar F, Qi L, *et al.* Obesity-Related Metabolomic Profiles and Discrimination of Metabolically Unhealthy Obesity. *J Proteome Res*. 2018;17(4):1452-1462.
44. Otto L, Budde K, Kastenmüller G, *et al.* Associations between adipose tissue volume and small molecules in plasma and urine among asymptomatic subjects from the general population. *Sci Rep*. 2020;10(1):1-11.
45. Martin FPJ, Montoliu I, Collino S, *et al.* Topographical body fat distribution links to amino acid and lipid metabolism in healthy non-obese women. *PLoS One*. 2013;8(9):e73445.
46. Schlecht I, Gronwald W, Behrens G, *et al.* Visceral adipose tissue but not subcutaneous adipose tissue is associated with urine and serum metabolites. *PLoS One*. 2017;12(4):e0175133.
47. Li X, Sun D, Zhou T, *et al.* Changes of branched-chain amino acids and ectopic fat in response to weight-loss diets: The POUNDS lost trial. *J Clin Endocrinol Metab*. 2020;105(10):e3747-e3756.
48. Naukkarinen J, Heinonen S, Hakkarainen A, *et al.* Characterising metabolically healthy obesity in weight-discordant monozygotic twins. *Diabetologia*. 2014;57(1):167-176.
49. Newgard CB, An J, Bain JR, *et al.* A Branched-Chain Amino Acid-Related Metabolic Signature that Differentiates Obese and Lean Humans and Contributes to Insulin Resistance. *Cell Metab*. 2009;9(4):311-326.
50. Yoon MS. The emerging role of branched-chain amino acids in insulin resistance and metabolism. *Nutrients*. 2016;8(7):405.
51. Krebs M, Krssak M, Bernroider E, *et al.* Mechanism of amino acid-induced skeletal muscle insulin resistance in humans. *Diabetes*. 2002;51(3):599-605.
52. Korner J, Cline GW, Slifstein M, *et al.* A role for foregut tyrosine metabolism in glucose tolerance. *Mol Metab*. 2019;23:37-50.
53. Oxenkrug G. Insulin resistance and dysregulation of tryptophan-kynurenine and kynurenine-nicotinamide adenine dinucleotide metabolic pathways. *Mol Neurobiol*. 2013;48(2):294-301.
54. Cheng S, Rhee EP, Larson MG, *et al.* Metabolite profiling identifies pathways associated with metabolic risk in humans. *Circulation*. 2012;125(18):2222-2231.
55. Yamakado M, Nagao K, Imaizumi A, *et al.* Plasma free amino acid profiles predict four-year risk of developing diabetes, metabolic syndrome, dyslipidemia, and hypertension in Japanese population. *Sci Rep*. 2015;5(1):1-12.
56. Yabut JM, Crane JD, Green AE, Keating DJ, Khan WJ, Steinberg GR. Emerging roles for serotonin in regulating metabolism: new implications for an ancient molecule. *Endocr Rev*. 2019;40(4):1092-1107.
57. Martin AM, Young RL, Leong L, *et al.* The diverse metabolic roles of peripheral serotonin. *Endocrinology*. 2017;158(5):1049-1063.
58. Weiss LA, Abney M, Cook EH, Ober C. Sex-specific genetic architecture of whole blood serotonin levels. *Am J Hum Genet*. 2005;76(1):33-41.
59. Menni C, Migaud M, Glastonbury CA, *et al.* Metabolomic profiling to dissect the role of visceral fat in cardiometabolic health. *Obesity*. 2016;24(6):1380-1388.

4. General discussion

Thousands of years ago Hippocrates wrote, “Corpulence is not only a disease itself but the harbinger of others”. Nowadays, epidemiological studies have largely confirmed that statement, pointing to the health consequences of obesity (Di Angelantonio et al., 2016; GBD 2015 Obesity Collaborators, 2017), and obesity has become a focus of attention in several countries and health organizations

Several factors are involved in the development of obesity, including genetic, environmental, and behavioural aspects. Nevertheless, it seems that the main causes of the current global obesity problem lie in environmental and behavioural changes such as an increase in the intake of high energy-dense food, together with low physical activity (Haslam and James, 2005; WHO Consultation on Obesity (1999: Geneva, 2000). Moreover, the classification of obesity becomes challenging as a subset of individuals with the same obesity level, seem to be protected from developing obesity-related diseases (Wildman et al., 2008).

This thesis showed that abdominal fat plays a central role in the health problems related to obesity. The excessive accumulation of fat in the abdominal cavity causes a cascade of physiological processes such as chronic inflammation and chronic organ failure in different body systems. Therefore, epidemiological studies should estimate obesity prevalence based on abdominal fat and not only BMI. To our knowledge, only one study (Wong et al., 2020) has reported on the global prevalence of central obesity based on WC measurements. They reported that the overall prevalence of central obesity was 41.5%, based on data from 288 selected studies from different countries. This prevalence increased with age and tended to be higher in women compared to men (Wong et al., 2020). In 2010, Moebus et al. reported that the prevalence of central obesity (WC > 102 cm in men or >88 cm in women) was 39.5% for the German population (Moebus et al., 2010), which is much higher than the BMI-based obesity prevalence reported by the Robert Koch Institute (23% of men and 24% of women) (Mensink et al., 2013).

To date, longitudinal studies have reported on the associations of excess abdominal obesity (VAT and SAT) with mortality (Koster et al., 2015)(Rao et al., 2021) and incidence of CVD risk factors (Britton et al., 2013)(Lee et al., 2016)(Abraham et al., 2015) in a relatively large sample size from different population-based studies. They similarly found weak or no effects of larger SAT volumes. For example, in the Jackson

study, only higher VAT volumes were associated with higher heart failure incidence after a follow-up of 10.6 years (Rao et al., 2021). Koster A *et al.* found that in older adults, VAT was a strong predictor of mortality in obese women while SAT was associated with lower mortality risk in normal and overweight women. Since only significant associations were found in women, they emphasized the importance of sex differences regarding adipose distribution and mortality (Koster et al., 2015).

In this thesis, I presented the validation of MRI and metabolomic techniques to acquire cardiometabolic risk markers. We validated a novel deep learning pipeline (termed FatSegNet) to reliably segment and quantify VAT and SAT on a fast acquisition abdominal DIXON MR protocol (approximately 1 minute for analyzing a subject's whole volume) in the Rhineland Study. This pipeline was able to show high robustness and generalizability across a wide range of ages, BMI, and body shapes. Furthermore, the pipeline showed high reliability when compared with manually labelled images. The fast acquisition performance and accuracy of FastSegNet positioned it as a suitable method to accurately quantify VAT and SAT in large population-based cohort studies that include MRI. This pipeline is open-source, which will allow for external validation in different populations.

This thesis also includes the validation of a single robust targeted method using UHPLC-ESI-MS/MS that quantified a broad coverage of metabolites from BCAA and AAA metabolism in a large sample set, requiring a low amount of biomaterial sample with a fast extraction. This method was validated using urine and plasma biomaterial from two independent epidemiological studies across the lifespan, in the Dortmund Nutritional and Anthropometric Longitudinally Designed (DONALD) Study and the Rhineland Study. The results established typical ranges for these metabolites in the human biofluids of two German populations.

Because of the important emerging role of BCAA, AAA, and AAA-breakdown metabolites on cardiometabolic risk, this method is applicable for large prospective cohort studies. The acquisition of MRI and metabolomics biomarkers, allowed me to address several questions on the complex link between abdominal adipose tissue and cardiometabolic risk markers. I compared how anthropometric measurements (indirect measurements of adiposity) correlated to direct MRI-abdominal fat. Furthermore, I evaluated the

association of several metabolites from the BCAA and AAA with VAT and SAT, and how those metabolites mediate the relationship between abdominal fat with cardiometabolic risk. Interestingly, our results confirm and expand upon previous findings by showing that men and women have different patterns of abdominal fat accumulation, and the impact of larger VAT and SAT volumes on cardiometabolic risk factors significantly differs between sexes.

The differences in fat accumulation between men and women have previously been emphasized as an evolutionary process, suggesting that a greater fat accumulation in thighs and buttocks in women was due to an adaptation for their functional reproduction and fertility (Power and Schulkin, 2008). However, the biological underpinning explanations remain poorly understood. Evidence has shown that sex differences may be determined by a complex interplay of genetic, epigenetic, and hormonal factors (Karastergiou et al., 2012). Furthermore, sex differences go beyond not only differences in anatomical fat accumulation but also in their interaction with cardiometabolic diseases. Our study demonstrated that women are significantly more susceptible to the metabolic harmful effects of increased amounts of VAT than men. Interestingly, we also observed that in men, the associations of VAT and SAT with cardiometabolic risk markers were equally strong. Evidence has suggested a healthier expansion of SAT in obese women (hyperplasia) when compared to men (Karastergiou et al., 2012). Nonetheless, the proportion of hepatic FFAs delivery from VAT in women is higher than in men (Nielsen et al., 2004), which may confirm the more harmful effect of larger VAT volume in women as compared to men.

The understanding of the mechanisms linking abdominal fat with cardiometabolic risk markers is essential to identifying individuals at risk before cardiometabolic diseases become present. In a more clinical perspective, these mechanisms will assist in finding and implementing targeted strategies to reduce abdominal fat. A reduction in abdominal fat, however, should not only be reflected as weight loss, but rather as changes in the functionality of adipocytes that can impact metabolic health. It has been proposed that diet and physical activity can improve the inflammation profile and enhance the functionality of adipose tissue. Specifically, certain food components have been associated with a healthy phenotype by impacting the metabolism in the adipose tissue (Nielsen et al., 2004). As a whole, dietary and physical activity interventions have been proven to have

positive effects on fat mobilization (Gepner et al., 2018). Specific exercise dosages and modalities have also been involved in reducing VAT and improving metabolic health (Chang et al., 2021) by stimulating positive adaptations in mitochondrial function in SAT (Mendham et al., 2020).

One of the main limitations of this thesis is the use of cross-sectional data, which makes it difficult to conclude causal associations of VAT and SAT with cardiometabolic risk. However, several strengths are worth mentioning. First, we included a large sample size with a broad age range. Second, we accurately quantified abdominal fat through MRI, which at a population-based scale, gives us the possibility to evaluate and compare VAT and SAT as two different metabolic fat compartments. We also included metabolites as putative biomarkers of metabolic health using a very sensitive technique to evaluate a broad number of cardiometabolic risk markers.

In summary, we can conclude that it is crucial to classify individuals at cardiometabolic risk based on accurate measures of abdominal obesity. The observed differences in the association of VAT and SAT with cardiometabolic risk markers, and the remarkable sex differences, insight into further research. The deep phenotyping in the Rhineland study and the upcoming follow-up examinations will create opportunities for further research questions that seek to understand the complex interaction of adiposity and cardiometabolic diseases. One example is identifying genetic and epigenetic components that determine the differences in VAT and SAT accumulation, and understanding how they might be involved in the complex connection of VAT and SAT with cardiometabolic risk in men and women. Additionally, examining the interaction of abdominal fat with environmental factors such as diet and physical activity could open a window to find targeted strategies that prevent the development of metabolic diseases by lowering VAT accumulation and improving its metabolic functionality.

References

- Abraham TM, Pedley A, Massaro JM, Hoffmann U, Fox CS. 2015. Association between visceral and subcutaneous adipose depots and incident cardiovascular disease risk factors. *Circulation* 132:1639–1647
- Britton KA, Massaro JM, Murabito JM, Kreger BE, Hoffmann U, Fox CS. 2013. Body Fat Distribution, Incident Cardiovascular Disease, Cancer, and All-cause Mortality. *J Am Coll Cardiol* 10:921–925
- Chang YH, Yang HY, Shun SC. 2021. Effect of exercise intervention dosage on reducing visceral adipose tissue: a systematic review and network meta-analysis of randomized controlled trials. *Int J Obes* 45:982–997
- Di Angelantonio E, Bhupathiraju SN, Wormser D, Gao P, Kaptoge S, de Gonzalez AB, et al. 2016. Body-mass index and all-cause mortality: individual-participant-data meta-analysis of 239 prospective studies in four continents. *Lancet* 388:776–786
- GBD 2015 Obesity Collaborators. 2017. Health effects of overweight and obesity in 195 countries over 25 years. *N Engl J Med* 377:13–27
- Gepner Y, Shelef I, Schwarzfuchs D, Zelicha H, Tene L, Meir AY, et al. 2018. Effect of distinct lifestyle interventions on mobilization of fat storage pools CENTRAL magnetic resonance imaging randomized controlled trial. *Circulation* 137:1143–1157
- Haslam D, James WP. 2005. Obesity. *Lancet* 366: 1197–209.
- Karastergiou K, Smith SR, Greenberg AS, Fried SK. 2012. Sex differences in human adipose tissues - The biology of pear shape. *Biol Sex Differ* 3:1
- Koster A, Murphy RA, Eiriksdottir G, Aspelund T, Sigurdsson S, Lang TF, et al. 2015. Fat distribution and mortality: The AGES-Reykjavik study. *Obesity* 23:893–897
- Lee JJ, Pedley A, Hoffmann U, Massaro JM, Fox CS. 2016. Association of Changes in Abdominal Fat and Cardiovascular Risk Factors. *J Am Coll Cardiol* 68:1509–1521
- Mendham AE, Larsen S, George C, Adams K, Hauksson J, Olsson T, et al. 2020. Exercise training results in depot-specific adaptations to adipose tissue

mitochondrial function. *Sci Rep* 10:1–14

- Mensink GBM, Schienkiewitz A, Haftenberger M, Lampert T, Ziese T, Scheidt-Nave C. 2013. Overweight and obesity in Germany Results of the German Health Interview and Examination Survey for Adults (DEGS1). *Bundesgesundheitsblatt - Gesundheitsforsch - Gesundheitsschutz* 56:786–794
- Moebus S, Balijepalli C, Lösch C, Göres L, Stritzky B Von, Bramlage P, et al. 2010. Age- and sex-specific prevalence and ten-year risk for cardiovascular disease of all 16 risk factor combinations of the metabolic syndrome - A cross-sectional study. *Cardiovasc Diabetol* 9:34.
- Nielsen S, Guo ZK, Johnson CM, Hensrud DD, Jensen MD. 2004. Splanchnic lipolysis in human obesity. *J Clin Invest* 113:1582–1588
- Power ML, Schulkin J. 2008. Sex differences in fat storage, fat metabolism, and the health risks from obesity: Possible evolutionary origins. *Br J Nutr* 99:931–940
- Rao VN, Bush CG, Mongraw-Chaffin M, Hall ME, Clark D, Fudim M, et al. 2021. Regional adiposity and risk of heart failure and mortality: The Jackson heart study. *J Am Heart Assoc* 10:e020920
- WHO Consultation on Obesity (1999: Geneva S& WHO. 2000. Obesity : preventing and managing the global epidemic : report of a WHO consultation. WHO Tech Rep Ser ; 894
- Wildman RP, Muntner P, Reynolds K, McGinn AP, Rajpathak S, Wylie-Rosett J, et al. 2008. The obese without cardiometabolic risk factor clustering and the normal weight with cardiometabolic risk factor clustering prevalence and correlates of 2 phenotypes among the US population (NHANES 1999-2004). *Arch Intern Med* 168:1617–1624
- Wong MCS, Huang J, Wang J, Chan PSF, Lok V, Chen X, et al. 2020. Global, regional and time-trend prevalence of central obesity: a systematic review and meta-analysis of 13.2 million subjects. *Eur J Epidemiol* 35:673–683

5. Acknowledgement

“Feeling gratitude and not expressing it is like wrapping a present and not giving it”

William Arthur Ward

I would first like to express my gratitude to my supervisor, Prof. Monique M.B. Breteler, for her guidance and feedback throughout my Ph.D., whose invaluable experience and epidemiological knowledge helped me to expand my epidemiological thinking, and inspired me to bring my work always to a higher level. I would also like to thank Prof. Ahmad Aziz for his assistance whenever I had a statistical question. And to our study assistance for making the bridge for us between data collection and data analysis.

I would like to thank all my colleagues for making a nice atmosphere at work and those who, more than colleagues, have also become friends.

Especially, Valentina, for her helpful feedback on this thesis. To Annabell for her prized friendship, with whom I shared frustrating and inspirational moments across this chapter of my life. And to Santiago, my Latin support, for his significant feedback and being always willing to help.

To Rika, Nersi, Weiyi, Dan, Xinwang, and Konstantinos, with whom I not only had discussions about our research but also expended many nice and funny moments that rested my mind when frustrating moments came across, and even when not.

In addition, I would like to thank all my friends and people with whom I came across during this important stage of my life and those who have supported me before starting this adventure. Vielen Dank, Angela und Mic, dass ihr in dieser Phase meines Lebens eine deutsche Familie geworden seid.

And lastly, I would extend my gratitude to my family, who despite being more than 9,800 kilometers far away always believed in me.

6. Statement

For the publication for which the doctoral student is the lead author, the doctoral student must have undertaken the predominant share of the planning of the academic work, data collection, evaluation, and interpretation, and have written the first version of the manuscript himself.

For the publications for which the doctoral student is a co-author, the doctoral student must have taken on a significant share of the planning of the academic work, data collection, evaluation, and interpretation. Relevant proof of the work carried out by the doctoral student is to be submitted to the publisher (sections 6(3), 7(1))